First Ramsey-type mass measurements with ISOLTRAP and design studies of the new PENTATRAP project

Dissertation zur Erlangung des Grades
Doktor der Naturwissenschaften
am Fachbereich 08: Physik, Mathematik und Informatik
der Johannes Gutenberg-Universität Mainz

Von Sebastian George
geb. in Hamm
Mainz 2009

Berichterstatter:

Tag der Promotion: 09.07.2009

Zusammenfassung

Der Einsatz von Penningfallen in der Massenspektrometrie hat zu einem einmaligen Genauigkeitssprung geführt. Dadurch wurden Massenwerte verschiedenster Atome zu wichtigen Eingangsparametern bei immer mehr physikalischen Fragestellungen. Dieser Prozess der Erschließung neuer Anwendungsgebiete setzt sich mit einer stetigen Entwicklung von Penningfallenmassenspektrometern hin zu höheren Genauigkeiten fort.
Die Massenspektrometrie mit Hilfe von Penningfallen basiert auf der Bestimmung der freien Zyklotronfrequenz eines Ions in einem homogenen Magnetfeld $\nu_c = qB/(2\pi m)$. Zwei grundsätzlich verschiedene Messmethoden stehen dabei zur Verfügung: Bei der destruktiven Flugzeitmethode (TOF-ICR) ist das Ion nach dem Messvorgang verloren. Insbesondere aufgrund ihrer schnellen Messfolge wird diese Methode standardmäßig zur Massenbestimmung kurzlebiger Radionuklide eingesetzt, wobei inzwischen eine relative Massenungenauigkeit $\delta m/m$ von wenigen 10^{-9} bei Nukliden mit Lebensdauern von $< 500\,ms$ erreicht wird. Dies wurde durch die im Rahmen dieser Arbeit erstmals in der Penningfallen-Massenspektrometrie eingesetzten Ramsey-Methode möglich. Im Gegensatz dazu wird bei der zerstörungsfreien Fouriertransformations-Ionenzyklotronresonanzmethode (FT-ICR) die Frequenz des in die Penningfallenelektroden induzierten Spiegelstroms des sich bewegenden Ions gemessen. Hierbei verbleibt das Ion in der Falle und kann weiter verwendet werden. Mit dieser Methode werden vorrangig Massen stabiler Nuklide mit relativen Genauigkeiten von weniger als $\delta m/m = 10^{-11}$ bestimmt.
Ein wesentlicher Bestandteil dieser Doktorarbeit war die Anwendung von zeitlich separierten, oszillierenden Feldern, genannt Ramsey-Methode zur resonanten Ionenanregung, um die Frequenzmessung durch die Flugzeitmethode zu verbessern. Damit wurden am Penningfallenmassenspektrometer ISOLTRAP an ISOLDE/CERN die Massen der Nuklide ^{26,27}Al und ^{38,39}Ca bestimmt. Alle Massen wurden in die "Atomic Mass Evaluation" eingebettet. Die Massenwerte von ^{26}Al und ^{38}Ca dienten insbesondere zu Tests des Standardmodells.
Des Weiteren wurden Dämpfungseffekte in der Penningfalle aufgrund von Stößen zwischen gespeicherten Ionen und Restgasatomen, sowie deren Auswirkungen auf die Flugzeitmethode ausführlich untersucht und beschrieben.
Um mit Massenwerten fundamentale Symmetrien oder die Quantenelektrodynamik (QED) in extremen Feldern zu testen wurde ein neues Penningfallenprojekt (PENTATRAP) für hochpräzise Massenmessungen an hochgeladenen Ionen konzipiert. In dieser Doktorarbeit wurde vornehmlich die Entwicklung der Penningfallen betrieben. Eine Neuerung bei Penningfallenexperimenten ist dabei der Einsatz so genannter "Monitorfallen", die eine permanente Beobachtung des Magnetfeldes B und seiner zeitlichen Fluktuationen ermöglichen sollen.

Summary

The application of Penning traps for mass spectrometry has led to a major step in the mass precision. Consequently, atomic masses became more and more important as input parameters in different research fields. This exploitation is still ongoing in line with a steady development of Penning trap mass spectrometers to even higher accuracies.
Penning trap mass spectrometry is based on the determination of the free cyclotron frequency $\nu_c = qB/(2\pi m)$ of an ion confined in a homogeneous magnetic field B. In principle two different measurement techniques are available: By applying the destructive time-of-flight detection method (TOF-ICR) the trap content is lost after the measurement. Since it is a fast measurement method it is usually used for mass determinations of short-lived radionuclides, whereas a relative mass uncertainty $\delta m/m$ of a few parts in 10^{-9} is routinely reached even for nuclides with half-lives well below $500\,ms$. This has been achieved by the implementation of the Ramsey method in Penning trap mass spectrometry within this work. By contrast the non-destructive Fourier Transform-Ion Cyclotron Resonance detection method (FT-ICR) determines the frequency of the image current introduced in the trap electrodes by the ion motion. Thus, the ion remains in the trap and can be used for further measurement cycles. This method is often applied for measurements of stable nuclides reaching a relative mass uncertainty of less than $\delta m/m = 10^{-11}$.
One part of this thesis was the application of time-separated oscillatory fields, called Ramsey method, for resonant ion motion excitation in order to improve the time-of-flight detection method. It was used to measure the nuclides ^{26,27}Al and ^{38,39}Ca with the Penning trap mass spectrometer ISOLTRAP. The mass values have been included in the "Atomic Mass Evaluation" (AME). Furthermore, the nuclides ^{26}Al and ^{38}Ca serve as input parameters for stringent tests of the Standard Model.
Additionally, damping effects in a Penning trap due to collisions between trapped ions and residual gas atoms as well as their impact on the time-of-flight detection method have been extensively investigated.
To exploit precise mass values to test fundamental symmetries or to study quantum electrodynamics (QED) in extreme fields a new Penning trap project (PENTATRAP) for mass measurements on highly-charged ions has recently been started. The main contribution within this thesis was the design of the Penning traps. For the first time so called "monitor traps" has been developed in order to observe permanently the magnetic field B and its time-dependent fluctuations.

Contents

List of Tables

List of Figures

Chapter 1

Introduction

$E = mc^2$, Einstein's famous energy-mass relation [Eins1905], accentuates in its simplicity the importance of the mass in Nature. It is one of the fundamental properties of all existing elementary particles. The nucleonic and atomic interactions are merged in the atomic mass. Ultimately, masses are unique like a fingerprint. The inherent connection of the mass and all forces acting in an atom allows accurate mass values to become elementary pillars in many research fields of physics. As different as the various applications of atomic mass values is the required precision. It ranges from $\delta m/m = 10^{-5}$ to below 10^{-8} for radionuclides, which often have half-lives considerably less than a second [Boll2001, Herf2003, Lunn2003], and even down to $\delta m/m = 10^{-11}$ for stable nuclides [Rain2004, VanD2004, Reds2008]. Some applications and their required precision are illustrated in Fig. 1.1. Presently masses of more than 3200 nuclides are known or estimated. A detailed overview about the actual status of atomic masses is given in the latest Atomic-Mass Evaluation AME2003 [Audi2003b, Waps2003]. The nuclear chart in Fig 1.2 shows the relative mass uncertainty of all known isotopes in a color-coded plot. The mass values are either obtained by different techniques of mass spectrometry or by estimations from systematic trends (see also [Blau2005a]).

The history of mass spectrometry was accompanied by a couple of Nobel Prize awards. Its beginning dates back to the year 1897, when Joseph John Thomson introduced the electron as an electrically charged particle and measured its charge-to-mass ratio [Thom1897, Thom1899]. Thomson was honored with the Nobel prize in physics in 1906. His student Francis William Aston developed the first velocity-focusing mass spectrograph by the use of magnetic and electric fields [Asto1919]. He was awarded with the Nobel Prize in chemistry in 1922 for the investigation of the abundance of isotopes. Aston measured the masses of more than 200 nuclides reaching a relative mass precision at the order of 10^{-4} [Asto1942]. These measurements were sufficient to proof that the binding energy per nucleon is about 8 MeV for most nuclides. In parallel to further improvements of the classical mass spectrometers up to a relative precision of 10^{-7} [Duck1950, Nier1951], a new method was invented by Paul and coworkers [Paul1953, Paul1955]. They used electric multipole fields to mass separate charged particles. This linear radiofrequency mass filter is nowadays widely used for residual gas analysis and molecular studies in chemistry. The two-dimensional storage device was later extended allowing for a complete

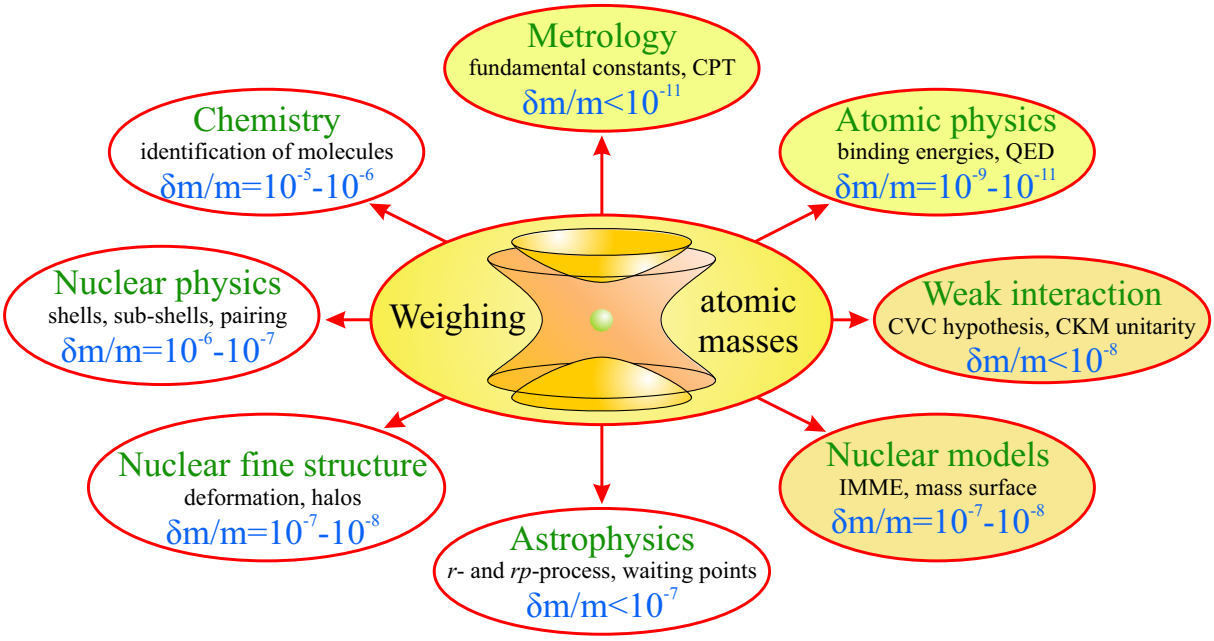

Figure 1.1: Applications of atomic masses for various research fields. The required relative uncertainties starting from general questions in chemistry at the level of $\delta m/m = 10^{-5}$ up to the determination of fundamental constants at the level of below $\delta m/m = 10^{-11}$ are included. Some special cases might even demand an order of magnitude higher mass precision. Fields from which mass measurements are presented in this work are underlayed with light brown. Light green fields mark research goals of the new Penning trap mass spectrometer introduced at the end of this thesis.

three-dimensional confinement [Paul1958, Fisc1959]. Today this device is known as a *Paul trap*. Beginning in the 1970's the study of reaction Q-values allowed routinely for mass determination at the level of 10^{-7} and better, now even for short-lived radionuclides. Since the mass resolution in Paul traps is limited by the stability of the electric fields, Paul traps are commonly used for ion beam preparation in high-precision mass mass spectrometry, but not for precise mass measurements itself. Today, another type of trap achieved the highest precision in mass measurements. The idea of this trap dates back to the 1930's when F.M. Penning used homogeneous magnetic fields for a two-dimensional confinement of charged particles [Penn1936]. A combination of an electrostatic field and a magnetic field for ion storage was developed for the first time by Pierce [Pier1949], before Hans G. Dehmelt performed his outstanding experiments and suggested the name *Penning trap*. The use of single ions in Penning trap mass spectrometry (PTMS) denoted a major progress in this field. Hans G. Dehmelt and Wolfgang Paul received for the ion trap technique the Nobel Prize in physics in 1989 [Dehm1990, Paul1990]. They shared the prize with Norman F. Ramsey, who was awarded for his invention of the separated oscillatory field technique to advance NMR experiments [Rams1990]. These three techniques, for the first time combined in one experiment, will form the fundament of this work.

Ion traps turned out to be ideal storage devices for charged particles. They are going to

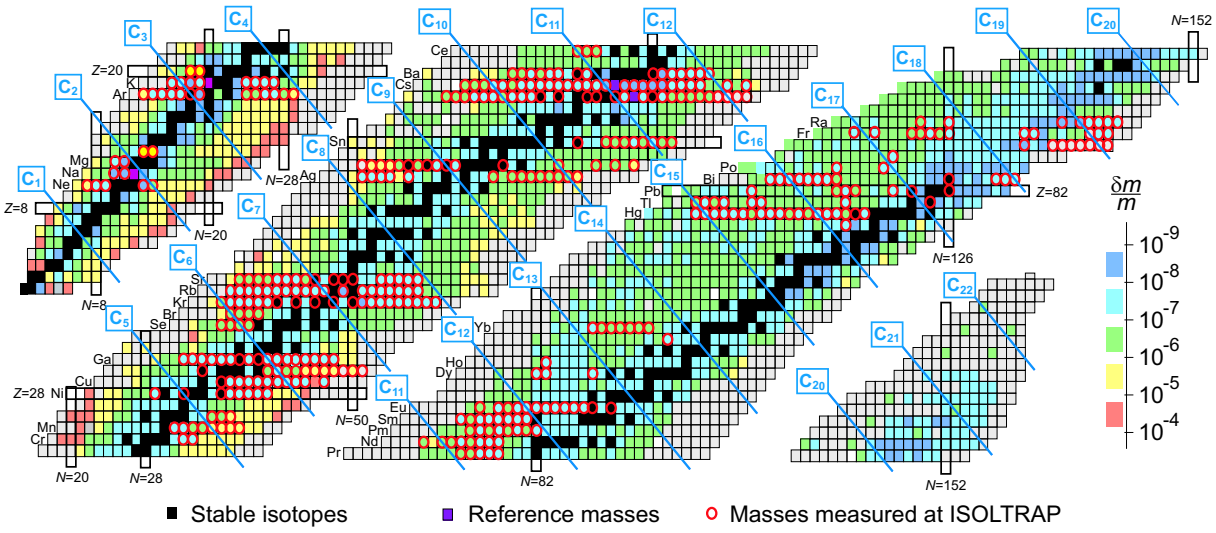

Figure 1.2: Nuclear chart with the relative mass uncertainty $\delta m/m$ of all to date known nuclides shown in a color code (see scale bottom right, stable nuclides are labeled in black). The masses of grey-shaded nuclides are estimated from systematic trends [Audi2003b]. Since the measurements presented in this thesis have been performed at the Penning trap mass spectrometer ISOLTRAP at ISOLDE/CERN [Blau2005a], all masses measured at this facility are highlighted with red circles. Furthermore, the measurements presented and discussed within this work are indicated by yellow dots with a red circle.

be employed not only for high-precision mass measurements itself, but for a multiplicity of applications such as nuclear decay studies, laser spectroscopy, magnetic moments measurements, and radioactive ion beam preparation [Boll2004, Majo2005]. Several features of ion traps offer the possibility of unique combinations of investigation methods at the border of atomic and nuclear physics: Single ions can be stored in a small volume. The storage time is in principle infinite and often only limited by the decay time of the investigated radionuclide. As it will be described extensively in the next chapter ion traps are ideally suited for the manipulation of ions. They cover the whole range from cooling and exact controlling of single ions up to bunching, cooling and cleaning of ion clouds and ion beams. The storage of single ions in vacuum reduces strongly the interaction with the environment and prevents ion-ion interactions, essentially for high-precision experiments. The unprecedented accuracy of Penning trap experiments is based on the observation of harmonic motions by means of frequency determinations, which are nowadays the most precise measurements [Häns2006]. A mass resolving power of up to $\Re = 10^7$ opens the window to studies of isobarically and even isomerically pure ion ensembles [Blau2004a]. An overview of the status of high-accuracy mass measurements with stored ions is given in the recent review article of K. Blaum [Blau2006]. The historical development is illustrated in Fig 1.3, where the relative mass uncertainty versus the year of publication represented by the nuclide ^{28}Si is shown.

With respect to the main goals of mass measurements one has to distinguish between radionuclides and stable isotopes. ISOLTRAP [Blau2003a, Mukh2008a], the pioneering experiment for high-precision mass measurements on short-lived radionuclides, allows

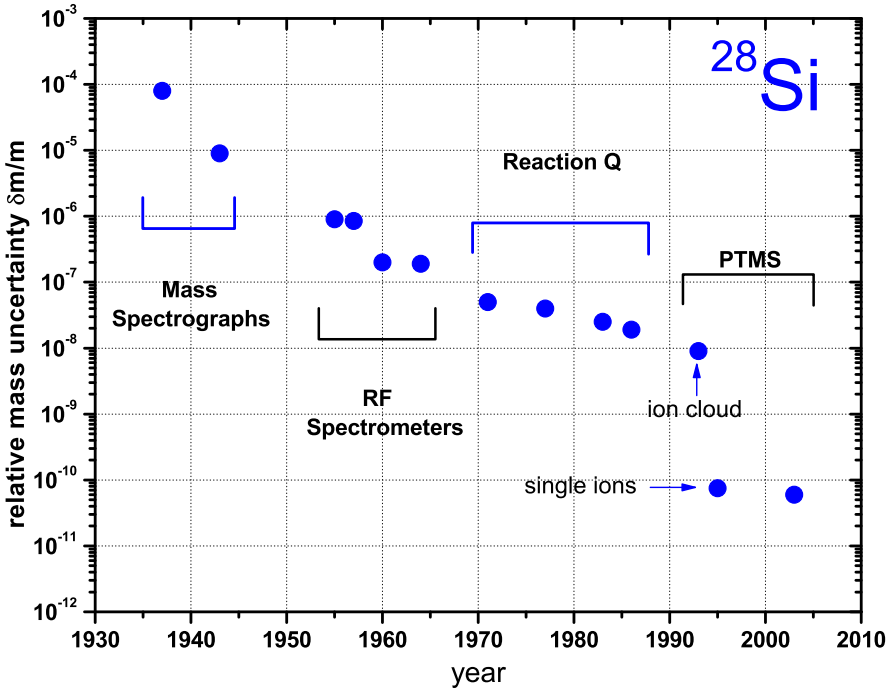

Figure 1.3: History of mass measurements displayed for the nuclide ^{28}Si. The average progress is approximately one order of magnitude in mass uncertainty per decade. Major steps have always been accompanied with the development of new mass spectrometers or the introduction of new techniques. The last big step forward came along by the use of single ion Penning trap mass spectrometry (PTMS) in the 1990s.

measurements down to a relative mass uncertainty of $\delta m/m = 8 \cdot 10^{-9}$ [Kell2003]. Since ISOLTRAP was used to perform the experiments presented within this work, the experimental setup and location will later be described in detail (see Chap. 3). Mass measurements with relative uncertainties down to a few parts in 10^{-9} allow one to address almost all questions with respect to short-lived radionuclides (see Fig. 1.1). A small overview mainly connected to the contribution of ISOLTRAP and relevant for the thesis presented, but also highlights from other PTMS facilities shall demonstrate the manifold applications of mass measurements.

Nuclear physics: The contribution of mass measurements to nuclear physics is one of the most successful stories of high-precision mass spectrometry. Extensive mass measurements along isotopic and isotonic chains have allowed to study the complex nuclear structure with its shell and sub-shell closures. Here, the differences of masses are equivalent to the nucleonic separation energies. Pairing effects become visible and shell structure studies by the determination of the two-neutron or two-proton separation energies have been performed [Guen2005, Dela2006, Guen2006]. Here, the study of proton-neutron interaction, expressed in the δV_{pn} values [Caki2005], will be in the focus of future mass measurements [Neid2009]. Information about the onset of deformation as well as halo nuclei [Geit2009] can be obtained by precise mass measurements. Extraordinary results

in this respect have recently been achieved at TITAN, a PTMS at TRIUMF, Vancouver, Canada [Ryjk2008]. In the context of nuclear structure and fine structure studies the resolution of ground and isomeric states in Penning traps was an important step forward [ISOL1992, Schw2001, Blau2004a]. A combination of mass spectrometry, resonant laser ionization, and nuclear spectroscopy was used for the first time to determine the low-energy nuclear structure of ^{70}Cu. By use of mass spectrometry the ground state ($T_{1/2}$ = 44.5 s) and the two low-lying excited states ($T_{1/2}$ = 33 s, E_{exc} = 101.1 keV) and ($T_{1/2}$ = 6.6 s, E_{exc} = 242.4 keV) were already distinguished and for the first time unambiguously identified as three beta-decaying isomers [Roos2004]. This was an unique example for the coaction of various measurement techniques from atomic and nuclear physics.

Astrophysics: The stellar nucleosynthesis [Rolf1988, Wall1997, Scha1998, Bosc2003] is one of the most studied fields in nuclear astrophysics. Reliable calculations depend on basic properties of unstable nuclei such as masses, half-lives, and cross section values. Masses of nuclides even far away from the valley of stability are important input parameters to calculate the rate and energetics of the nuclear transformations. Ultimately, the abundance and distribution of elements in the universe shall be explained. The pathway of stellar nucleosynthesis is mainly described by the following scenarios: Nuclei close to the valley of β-stability are created by the slow neutron capture *s-process*. It is expected that most of the heavy nuclei in our solar system such as uranium are produced in the explosive rapid neutron capture *r-process*. The rapid proton capture *rp-process* is responsible for the creation of nuclei close to the proton drip line. Most nuclei involved in the *s*-process are quite easy accessible at radioactive ion beam facilities and consequently extensively studied. Thus, it is believed that this process is well understood [Kaep1998]. Unfortunately, a lot of the nuclei in the *r*- and *rp*-process are far away from stability, and thus difficult to investigate. Recently, some masses of nuclides in the vicinity of the *rp*-path have been measured at the Penning trap mass spectrometer ISOLTRAP, CPT (Argonne, US), SHIPTRAP (GSI), and JYFLTRAP (Jyväskylä). Direct measurements have been performed on ^{74}Kr, which are important waiting point nuclei [Rodr2004]. Masses of the short-lived nuclei ^{21}Na and ^{22}Mg involved in the reaction ^{21}Na(p,γ)^{22}Mg serve as input parameters for nova models [Mukh2004]. Furthermore, quite a few masses have been measured at SHIPTRAP and JYFLTRAP and were published in a common article [Webe2008].

Nuclear models: Beside the investigation of nuclear structure effects like shell closures, precise mass values of radioactive nuclides can be used to test nuclear mass models and mass formulas in general [Lunn2003]. A nucleus is a many-body system involving interactions of the strong, weak, and electromagnetic forces. Thus, it is far away from being analytically describable. Instead, mass models for the prediction of the total binding energies of nuclei and mass formulas for numerical calculation of masses shall approximate the complex system. The valley of stability delivers suited set of data to test the predictive power of mass models. Mass formulas are based on a set of free parameters which have to be connected to experimental data on a local [Jänn1988] or global [Tach1988] scale. More details can be found in the review article of D. Lunney, J.M. Pearson, and

C. Thibault [Lunn2003]. One of the most powerful local mass formulas is the isobaric-multiplet mass equation (IMME) [Bene1979]. It relates the masses of the members of an isospin multiplet. The main use is the prediction of unmeasured masses at the proton drip line to determine the pathway of the *rp*-process. The accepted structure of the formula is of the quadratic form $M(T_z) = a + bT_z + cT_z^2$ with T_z being the z-projection of the isospin and a, b, c being numerical parameters. Thus, a cubic term dT_z^3 would lead to a failure of IMME. ISOLTRAP contributed with several mass measurements to stringent tests of the quadratic form of IMME [Blau2003b, Yazi2007].

Weak interaction studies: The Cabibbo-Kobayashi-Maskawa (CKM) quark-mixing matrix describes the weak interactions of quarks. The Standard Model demands the unitarity of the CKM matrix. Nevertheless, the matrix elements itself are not predicted by the Standard Model. They are determined from weak decays of the related quarks. V_{ud}, the largest matrix element, can be extracted from the Fermi coupling constant of the myon decay G_μ in connection with the vector coupling constant G_V derived from the mean $\mathcal{F}t$ value, called comparative half-life, of superallowed β-decays. According to the conserved-vector-current hypothesis (CVC) the mean $\mathcal{F}t$ value is constant, since the vector part of the weak interaction is not influenced by the strong interaction [Hard2001]. The comparative half-life depends to the fifth power on the Q-value of the superallowed transition and is thus direct accessible via mass measurements in combination with measurements of the half-life. The required relative mass uncertainty in this field is about 10^{-8} and below, which has been reached at ISOLTRAP, CPT, LEBIT, and JYFLTRAP in the determination of the decay energies of ^{22}Mg(β^+)^{22}Na [Mukh2004], ^{46}V(β^+)^{46}Ti [Sava2005], ^{38}Ca(β^+)^{38}K [Boll2006], and ^{42}Sc(β^+)^{42}Ca [Eron2006a].

Stable mass measurements: Mass measurements on stable and very long-lived nuclides at the level of better than $\delta m/m = 10^{-9}$ have a wide range of applications in physics. Up to now only five groups in Harvard [Gabr1999], at MIT [Brad1999], in Stockholm [Berg2002], in Seattle [VanD2004], and in Tallahassee [Reds2008] have reached a precision of 10^{-10} or better. Recently even a relative mass precision of about $1 \cdot 10^{-11}$ was achieved [Rain2004, Shi2005]. High-precision mass measurements at that level are used for the determination of the fine structure constant α [Brad1999, Hann2008], a new definition of the kilogram [DiFi1994, Berg2002], the provision of input data for the determination of the neutrino rest mass [Born2005, Nagy2006], and the search for neutrinoless double beta decay [Douy2001, Klap2004, Raha2008]. Furthermore, the so far most precise test of Charge, Parity, and Time Reversal (CPT) symmetry on the baryonic sector has been performed by a mass comparison of the proton and the antiproton at the level of $9 \cdot 10^{-11}$ [Gabr1999]. There are more applications for mass measurements on stable nuclids, for which relative precisions of 10^{-11} or even below are required. One of such fields is the quantum electrodynamic (QED). QED is the theory about the interaction of electric charges by photon exchange and is currently tested experimentally by X-ray spectroscopy down to 10^{-14} [Beie1998]. Thus, it is the most accurate tested theory in physics today. With mass measurements it is possible to contribute to these stringent tests of bound-state QED. Ideally suited are tests in extreme strong electrical fields, such as binding energy measurements of the last electrons in lead and uranium. Mass measure-

ments with uncertainties at the level of 2 eV, corresponding to a relative mass precision of approximately 10^{-11} are therefore required.

The presented applications and measurements cannot report the use of mass measurements in total, but a more detailed overview would go beyond the introduction of this thesis and can be found in [Blau2006]. Despite the achieved precision in mass spectrometry the nowadays available methods and experiments cannot cover all open questions. Thus, there is continuous improvement regarding the precision of mass measurements as well as the accessibility of very short-lived, exotic nuclei. Thereby the demands on measurements of radioactive and stable nuclides differ as much as the techniques developed for their investigation. On the one hand the actual routinely achieved precision of 10^{-8} for radionuclides is sufficient for almost all applications nowadays. But foreseeable is that weak interaction studies will require a mass precisions of 10^{-9} for more stringent tests of the CVC hypothesis and the CKM unitarity [Hard2005a, Hard2005b]. More challenging is the task to reach exotic nuclides, rarely produced at radioactive ion beam facilities, with half-lives of only a few milliseconds and production rates as low as a few ions per second. Therefore it is essential to develop new cooling, excitation, and detection techniques of stored charged particles as ongoing at many high-precision mass spectrometry facilities worldwide [Lunn2003, Boll2004]. On the other hand reaching a relative mass precision of 10^{-11} and below for stable and long-lived nuclides is experimentally challenging. Advanced shielding and stabilization systems for the superconducting magnets have to be developed and carefully optimized to decouple the experiment from the environment as much as possible.

This thesis reports on the application of time-separated oscillatory fields for the ion motion excitation at the triple-trap mass spectrometer ISOLTRPAP at CERN, Geneva, Switzerland. The method was invented by Norman F. Ramsey for the improvement of nuclear magnetic resonance (NMR) experiments. As mentioned, he received therefore the Nobel Prize in physics together with H.G. Dehmelt and W. Paul in 1989. After the successful offline implementation of the Ramsey technique at ISOLTRAP reported in my diploma thesis [Geor2005], the method was further improved, *e.g.* in consideration of damping effects in a Penning trap (see Chap. 4). The first online application by measuring the masses of ^{26,27}Al and ^{38,39}Ca is presented in Chap. 5. Regarding possible binding energy measurements of highly-charged ions, as mentioned above in the context of QED tests in strong fields, the new Penning trap project "PENTATRAP" has been started within this thesis. It will be the first one combining singly isolated and highly-charged ions for precise mass measurements. The project as well as the Penning trap setup including novel monitoring traps calculated, simulated, designed, and constructed as part of this thesis will be discussed in Chap. 7.

Chapter 2

Penning traps

As introduced in Chap. 1, Penning traps are nowadays the tools of choice for reaching highest precision in mass spectrometry. In this chapter, the Penning trap as a device for storage of charged particles is described in detail. Common techniques for the manipulation of the ion motion such as cooling as well as excitation are discussed in the context of this work. They establish the basis for precision frequency measurements in Penning trap mass spectrometry.

2.1 Ion confinement

A three-dimensional confinement of particles requires a potential minimum in each spatial direction. The motion of a trapped particle is desired to be harmonic, which requests confining forces that are proportional to the particles distance from the trapping center. Electric $\vec{E}$ and magnetic $\vec{B}$ fields are excellent suited for such confinement of charged particles, since they are at most sensitive to the electromagnetic force. In general, this interaction is described by the Lorentz equation

$$\vec{F} \;=\; q \cdot \left[\vec{E}(\vec{r},t) + \vec{v} \times \vec{B}(\vec{r},t)\right]. \tag{2.1}$$

Confining the particle via electric fields would imply that the mean value of the electric field with respect to time vanishes:

$$\left\langle \vec{E}(\vec{r},t) \right\rangle_t = \left\langle \vec{\nabla} \cdot \Phi(\vec{r},t) \right\rangle_t = 0. \tag{2.2}$$

Furthermore, the potential of the electrostatic field $\vec{E}(\vec{r}) \neq \vec{E}(\vec{r},t)$ has to fulfill the Laplace equation:

$$\Delta\Phi(\vec{r}) \;=\; 0. \tag{2.3}$$

Hence, with a pure electrostatic potential a full three-dimensional confinement is impossible. In principle, two concepts are available to allow the 3D storage of charged particles, the *Paul trap* [Paul1958] and the *Penning trap* [Brow1986] configuration. In the following the text focuses on the latter one, since it is the key technology used in this work.

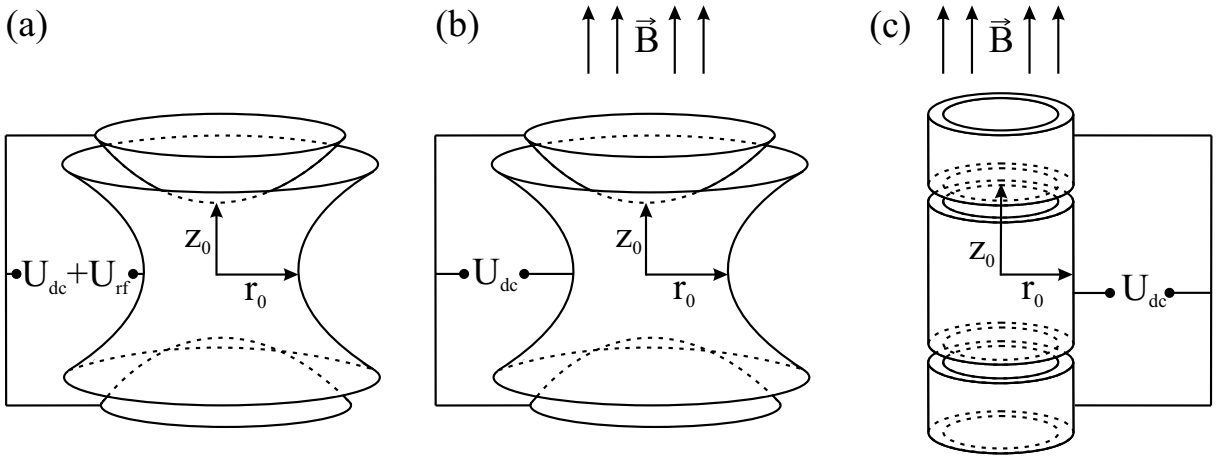

Figure 2.1: Electrode configurations of Paul (a) and Penning (b,c) traps. The electrodes are either hyperbolical (a,b) or cylindrical shape (c). A minimum of three electrodes, two end-caps and one ring, is required. Further correction electrodes to improve the quality of the trapping potential can be added. For axial ion confinement a voltage U_{dc} with a proper polarity is applied. In (a) a radiofrequency quadrupole (RFQ) field U_{rf} is added to fulfill the trapping condition. The homogeneous magnetic field B used in the Penning trap configuration (b,c) is parallel to the trap axis z.

2.1.1 The electric potential

In Fig. 2.1 typical electrode configurations used in Paul and Penning traps are shown. The traps consist in the simplest way of two end-cap electrodes and one ring electrode. In the ideal case these electrodes are infinite hyperboloids of revolution (see Fig. 2.1 (a,b)), which create a perfect axially symmetric electric quadrupole potential

$$\Phi = \frac{U_{dc}}{4d^2}(\rho^2 - 2z^2). \tag{2.4}$$

Here, U_{dc} is the potential difference between the ring end the end-cap electrodes. Such a potential is qualitatively shown in Fig. 2.2 (a). $(\rho^2 - 2z^2) = \rho_0^2$ and $(\rho^2 - 2z^2) = -z_0^2$ define the geometry of the ring electrode as well as of the end-cap electrodes, respectively. An indicator for the characteristic trap dimension is the parameter

$$d^2 = \frac{1}{2}\left(z_0^2 + \frac{r_0^2}{2}\right), \tag{2.5}$$

which is defined by the minimum axial z_0 and radial r_0 distances to the electrodes.
A second type of electrodes commonly used for Penning traps are of cylindrical shape. They offer a larger storage volume and open access from outside, *e.g.* for laser beams. Cylindrical electrodes are in general easier and more precise to machine and to align, but unfortunately lead to unwanted higher-order terms of the electric field. Nevertheless, effective ion cooling techniques confine the particles near the trap center, which allows one to neglect the higher order terms of the electric potential in a first order approximation. Thus, cylindrical Penning traps are widely used in high-precision experiments [Gabr1984].

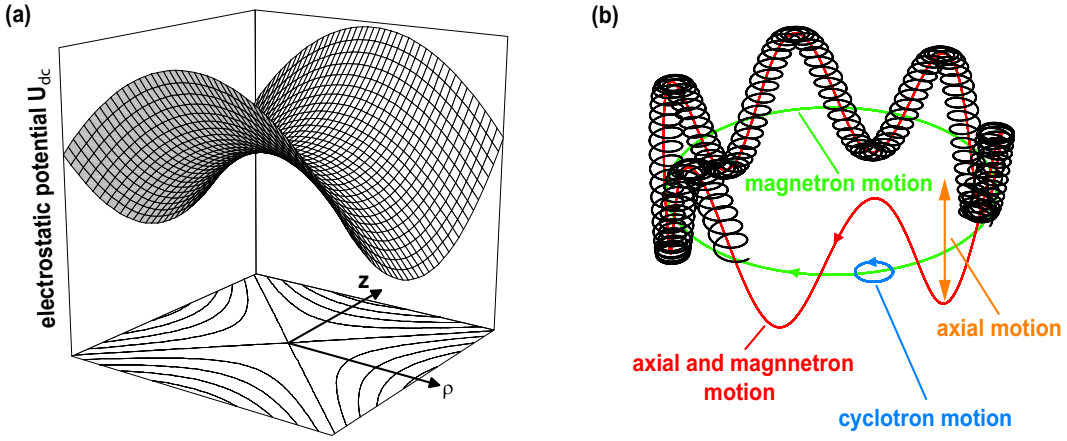

Figure 2.2: (a) Quadrupole potential as a function of the cylindrical coordinates ρ and z. The overall shape has the form of a saddle. The bottom is depicted by a projection of the equipotential lines. (b) Trajectory of a charged particle in a Penning trap (black) as a superposition of the magnetron motion with frequency ν_- (green), the cyclotron motion (blue) with modified frequency ν_+, and the axial motion ν_z (orange). The superposition of magnetron and axial motion is additionally shown (red). The figure is just qualitatively and the frequencies are not to scale.

2.1.2 Three-dimensional confinement

A superimposed radiofrequency field U_{rf} between the end-cap and ring electrodes complete the three-dimensional confinement in a Paul trap (see Fig. 2.1 (a)). This configuration is mass-dependent and the ratio of the amplitudes U_{dc} and U_{rf} control the storage conditions for a certain mass. Hence, Paul traps are suited for mass filtering ion ensembles and are routinely used in form of linear radiofrequency quadrupole structures (RFQ) to mass separate low energy ion beams. Unfortunately, the precision of a Paul trap is hampered by voltage fluctuations and thus not in use as a precision tool in mass spectrometry.
In the Penning trap configuration a strong homogeneous magnetic field $\vec{B}$ for the radial confinement is combined with an electric quadrupol field for the axial trapping (see Fig. 2.1 (b,c)). Due to the excellent temporal stability of magnetic fields, Penning traps are widely used for high-precision experiments. An extensive introduction in the physics of charged particles in a Penning trap is given in the review article by Brown and Gabrielse [Brow1986] and in the text book of Major, Gheorghe, and Werth [Majo2005]. Important issues regarding high-precision mass spectrometry shall be discussed here.

2.2 The ideal Penning trap

An ion with mass m and charge q moving in a homogeneous magnetic field $\vec{B} = \vec{B}(z)$, oriented in the z-direction, is subjected to the Lorentz force (see Eq. 2.1). As a result the velocity component v of the ion motion, which is perpendicular to the magnetic field, is bend on a circular motion around the magnetic field lines. The revolving frequency of the

Table 2.1: Eigenfrequencies of the singly-charged reference ion species used in the precision Penning trap at ISOLTRAP. The trap parameters are $B = 5.9$ T, $U_0 = 9.2$ V, $z_0 = 11.18$ mm, and $r_0 = 13$ mm.

Ion species	ν_c / Hz	ν_+ / Hz	ν_- / Hz	ν_z / Hz
^{39}K	2331416	2330338	1078	70882
^{85}Rb	1069815	1068737	1078	48002
^{133}Cs	683492	682414	1078	38357

ion is called *cyclotron* frequency

$$\nu_c = \frac{1}{2\pi} \cdot \frac{q}{m} \cdot B\,, \tag{2.6}$$

with $\omega_c = 2\pi\nu_c$. The radius of the harmonic motion is determined by conservation of momentum and energy. Still, the motion of the ion along the magnetic field is unbound. The superposition with the electric quadrupole field allows full three-dimensional confinement, but distorts the circular motion. Then, the ions' motion in all three dimensions is now described by the Newtonian equation $m\ddot{\vec{x}} = \vec{F}$:

$$\ddot{x} - \omega_c\dot{y} - \frac{1}{2}\omega_z^2 x = 0 \tag{2.7}$$

$$\ddot{y} + \omega_c\dot{x} - \frac{1}{2}\omega_z^2 y = 0 \tag{2.8}$$

$$\ddot{z} + \omega_z^2 z = 0\,. \tag{2.9}$$

The motion of the particle in the z-direction is determined only by the electrostatic potential $E_z = -U_{dc}/d^2$ of the electrodes (see Eq. 2.9) and is decoupled from the radial motion. Fulfilling the trapping condition $q \cdot U_{dc} > 0$ leads to a harmonic oscillation parallel to the z-axis. The characteristic eigenfrequency is

$$\omega_z = \sqrt{\frac{qU_{dc}}{md^2}}\,. \tag{2.10}$$

The motion in the radial plane is more complicated. To analyze it, the complex variable $u = x + iy$ is introduced [Kret1991]. The two linear differential equations (2.7, 2.8) are then reduced to the complex equation

$$\ddot{u} + i\omega_c\dot{u} - \frac{1}{2}\omega_z^2 u = 0\,. \tag{2.11}$$

Solving (2.11) with the ansatz $u = e^{-i\omega t}$ leads to the algebraic condition

$$\omega^2 - \omega_c\omega + \frac{1}{2}\omega_z^2 = 0\,. \tag{2.12}$$

The two characteristic eigenfrequencies

$$\omega_\pm = \frac{1}{2}\left(\omega_c \pm \sqrt{\omega_c^2 - 2\omega_z^2}\right)\,, \tag{2.13}$$

are called magnetron (ω_-) and modified cyclotron (ω_+) frequency, respectively. The slow magnetron or drift motion is centered at the potential minimum. On top of the drift is superimposed the cyclotron motion. The single harmonic motions as well as their superposition are shown in Fig. 2.2 (b). Important to note is that the figure is just a schematic drawing. All sizes of the radii and their frequencies are not to scale. As an example the typical frequencies in the precision trap at ISOLTRAP for three usually used reference ion species, namely ^{39}K, ^{85}Rb, ^{133}Cs, are presented in Table 2.1. Obviously from Eq. (2.13) is that for ion trapping the condition $\omega_c^2 - 2\omega_z^2 > 0$ has to be fulfilled. Combining the trapping condition with Eqs. (2.6) and (2.10) allows one to express the requirements for stable trapping in terms of the applied fields:

$$\frac{|q|}{m} B^2 > \frac{2\,|U_{dc}|}{d^2} \tag{2.14}$$

$$qU_{dc} > 0\,. \tag{2.15}$$

This determines the magnetic field strength needed to counteract the radial component of the electric field. Using the defined frequency $\omega_1 = \sqrt{\omega_c^2 - 2\omega_z^2}$ the eigenfrequencies can be be written in the form

$$\omega_+ = \frac{1}{2}\left(\omega_c + \omega_1\right) \tag{2.16}$$

and

$$\omega_- = \frac{1}{2}\left(\omega_c - \omega_1\right)\,. \tag{2.17}$$

Amplitudes and phases of the motional modes depend on the trapping fields as well as on the initial condition of the ion motion at that time when they are trapped. The characteristic trap dimension d, the trapping potential U_{dc}, and the magnetic field strength B define the boundary conditions and determine all eigenfrequencies. The position and velocity of the ion at the moment of creation or the circumstances of the injection from external sources decide the specific pathway. Amplitudes, phases, and position can be manipulated and controlled by external radiofrequency fields. This will be extensively discussed in Sec. 2.4. The radial eigenfrequencies can be expressed via the trap parameters. A serial expansion leads to the approximations

$$\omega_- \approx \frac{U_{dc}}{2d^2 B} \tag{2.18}$$

and

$$\omega_+ \approx \omega_c - \frac{U_{dc}}{2d^2 B}\,. \tag{2.19}$$

Important to note is the mass independence of the magnetron frequency (2.13) in a first order approximation (see Table 2.1). The eigenfrequencies and the characteristic cyclotron frequency obey the following order

$$\omega_- < \omega_z < \omega_+ < \omega_c\,, \tag{2.20}$$

whereas they differ by several orders of magnitude. The potential energies $-e(U_{dc}/d^2)r_\pm^2$ of the two radial motions are negative due to the potential hill in the radial plane. But

here, the positive kinetic energies of the motions are counteracting. Since $\omega_+ > \omega_-$, the total energy of the cyclotron mode is in general positive, while the magnetron motion is always negative (see Sec. 2.4). The sum of the kinetic and potential energy of each eigenmotion results in the total energy of the trapped ion [Brow1986]. Some important relations between the eigenfrequencies shall be mentioned:

$$\omega_c = \omega_+ + \omega_- \tag{2.21}$$

$$\omega_z^2 = 2\omega_+\omega_- . \tag{2.22}$$

2.3 The real Penning trap

The behavior of an ion in a real Penning trap is more complicated than it is the case for the ideal Penning trap. In reality a Penning trap deviates from the ideal trap with its pure quadrupole electric field and uniform magnetic field due to several reasons, which are discussed extensively in [Brow1986, Majo2005]. Field inhomogeneities, imperfections and misalignment of the trap, ion-ion interactions, collisions of ions with residual gas atoms or molecules as well as image charges disturb the ideal motions in the trap.

2.3.1 Electric field imperfections

The electrostatic quadrupole potential (see Eq. 2.4) in a real trap is inaccurate when unavoidable geometrical imperfections are considered. Due to practical reasons all electrodes have to be truncated at a certain point. Additional holes for injection and ejection of ions, as well as slits in the electrodes for ion manipulation purposes perturb the electric potential. Furthermore, all surfaces are only accurate within fixed production limits. Accounting for the deviations from the ideal quadrupole potential calls for a higher order multipole expansion of the trapping potential. Consequential frequency shifts for the octupole and dodecapole contributions, which are mainly depending on the amplitudes of the eigenmotions, have been calculated [Boll1990]. Especially crucial for mass measurements is the frequency shift $\Delta\omega_c^{elec}$ of the sum frequency $\omega_c = \omega_+ + \omega_-$:

$$\Delta\omega_c^{elec} = \frac{\omega_z^2}{\omega_+ - \omega_-}\left[\frac{3}{4}\frac{C_4}{z_0^2}\left(\rho_+^2 - \rho_-^2\right) + \frac{15}{8}\frac{C_6}{z_0^4}\left[3\rho_z^2\left(\rho_-^2 - \rho_+^2\right) + \left(\rho_+^4 - \rho_-^4\right)\right]\right] \tag{2.23}$$

C_4 and C_6 are higher order coefficients of the electric field. In order to cancel out the higher order terms of the quadrupole potential and thus minimize the resulting frequency shifts correction electrodes are added to the basic Penning trap configuration. As examples for real trap configurations shall serve the preparation and precision trap of ISOLTRAP (see Fig. 3.2 and 3.3). Approximating the first part of Eq. (2.23)

$$\frac{\omega_z^2}{\omega_+ - \omega_-} = \frac{2\omega_-}{1 - \frac{\omega_-}{\omega_+}} \approx \omega_- \approx \frac{U_{dc}}{2d^2B} \tag{2.24}$$

shows that further minimizing of unwanted frequency shifts can be achieved by use of a trap with large characteristic dimension d and small trapping potential U_{dc}. Furthermore, a relative deviation of the electric and magnetic field axis leads to shifts in the sum

frequency ω_c as approximated for small tinting angles $\Theta \ll 1$ and ellipticity $\epsilon \ll 1$ in [Gabr2009]:

$$\Delta\omega_c^{tilt} \approx \omega_- \left(\frac{9}{4}\Theta^2 - \frac{1}{2}\epsilon^2 \right) . \tag{2.25}$$

2.3.2 Magnetic field imperfections

Inhomogeneities and fluctuations of the magnetic field are one of the most crucial points limiting the precision in Penning trap mass spectrometry. Four main contributions shall be briefly discussed. First, due to the finite dimension of the magnetic coils, the homogeneity of the three dimensional magnetic field is limited. Second, the non-zero susceptibilities of the Penning trap materials itself as well as ferromagnetic or paramagnetic materials within a short distance of a few meters around the magnet influence the magnetic field lines. Third, the current in the superconducting coils decreases with time due to the *flux creep* phenomenon [Ande1962, Ande1964]. It describes the effect when flux lines, which are pinned to inhomogeneities of the superconducting material, jump from one pinning site to another. For modern superconducting magnets in principle logarithmic decay can be linearly approximated for time intervals up to years. Fourth, temperature and pressure fluctuations in the nitrogen and helium reservoirs of the superconducting magnet cause changes in the permeability of all materials inside the bore of the magnet and consequently disturb the magnetic-field homogeneity and strength [VanD1992]. Therefore, parts such as the vacuum chamber and the trap electrodes itself are made of oxygen free materials to reduce the permeability in general. Additional correction coils are used for stabilization, correction, and alignment of the magnetic field.
Today homogeneities of $\Delta B/B < 10^{-7}$ within one cubic centimeter and relative field stabilities of $\frac{\delta B}{\delta t}\frac{1}{B} < 17\,ppb/h$ can be achieved [VanD1999]. Frequency shifts occur if the magnetic field can be expressed in a series expansion of the even powers of the distance from the trap center [Brow1986]. Then the ion sees an average magnetic field, which depends on the amplitude of its motion. The lowest multipole term is the component β_2 and creates a frequency shift of

$$\Delta\omega_c^{magn} \approx \beta_2\omega_c \left(\rho_z^2 - \rho_-^2\right) . \tag{2.26}$$

In contradiction to the frequency shifts obtained from electric field imperfections this one depends on the cyclotron frequency of the ion. If the frequencies and motional amplitudes ρ_z and ρ_- of the different ions species are identical this frequency shift does not effect an error in the mass determination. Nevertheless, the design of the trap should account for the minimization of magnetic inhomogeneities.
Despite frequency shifts of the eigenmotions due to elecric and magnetic field imperfections and trap misalignment a special relation between the trap frequencies and the free cyclotron frequency is still valid:

$$(\omega_c)^2 = (\widetilde{\omega}_+[\Theta,\Phi,\epsilon])^2 + (\widetilde{\omega}_-[\Theta,\Phi,\epsilon])^2 + (\widetilde{\omega}_z[\Theta,\Phi,\epsilon])^2 , \tag{2.27}$$

$$\tag{2.28}$$

with distorted eigenfrequencies $\widetilde{\nu}_+ = \frac{\widetilde{\omega}_+[\Theta,\Phi,\epsilon]}{2\pi}$, $\widetilde{\nu}_- = \frac{\widetilde{\omega}_-[\Theta,\Phi,\epsilon]}{2\pi}$, and $\widetilde{\nu}_z = \frac{\widetilde{\omega}_z[\Theta,\Phi,\epsilon]}{2\pi}$. Θ and Φ are misalignment angles between the electric and magnetic fields and ϵ is a harmonic distortion factor of the electrostatic potential. The relation (2.27) is called the *Brown-Gabrielse Invariance Theorem* [Brow1982, Gabr2009].

2.3.3 Ion-ion interactions

Ideally only a single, isolated ion is stored in the trap for high-precision experiments. Additional charged particles would interact via the Coulomb force and disturb the harmonic eigenmotions resulting in a change of the frequencies. Detailed investigations of these effects in Penning traps have been performed already many years ago [Jeff1983, Gabr1993, ISOL1992]. One has to distinguish two cases. In the first one all stored ions are of the same species. Then a driving frequency acts on the q/m center of the stored ion cloud. In this scenario no frequency shift is observed [Wine1975], but the trapping potential is changed due to the space charge. The situation becomes more complicated in the case of two or more ion species with different charge-to-mass ratios stored simultaneously in the trap. With a sufficient resolving power of the Penning trap a separated resonance appears for each ion species. When the resolving power is insufficient, a single resonance is observed. The width of the obtained resonance is smaller than the expected width of a superposition of the initial resonances. The center frequencies of two separated resonances are successively approaching each other with increasing number of trapped ions, whereas both centers are shifted to lower values compared to the unperturbed resonances. The size of the shift of one species depends on the number of stored ions of the other species and vice versa. For a quantitative description the coupling of the eigenmotions due to the Coulomb force has to be considered. The procedure of frequency determination and measurement of the cyclotron resonance is described in Sec. 2.5. Until now no analytical solution for such an equation of motion has been found. Despite an insufficient analytical description observations could be confirmed by ion motion simulations of simultaneously stored particles [ISOL1992, Beck2001]. Due to the difficulties with contaminated ion ensembles it is preferable to work with clean ion clouds. Cleaning techniques for such purposes will be explained later.

2.3.4 Image charges

The oscillating ions in the trap induce image charges in the trap electrodes, which acts in turn on the ions in the trap. This causes a frequency shift of the motional frequencies. Image charge effects have already been investigated in the past [VanD1989, Port2001]. Approximating the trap as a cylindrical shell with radius a, the image charge creates an electric field:

$$\vec{E} = \frac{1}{4\pi\epsilon}\frac{qa}{(a^2-r^2)^2}\vec{r}. \tag{2.29}$$

This additional electric field shifts the frequency of the axial mode by

$$\Delta\omega_z = -\frac{1}{4\pi\epsilon}\frac{q^2}{2ma^3\omega_z}. \tag{2.30}$$

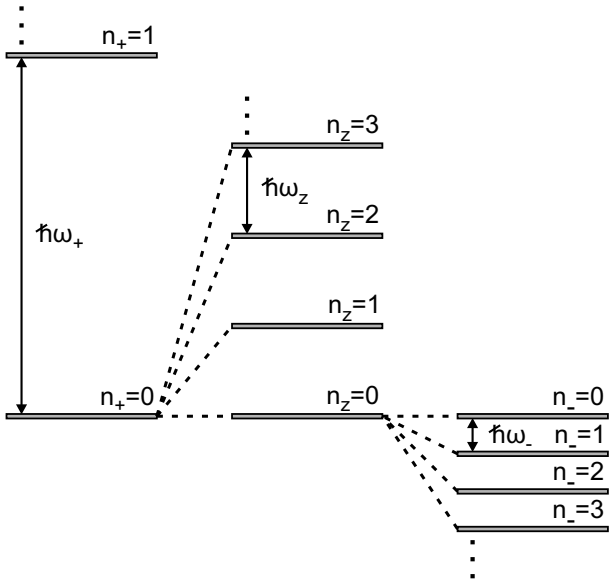

Figure 2.3: Energy level scheme of harmonic oscillators for spin-less charged particles in an ideal Penning trap. ω_+ is the modified cyclotron frequency, ω_z is the axial frequency, and ω_- is the magnetron frequency. n_+, n_z, and n_- denote the corresponding quantum numbers. The total energy is given by the sum of the energies of the three independent harmonic oscillations.

Small traps and large number of stored ions increase this shift.

2.4 Excitation of the ion motion

Controlling and manipulation of the ion motion is the key to high-precision mass measurements in Penning traps. In the ideal trap each of the three ion motions are decoupled and can be described by the simple picture of a quantized harmonic oscillator with a fixed eigenfrequency [Kret1992]. The quantum mechanical energy levels, called *Landau levels*, add up to the total energy of the system. It follows that the total energy for a stored spin-less particle is expressed by:

$$E = \hbar\omega_+\left(n_+ + \frac{1}{2}\right) + \hbar\omega_z\left(n_z + \frac{1}{2}\right) - \hbar\omega_-\left(n_- + \frac{1}{2}\right). \tag{2.31}$$

Fig. 2.3 shows the energy level scheme of the ideal Penning trap. In the center of the trap the potential energy is set to zero. The potential energy of both radial motions is a negative potential hill. The kinetic energy of the fast cyclotron motion overcomes its negative potential energy leading to a positive total energy in this motional mode. In contradiction the low kinetic energy of the slow magnetron drift is not able to compensate the negative potential energy. Thus, the contribution of the magnetron mode in Eq. (2.31) has a negative sign. Electric driving fields can be used to manipulate the ion motion. In Penning traps usually dipolar and quadrupolar fields in the plane of the specific motional mode are applied for such purposes. In the following subsections the manipulation and its applications will be discussed.

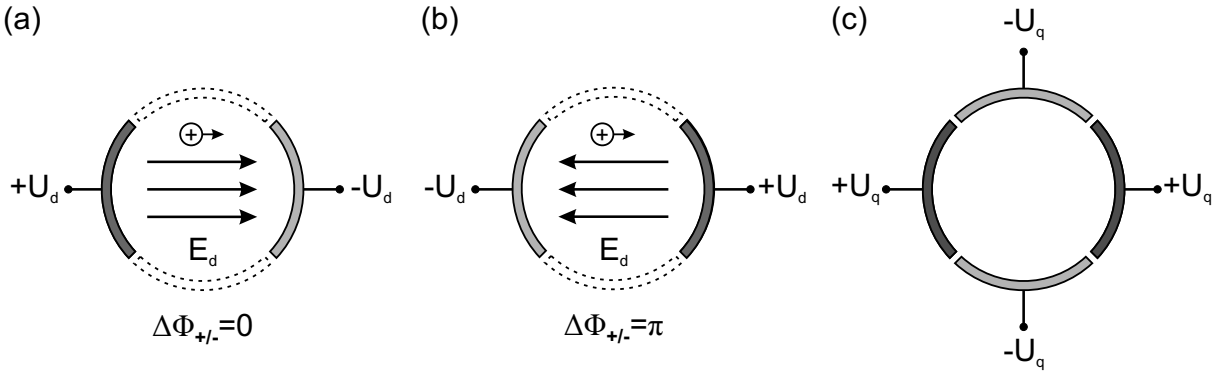

Figure 2.4: Radial segmented ring electrode (top view) of a Penning trap to apply an electromagnetic radiofrequency field. (a) Dipolar radiofrequency field between two opposite ring segments in phase with the ion motion. (b) Dipolar radiofrequency field with a phase shift of 180° compared to the ion motion. (c) A quadrupolar field can be generated by applying a radiofrequency between each opposite pairs of the four-fold segmented ring electrode.

2.4.1 Dipolar excitation

Due to the high importance of radial mode control with respect to high-precision mass spectrometry only the effect of dipolar fields on the radial modes shall be discussed in detail. The excitation of the axial mode is carried out by applying an rf field with frequency ν_z between the two end-caps. Furthermore, only the ideal Penning trap without any damping effects due to collisions of ions with rest-gas atoms/molecules shall be examined in this section. Damping effects in Penning traps will be discussed and confirmed with experimental data in Chap. 4.
A dipolar excitation of the radial motions is achieved via the application of an alternating voltage to opposite segments of a splitted ring electrode as shown in Fig. 2.4 (a,b) and is used to control the individual motional modes. Consequently, for the axial mode the alternating field is applied to the end-cap electrodes. A frequency scan with a dipolar field allows for a determination of the eigenfrequencies. Due to the mass independence of the magnetron frequency a dipolar excitation at ν_- offers the possibility to change the motional amplitude of all trapped ion species simultaneously. Since the cyclotron motion is mass dependent, a dipolar excitation at ν_+ can be used *e.g.* as a mass selective cleaning procedure to remove unwanted ion species from the trap [Sava1991]. A driving field created by an rf voltage with frequency ω_d and phase Φ_d is expressed by

$$\vec{E}(t) \;=\; (d_x\vec{e}_x + d_y\vec{e}_y)\cos(\omega_d + \Phi_d)\,. \tag{2.32}$$

The strongest parameter beside the amplitude is the phase difference between the rf driving field and the ion motion, which influences the evolution of the motional amplitudes. The phase difference $\Delta\phi_\pm = \phi_d - \phi_\pm$ of a dipolar excitation is illustrated in Fig. 2.4, where in (a) a coherent excitation with no phase difference and in (b) an excitation with a phase difference of π are shown. With no phase difference the magnetron radius (Fig. 2.5 (a)) as

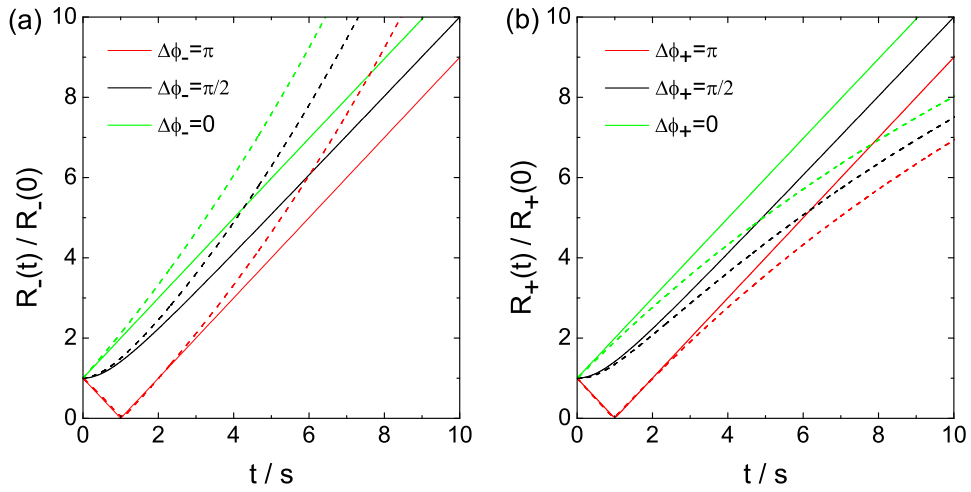

Figure 2.5: (a) Development of the normalized magnetron radius as a function of the dipolar excitation time in resonance. The solid green line shows the direct increase of the radius when there is no phase difference between the dipolar driving field and the ion motion. The solid red and black lines demonstrate the evolution with a phase difference of π and $\pi/2$, respectively. Dashed lines show the corresponding development for a damped motion (see Chap. 4). In (b) the same is shown as in (a), but for the cyclotron radius.

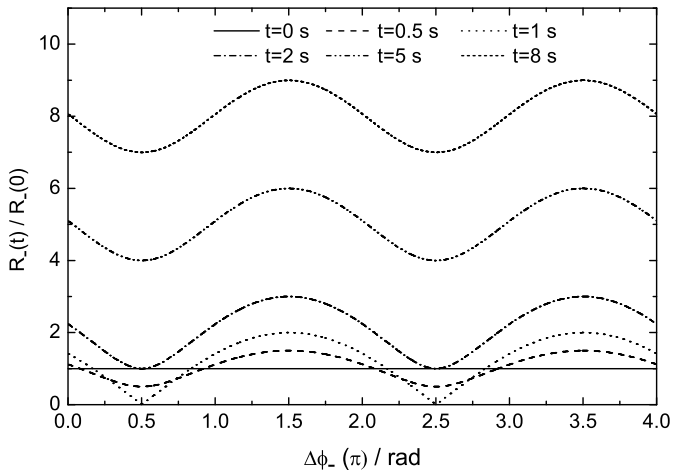

Figure 2.6: Normalized magnetron radius in dependence of the phase difference in resonance for various excitation times. The amplitude of the rf field is kept constant.

well as the cyclotron radius (Fig. 2.5 (b)) increases linear from the very beginning on, if the excitation frequency matches the specific mode frequency. When the phase difference is π the two radii decrease first before they increase again. Due to the high frequency in

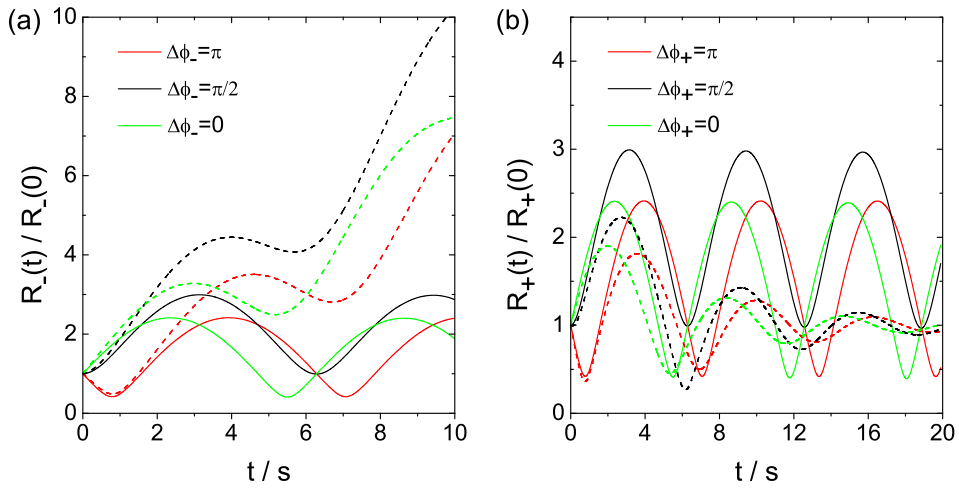

Figure 2.7: (a) Development of the normalized magnetron radius as a function of the dipolar excitation time for an off resonance excitation. The green line shows the evolution of the radius when there is no phase difference between the dipolar driving field and the ion motion. The red and black lines demonstrate the evolution with a phase difference of π and $\pi/2$, respectively. Dashed lines show the corresponding development for a damped motion (see Chap. 4). In (b) the same is shown as in (a), but for the cyclotron radius. Remarkable is the beating of the final radius between minimal and maximal radii, when the excitation is off resonance.

the cyclotron mode compared to the uncertainty in the capture time a phase locking of the cyclotron excitation can hardly be done in Penning trap experiments nowadays, but a phase locked excitation of the up to three orders of magnitude lower magnetron frequency is important for time-of-flight mass spectrometry [Blau2003a]. The final magnetron radius for a certain excitation time τ in resonance depends periodically on the initial phase difference as shown in Fig. 2.6. A dipolar excitation off resonance results in a periodic increase and decrease of the motional amplitude (see Fig 2.7). In this case there is no net effect of the driving field. The difference between maximum and minimum amplitude depends on the rf field strength.

2.4.2 Quadrupolar excitation

A quadrupolar driving field at the sum frequency of the individual eigenfrequencies (e.g. $\nu_c = \nu_- + \nu_+$) couples these two motions. This coupling creates a periodic conversion of the energy between the two modes with the beat frequency $\Omega_0 = \frac{2g}{\pi}$. g is a coupling constant. The sideband frequency measurement $\nu_c = \nu_- + \nu_+$ is a good approximation of the invariance theorem for an almost ideal Penning trap with only small distortions. Its validity for high-precision mass measurements has been theoretically derived [Gabr2009]. In case of mass spectrometry of short-lived radionuclides the coupling of the two radial

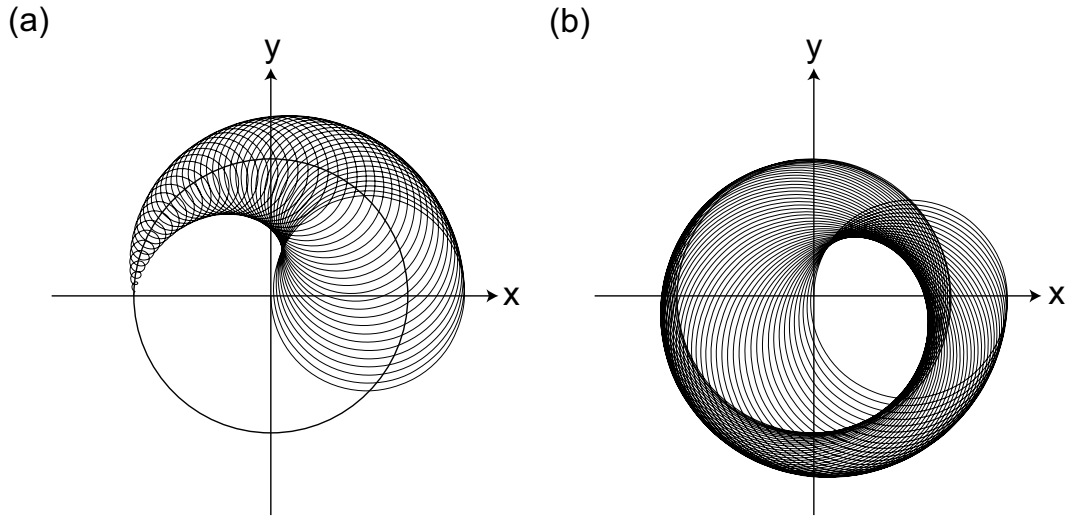

Figure 2.8: Conversion of motion from pure magnetron mode into pure cyclotron mode by applying a quadrupolar rf field at $\nu_c = \nu_+ + \nu_-$. Again the motion starts in a pure magnetron state, indicated by the solid circle. Part (a) and (b) show the first and second half of the conversion. Here, the ideal Penning trap environment without any residual gas is adopted.

modes is the most important one. First, a direct determination of the cyclotron frequency via a time-of-flight detection method is possible [Gräf1980] (see Sec. 2.5). Second, it plays an essential role for buffer-gas cooling in Penning traps (see Sec. 2.6).
For the two radial modes an azimuthal quadrupolar driving field with $\nu_q = \nu_c = \nu_+ + \nu_-$ is applied simultaneously to the opposite segments of the four-fold segmented ring electrode, as shown in Fig. 2.4 (c):

$$\vec{E_x} = C_q \cdot \cos(\omega_q t + \phi_q) \cdot y\vec{x} \tag{2.33}$$
$$\vec{E_y} = C_q \cdot \cos(\omega_q t + \phi_q) \cdot x\vec{y}\,. \tag{2.34}$$

Starting initially with pure magnetron motion a full conversion into the cyclotron mode is obtained after a certain time τ_{conv}, which depends on C_q, a constant factor including the amplitude U_q of the quadrupolar field as well as parameters of the trap geometry. Consequently, the magnetron motion disappears while the amplitude of the cyclotron motion approaches the initial magnetron radius [Boll1990]. The conversion between the two radial modes is qualitatively shown in Fig. 2.8 (a,b). The radial kinetic energy E_r is proportional to the revolving frequency of the trapped ion [Köni1995]:

$$E_r(t) \propto \omega_+^2 \rho_+^2(t) + \omega_-^2 \rho_-^2(t) \approx \omega_+^2 \rho_+^2(0)\,. \tag{2.35}$$

Since $\omega_+ \gg \omega_-$ the resonant coupling of magnetron and cyclotron mode increases the radial kinetic energy in total and consequently as well the associated magnetic moment. Out of resonance ($\omega_q \neq \omega_c$) the conversion is not complete and therefore the radial energy lower. The exact functional relation of the energy gain depends on the overall shape of the excitation signal. Usually a rectangular profile is used, where the quadrupolar excitation

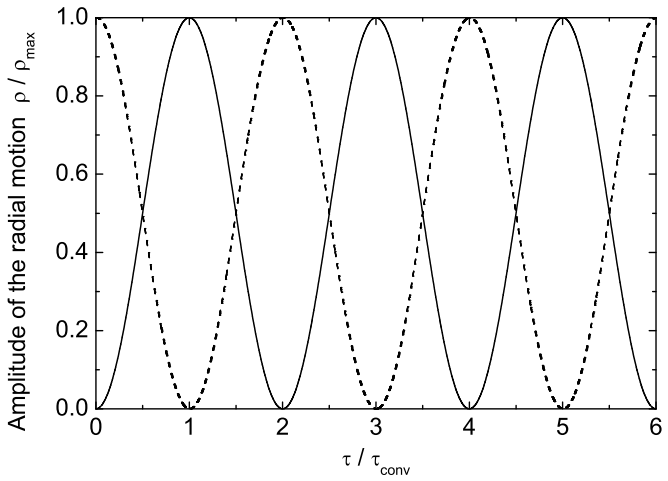

Figure 2.9: Calculated amplitudes of the radial motions. The so-called Rabi oscillations between magnetron (dashed line) and cyclotron (solid line) amplitudes as a function of the ratio τ/τ_{conv} are plotted.

is applied with a constant amplitude during the excitation intervall τ. This results in the following normalized energy gain:

$$E_r(\delta, \tau, g) \;=\; \frac{4g^2}{\omega_R^2} \cdot \sin^2 \frac{\omega_R \tau}{2}\,, \tag{2.36}$$

with the so-called Rabi-frequency $\omega_R = \sqrt{(2g)^2 + \delta^2}$. g is the coupling constant, τ the excitation time, and δ the frequency detuning between the excitation frequency ω_{rf} and the resonance frequency ω_c. The overall effect of the resonant coupling of magnetron and modified cyclotron motion is a harmonic beating between these two radial motions as depicted in Fig. 2.9 [Boll1990]. The beating frequency at resonance is half the Rabi frequency ω_R and is proportional to the amplitude of the driving field.

2.5 Frequency measurement techniques

In Penning trap mass spectrometry the cyclotron frequency is the observable to be measured. In general, two basically different measurement principles for its determination are available: a destructive and a non-destructive technique. In case of the destructive technique the information about the frequency is deduced from a time-of-flight measurement of the ions from the trap center to a particle detector. Thus, the ions are lost after a measurement and the trap has to be reloaded for further measurements. In opposition to that the non-destructive technique, which measured the image current of the particles induced in the trap electrodes, preserves the ions in the trap. A series of measurements with the same ion or ion ensemble is possible. For high-precision mass measurements of short-lived radionuclides with half-lives of below a second the destructive detection technique does

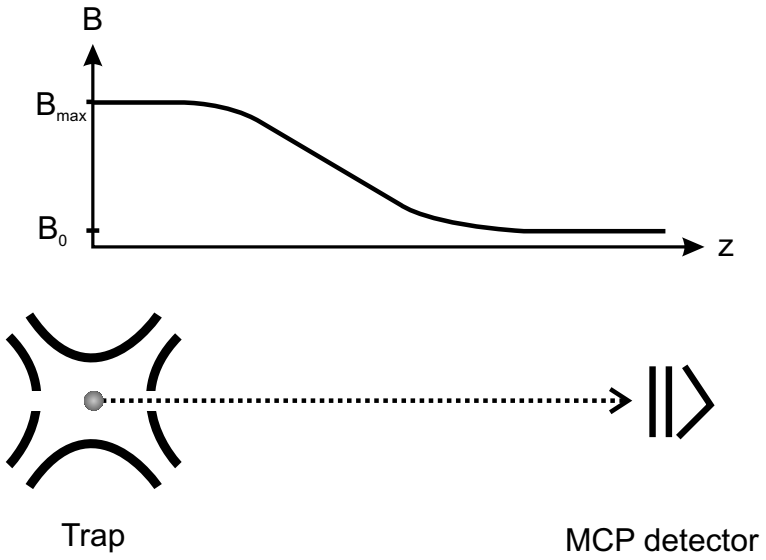

Figure 2.10: Principle of the time-of-flight cyclotron resonance detection technique. The magnetic field gradient, where the excited ion is passing through, as well as the drift from the trap to the MCP detector are shown.

not hamper the measurement procedure, since the ion would anyhow decay in a short time. As it will be seen later the advantage of destructive detection technique is the fast preparation and measurement cycle, which for the first time allows mass measurements of short-lived radionuclides. The very precise non-destructive technique is ideally suited for long-lived radioactive or stable ions, where the measurement process is not subjected to any ion losses due to a decay.

2.5.1 Time-of-flight detection technique

The time-of-flight ion cyclotron resonance (TOF-ICR) detection technique [Gräf1980] is destructive, since the ion is ejected out of the trap and detected at a particle detector outside the magnetic field. The information about the frequency is deduced from a time-of-flight measurement from the trap to the detector. Therefore, the ions are first prepared in the trap on a well-defined magnetron radius. Due to the relative low magnetron frequency in the trap the ions orbital magnetic moment $\vec{\mu}$ and subsequently the radial energy $E_r(t) \approx \omega_-^2 \rho_-^2(t)$ are small. The application of a resonant quadrupolar field with an appropriate choice of amplitude and excitation time leads to a full conversion into the cyclotron mode (see Sec. 2.4.2) with the radial energy $E_r(t) \approx \omega_+^2 \rho_+^2(t)$. The radial energy increases significantly, since the frequency is several orders of magnitude higher (see Table 2.1) while the radius remains constant. Afterwards the ions are ejected adiabatically from the trap along the magnetic field axis towards the detector. Thus, the ions are axially accelerated by the interaction of their orbital magnetic moment with the gradient of the decreasing magnetic field (see Fig. 2.10). The force is proportional to the magnetic moment and

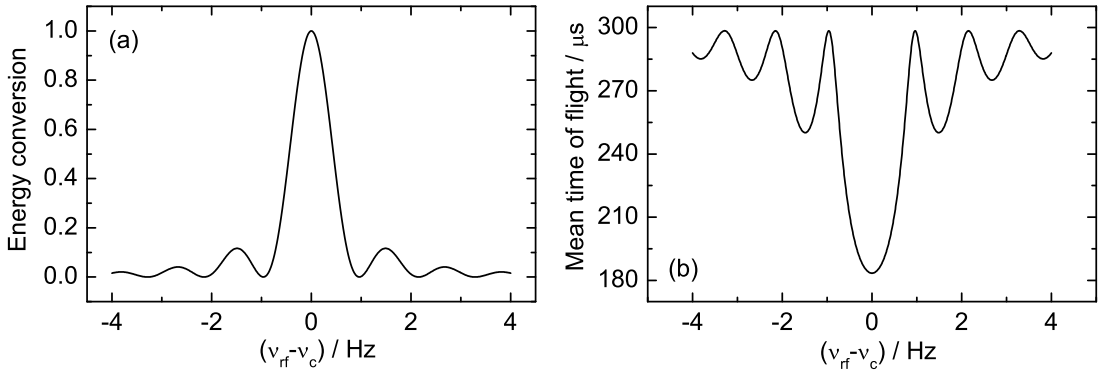

Figure 2.11: (a) Radial energy gain of the ion motion in case of a quadrupolar excitation around ω_c. The energy is normalized to its maximum. (b) Theoretical lineshape of the corresponding mean time of flight from the trap to the detector. For the calculations the dimensions of ISOLTRAP and $^{39}K^+$ as ion species were used.

hence to the radial energy:

$$\vec{F} \;=\; -\vec{\mu}(\vec{\nabla}\vec{B}) = -\frac{E_r}{B}\frac{\partial B}{\partial z}\hat{z}\,. \tag{2.37}$$

The higher the initial radial energy at the time of ejection, the shorter the time of flight to the detector. It is a non-linear function of the radial energy and can be calculated by:

$$T_{tot}(\omega_q) \;=\; \int_0^z \sqrt{\frac{m}{2(E_0 - qU(z) - \mu(\omega_q)B(z))}}dz \tag{2.38}$$

where E_0 denotes the initial axial energy of the ion, $U(z)$ and $B(z)$ the electric and magnetic potential differences, respectively. The minimum time of flight is observed for an excitation with a frequency matching exactly the free cyclotron frequency. For a non-resonant excitation the conversion is not complete. In order to determine the cyclotron frequency a series of time-of-flight measurements is done with discrete frequency steps around the adopted value of the cyclotron frequency. In this way a resonance curve of discrete points is taken. The center of the resonance is identified as the free cyclotron frequency ν_c. In Fig. 2.11 the percentage of conversion (see Eq. 2.36) (a) from pure magnetron motion to cyclotron motion and the corresponding time-of-flight resonance curve (b) are shown. As an example in Fig. 2.12 a time of flight resonance curve of $^{39}K^+$ for an excitation time of τ=900 ms is shown. The data have been taken at the Penning trap mass spectrometer ISOLTRAP. A fit of the theoretically expected line shape (2.36) to the data is added [Köni1995]. To obtain such a resonance the frequency scan is repeated several times to record a few hundred or even a few thousand ions. From all time-of-flight measurements with identical excitation frequency the mean time of flight is calculated. The inset shows two time-of-flight distributions in and off resonance, each with a few hundreds of events.

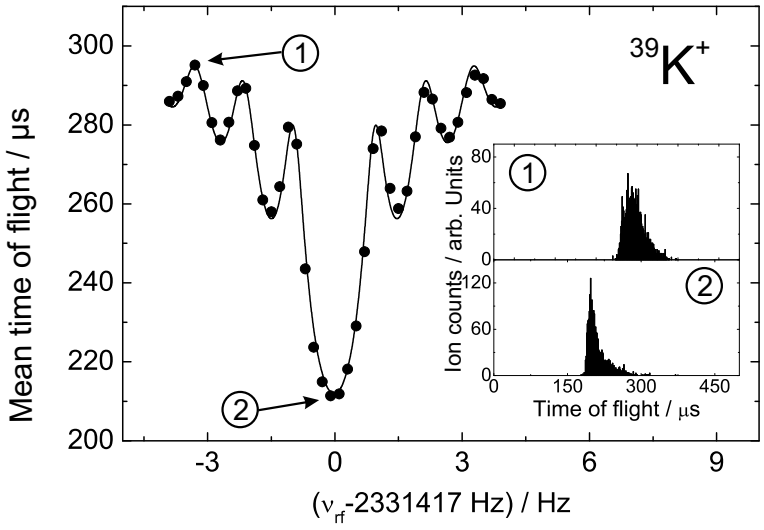

Figure 2.12: Cyclotron resonance curve of $^{39}K^{+}$ for an excitation time of τ=900 ms. A fit of the theoretically expected lineshape to the data is added [Köni1995]. The inset shows two time-of-flight distributions off and in resonance, labeled with (1) and (2), respectively.

2.5.2 Fourier-transform ion-cyclotron-resonance detection

In principle only one ion is needed for the non-destructive Fourier-transform ion cyclotron resonance (FT-ICR) detection. The measurement can be repeated as often as required with the same trapped ion as long it is not lost due to a mechanism such as a decay process or charge exchange. The technique is based on the detection of the image current induced in the trap electrodes by the motion of the trapped particle itself (see Fig. 2.13). It can be performed either with broad-band or with a narrow-band frequency detection. For high-precision mass measurements the narrow-band detection has to be chosen. The signal-to-noise-ratio is given by

$$\frac{S}{N} = \frac{\sqrt{\pi}}{2} \cdot \frac{r_{ion}}{d} \cdot \sqrt{\frac{\nu}{\Delta\nu}} \cdot \sqrt{\frac{Q}{kT \cdot C}}, \tag{2.39}$$

where r_{ion} is the radius of the ion motion and q the charge state of the ion. d is the characteristic trap dimension (see Eq. 2.5), $\nu/\Delta\nu$ the ratio of the ion frequency to the bandwidth of the spectrum, T the temperature, C the capacity, and Q the quality factor of the detection system. For single-ion detection a cryogenic environment is mandatory to detect the image current, which is for a singly-charged ion at the level of only a few femtoampere. The determination of all three eigenfrequencies offers an access to the free cyclotron frequency via the invariance theorem given in Eq. (2.27).

The advantage in comparison with the time-of-flight method is that it allows to obtain a full resonance spectrum after one experimental cycle. The disadvantage is that the minimum time required for such a measurement cycle is more than a second, which makes very exotic nuclei with half-lives in the range of some ten milliseconds unaccessible for this detection technique.

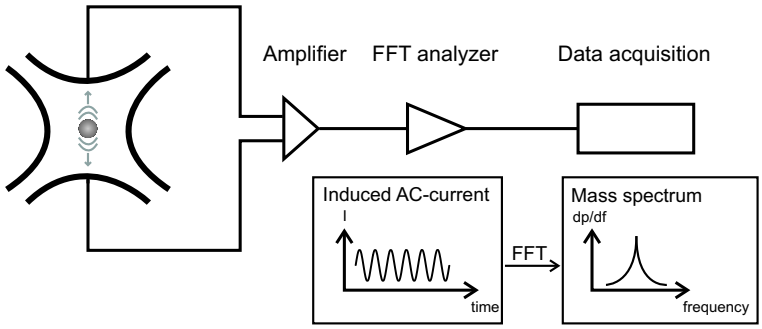

Figure 2.13: Sketch of the non-destructive Fourier-transform ion cyclotron mass spectrometry. The image current of the oscillating ion induced in the trap electrodes is first amplified and later transformed in the frequency domain to measure the eigenfrequencies.

2.6 Cooling techniques

Cooling is an important tool for the manipulation of stored ions and is in the case of the axial as well as the cyclotron mode associated with a lowering of the motional amplitude. In contrast the motional amplitude of the magnetron mode is slowly increased. Thereby the uncertainty of the ions' energy and location is reduced. Consequently, the effects of field inhomogeneities are minimized and further manipulation and transfer is simplified. Thus, the control about the ion motion is increased, when the ion is cooled to a well-defined temperature. Several cooling techniques were invented in the past, for a summary see [Majo2005]. Buffer-gas cooling, resistive cooling, electron cooling, and laser cooling are the most important techniques concerning ion traps. Within the context of this work only the buffer-gas cooling and the resistive cooling will be described in the following.

2.6.1 Buffer-gas cooling

Most common in connection with the time-of-flight measurement technique is buffer-gas cooling in Paul and Penning traps. In the presence of a buffer-gas in the trap region the ions lose kinetic energy by collisions with the buffer-gas atoms. The damping force depends on the ions velocity and can be described by a viscous drag force

$$\vec{F} \;=\; -2m\gamma\vec{v}\,, \tag{2.40}$$

where $m\vec{v}$ is the ion momentum with ion mass m and ion velocity $\vec{v}$, and γ is the damping coefficient describing the effect of the buffer-gas. With the ion mobility K_{ion} the damping constant γ can be written as

$$\gamma \;=\; \frac{q}{2m}\cdot\frac{1}{K_{ion}} = \frac{q}{2m}\cdot\frac{1}{K_0}\cdot\frac{p/p_0}{T/T_0}\,. \tag{2.41}$$

Here, q/m is the ions charge-to-mass ratio and K_0 is the reduced ion mobility referring to room temperature $T_0 = 300\,\mathrm{K}$ and atmospheric pressure $p_0 = 10^5\,\mathrm{Pa}$. Typical values for K_0 are ranging from 1 to 3 $\mathrm{cm}^2/\mathrm{Vs}$ for ions in nitrogen and from 10 to 20 $\mathrm{cm}^2/\mathrm{Vs}$ for

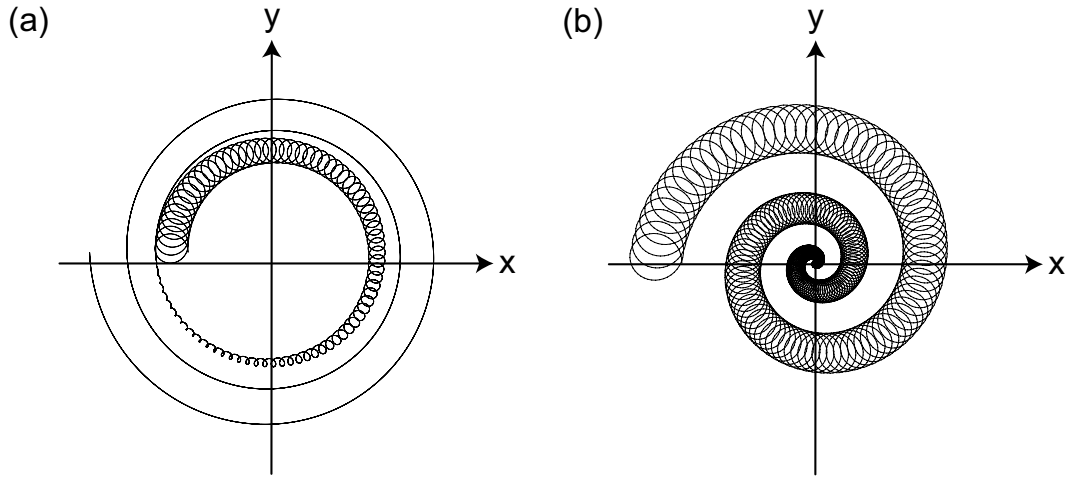

Figure 2.14: Calculated radial ion trajectories in a plane perpendicular to the magnetic field of the buffer-gas filled Penning trap. The cross marks the center of the trap. A velocity dependent damping force representing the buffer-gas cooling has been included in the equations of motion. In (a) a fast damping of the cyclotron motion and a slow increase of the magnetron motion is observed. In (b) the effect of an additional excitation with an azimuthal quadrupolar field at the resonance frequency ν_c is shown. Both, cyclotron and magnetron motions decrease and a mass-selective centering to the trap center is achieved.

ions in helium, respectively. The lower values are corresponding to heavy ions and vice versa [Moor2002].
Normally nobel gases are used as buffer-gas because of their high ionization potential and thus minimal charge-exchange losses of the ions of interest. The damping reduces the amplitudes of the reduced cyclotron motion and the axial motion, but increases the magnetron radius due to the negative potential energy of the magnetron motion. These effects are shown in Fig. 2.5 and 2.7, where the evolution of the radii with the presence of additional neutral gas are added (dashed lines). A loss of ions can be prohibited by a coupling of the magnetron motion to another proper motion via a quadrupolear driving field (see Sec. 2.4.2). Due to the relation $\omega_+ \gg \omega_-$ the reduced cyclotron motion is cooled much faster than the magnetron motion. This is demonstrated in Fig. 2.14 (a) and (b). The coupling by the quadrupolar driving field with appropriate excitation amplitude and adjusted gas pressure leads to a reduction of all amplitudes of the ion motion. If the excitation with the quadrupolar frequency ω_{rf} is in resonance with the cyclotron frequency $\omega_c = qB/m$ of the ion of interest, a mass selective centering of one specific ion species will occur [Sava1991].

2.6.2 Resistive cooling

Resistive cooling of the motional energy of the stored charged particles takes place when the trap electrodes are connected to an external circuit that is continuously kept in resonance with the eigenfrequency of the ions motion. The kinetic energy of the ions is dissipated in the resistor of the circuit via the image currents induced in the trap elec-

trodes. The ion energy is lowered down to the temperature of the resistor. Thus, it is desirable to cool the circuit down to cryogenic temperatures.
As a simple model the ion with a charge-to-mass ratio q/m oscillates between two parallel infinite plates separated by a distance l [Ghos1995]. Then the image charges induced by an ion with velocity v cause a current

$$i = \frac{qv}{l}\,. \tag{2.42}$$

This current dissipates an energy of i^2R per unit time and damps subsequently the ion motion as

$$\frac{dE}{dt} = -r \cdot i^2 = -R \cdot \frac{q^2v^2}{l^2} = -R \cdot \frac{q^2E}{ml^2} = -\frac{1}{\tau}E\,, \tag{2.43}$$

where E is the total energy of the particle. The energy evolution of a single, trapped ion shows an exponential behavior $E = E_0 \exp(-\gamma t)$. The time constant $\tau = 1/\gamma$ of the cooling process can be described by

$$\tau = \frac{ml^2}{Rq^2}\,. \tag{2.44}$$

Obviously, resistive cooling is favorable for ions with a large charge-to-mass ratio q/m. Furthermore, the time constant can be reduced by use of a large resistor R. In real traps resistive cooling is permanent present, since the voltage supply for the electrodes acts like a resistor. The long cooling times make this cooling technique inconvenient in the case of short-lived radionuclides, where most often buffer-gas cooling is applied.

Chapter 3

Experimental setup

High-precision mass measurements of short-lived radionuclides as well as extensive experimental studies of damping effects in a Penning trap are the main research projects within in this thesis. Most of the experimental data including all high-precision mass measurements have been taken at the triple trap mass spectrometer ISOLTRAP [Herf2003, Blau2005a, Mukh2008a] at the on-line mass separator ISOLDE/CERN [Kugl2000]. Thus, a detailed description of the setup and measurement procedure at ISOLTRAP is given in this chapter. Investigations of damping effects with respect to Penning trap mass spectrometry have been performed both at ISOLTRAP as well as at the double Penning trap mass spectrometer SHIPTRAP [Dill2000, Bloc2005], located at the velocity filter SHIP [Münz1979] at GSI.

3.1 The ISOLTRAP experiment

The Penning trap mass spectrometer ISOLTRAP is especially dedicated to mass measurements of short-lived radionuclides [Blau2004b, Blau2006, Mukh2008a]. More than 300 masses of radionuclides have been measured in the last 15 years. Improving both the experimental setup as well as the measurement procedure continuously pushed the systematic uncertainty down to $\delta m/m = 8 \cdot 10^{-9}$ [Kell2003] allowing us to reach routinely a relative mass uncertainty at the level of $\delta m/m \approx 1 \cdot 10^{-8}$ [Blau2003a, Blau2003b, Blau2005a]. Thereby, a resolving power of up to ten millions, enough to separate isomers [Blau2005b, Webe2005], is achieved. Furthermore, ISOLTRAP can address nuclides with half-lives down to 65 ms [Kell2004a, Kell2004b, Kell2007]. The on-line isotope separator ISOLDE [Kugl2000, Lind2003] and the present ISOLTRAP setup will be described in the following.

3.1.1 On-line isotope separator ISOLDE

The experimental study of radioactive nuclides requires their production at radioactive ion-beam facilities. Alltogether, more than 3000 nuclides can be produced at different facilities with several complementary techniques. The ISOLDE facility (see Fig. 3.1) as part of the European Organization for Nuclear Research (CERN) employs the isotope

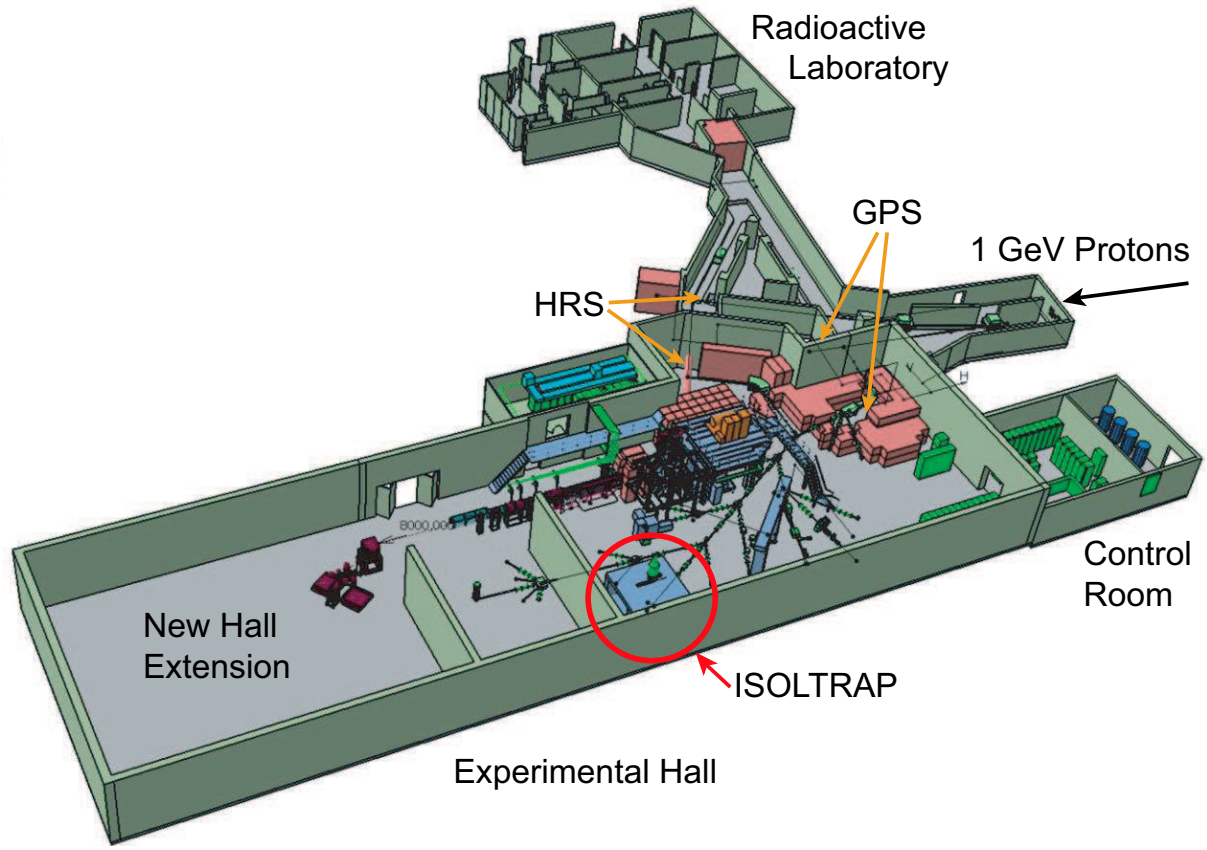

Figure 3.1: Floor plan of the ISOLDE facility including target areas, control room, and experimental hall with the new extension. The proton beam from the PS-booster enters from the upper right and is guided to the target areas. The two mass separators, the GPS and the HRS, as well as the beam distribution system in the experimental hall are shown. ISOLTRAP is installed at the central beam-line in the lower middle and extends over a three-story platform.

separation on-line (ISOL) technique [Ravn1992]. Here, protons produced via ionization of hydrogen are prepared and accelerated by a linear accelerator (LINAC) and a Proton-Synchrotron-Booster (PSB) to an energy of 1-1.4 GeV. Proton pulses with up to $3 \cdot 10^{13}$ protons per pulse ($\widehat{=} 5\mu$A average beam current) impinge on a thick target. The radioactive nuclides are produced through fragmentation, spallation, and fission reactions within the target. Depending on the desired radioactive species, different target materials, such as calcium oxide or uranium carbide, are used. The produced nuclei are stopped in a target matrix or solid catcher. To release the nuclei from the target the matrix is heated in some cases above 2000 K. Thus, the reaction products evaporate and diffuse out of the target towards an ion source.

Three different types of ion sources are available: Surface ionization, plasma ionization and resonant laser ionization [Köst2003] take advantage of physical and chemical properties of the different species to efficiently ionize the desired nuclide and heavily suppress all unwanted contaminants. Not all isotopes of the nuclear chart can be produced with the

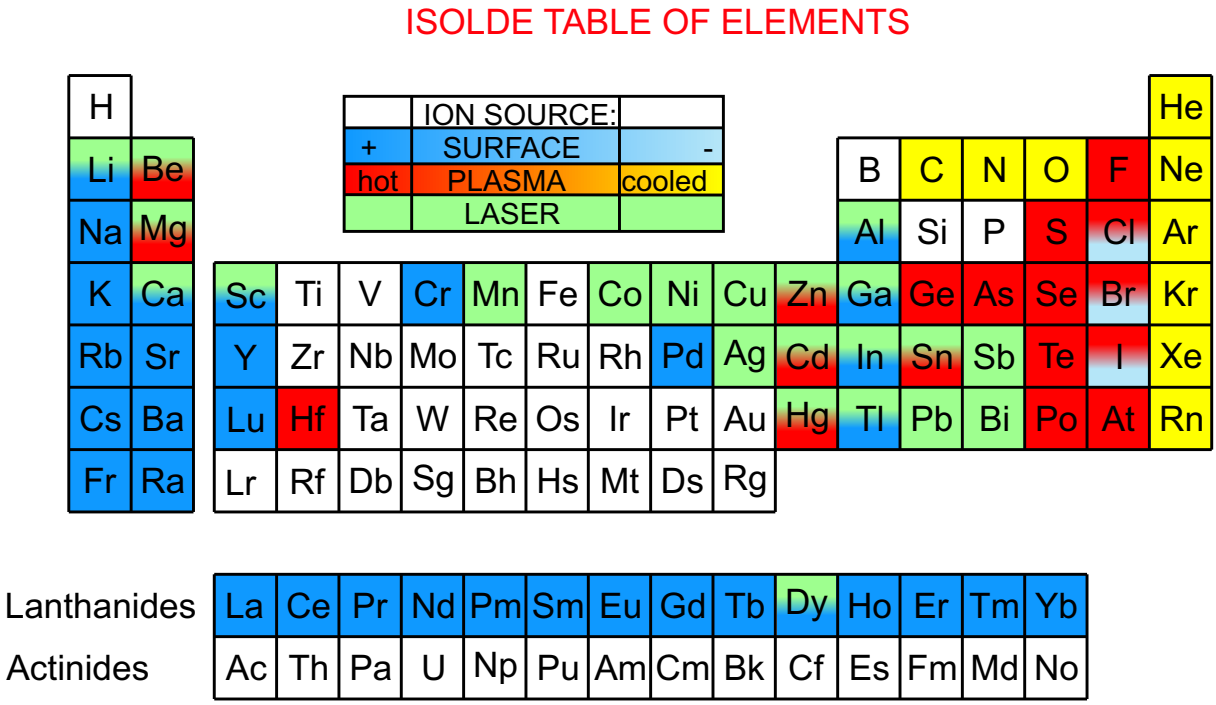

Figure 3.2: Color coded periodic table of available elements at ISOLDE/CERN and the corresponding type of ion source (see http://isolde.web.cern.ch/ISOLDE/).

ISOL technique, e.g. refractory elements are suppressed due to their long release time. At ISOLDE more than 70 elements and about 1100 isotopes ranging from He (Z=2) to Actinium (Z=89) with half-lives down to a few milliseconds are available. The obtained yield varies from a few ions per second up to a few ten nA. In the periodic table of Fig. 3.2 the accessible elements at ISOLDE as well as the specific type of ionization are shown. After extraction from the ion source the usually singly-charged ions are accelerated to 60 keV kinetic energy and sent through magnetic mass separators. Two separators, the general-purpose separator (GPS) with a resolving power of $R = m/\Delta m \approx 1000$ and the high-resolution separator (HRS) with R up to 6000 are therefor available [Kugl2000]. In the experimental area of ISOLDE the ion-beam is distributed to the various experiments by an electrostatic beam-line system.

3.1.2 Experimental setup of ISOLTRAP

The setup of ISOLTRAP, shown in Fig. 3.3, consists of three main parts relying on ion traps. The first part (a) is a linear gas-filled radio-frequency quadrupole (RFQ) trap placed on a high-voltage platform adapted to the acceleration voltage of the ISOLDE ion source. Thus, the continuous ISOLDE ion-beam is decelerated and captured in the RFQ. It is meant for accumulation, bunching, and cooling of the ion-beam [Herf2001a, Herf2001b, Kell2001]. A detailed sketch of the RFQ is shown in Fig. 3.4. The injection electrode decelerates the ions and focuses them through the 6-mm entrance opening. Their remaining radial and longitudinal energies are efficiently and fast damped in collisions with

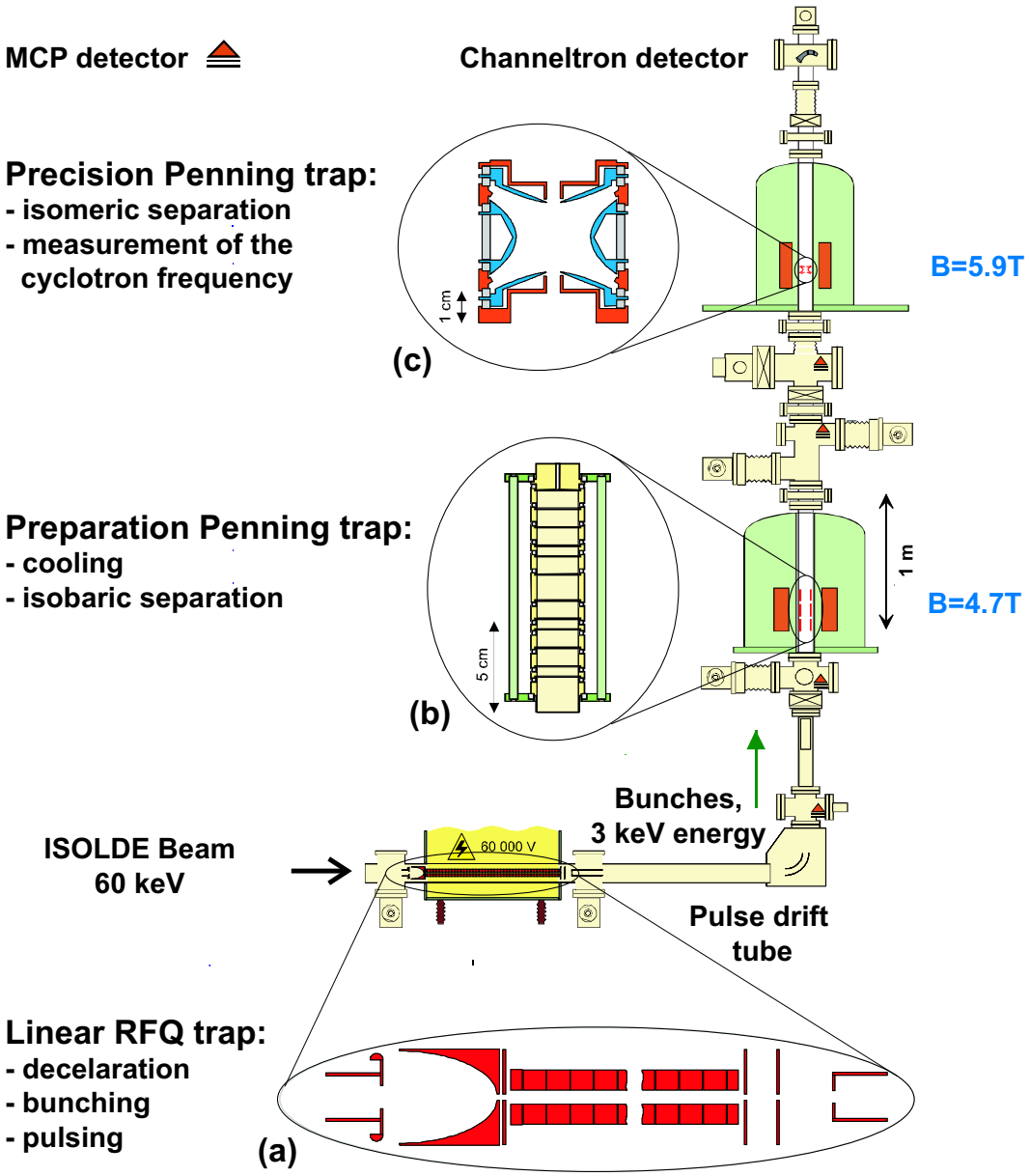

Figure 3.3: Schematic layout of the ISOLTRAP experiment. The main components are a radiofrequency quadrupole trap (a) for ion-beam cooling and bunching, a preparation Penning trap (b) for isobaric cleaning and further cooling of the radioactive ion ensemble, and a 5.9-T Penning trap mass spectrometer (c). Micro-channel-plate (MCP) detectors are used to monitor the ion transfer. Measurements of the time-of-flight cyclotron resonance for the determination of the cyclotron frequency are performed with a high-efficient channeltron detector [Yazi2006].

buffer-gas. For this purpose typically helium with a purity of 5.9 is used. An axial DC field applied to the segmented rods of the RFQ, whose potential has a minimum near the end of the exit side, allows the three-dimensional confinement. After a cooling and accumulation time of a few (5-10) ms (see also Fig. 3.7), the axial potential is lowered towards the exit orifice. Thereby, the ion bunch is ejected with a temporal width of less

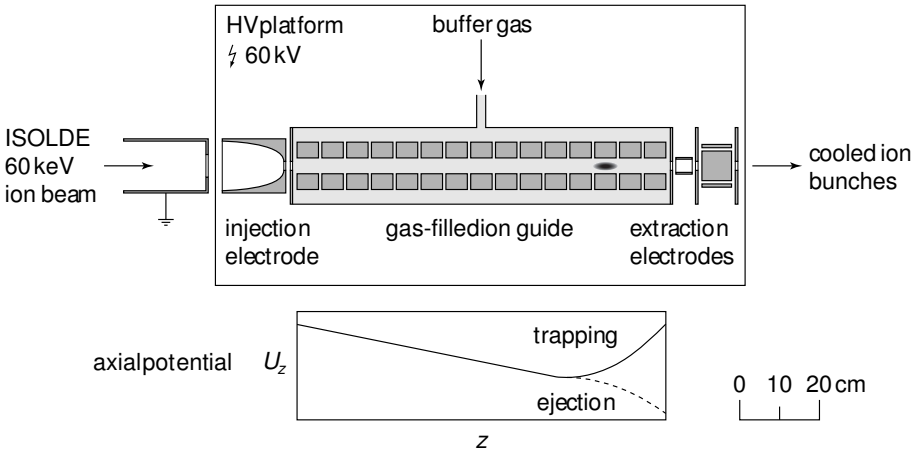

Figure 3.4: The upper figure shows a sketch of the 26-fold segmented RFQ trap at ISOLTRAP [Herf2001a]. Below the corresponding axial voltage for trapping and ejection is plotted. The continuous ion-beam is decelerated by placing the whole setup close to 60 keV. In the radial plane the ions are confined in the pseudo-potential well of the radiofrequency quadrupole field. Usually helium as buffer-gas is used to lower the ions kinetic energy in the ion guide by collisions. The ions are accumulated in the axial potential minimum at the end of the RFQ structure provided by the segmented rods. Via extraction electrodes and lenses the ion clouds are ejected to the first Penning trap.

than 1 μs at a beam emmitance of $< 10\pi$ mm mrad and passed through a pulsed drift tube in which the energy of the ion cloud is lowered from initially 60 keV to approximately 2.7 keV.

For injection into the first Penning trap in the vertical part of the setup the energy of the ion cloud has to be further reduced to only a few hundred eV. To this end, a second pulsed drift tube is used. This preparation Penning trap (b), second main part of the experiment, is a gas-filled cylindrical trap placed in a superconducting magnet with 4.7-T field strength. The ion bunch is captured in flight, further cooled, and purified by a mass-selective buffer-gas-assisted cooling [Sava1991]. A resolving power of up to 10^5 can be obtained. The preparation Penning trap ensures optimal and reproducible starting conditions for a later frequency determination. A detailed sketch of this trap and its potential distribution is shown in Fig. 3.5.

After the transfer to the third main part (c), a precision hyperbolical Penning trap [Boll1996] installed in a 5.9-T superconducting magnet, the ion cyclotron frequency ν_c is determined by a time-of-flight cyclotron-resonance detection technique (see Chap. 3) [Gräf1980]. The precision Penning trap is designed to have minimal electric and magnetic field inhomogeneities and is operated under vacuum conditions of typically 10^{-9} mbar. A resolving power of up to ten millions, depending on the excitation time of the quadrupolar driving field, can be achieved. This even allows to resolve and isolate excited nuclear states (see Chap. 4), so called isomers [Schw2001, Blau2004a]. A detailed sketch of the precision Penning trap is shown in Fig. 3.6.

Another important part of the ISOLTRAP setup not yet discussed is the reference ion

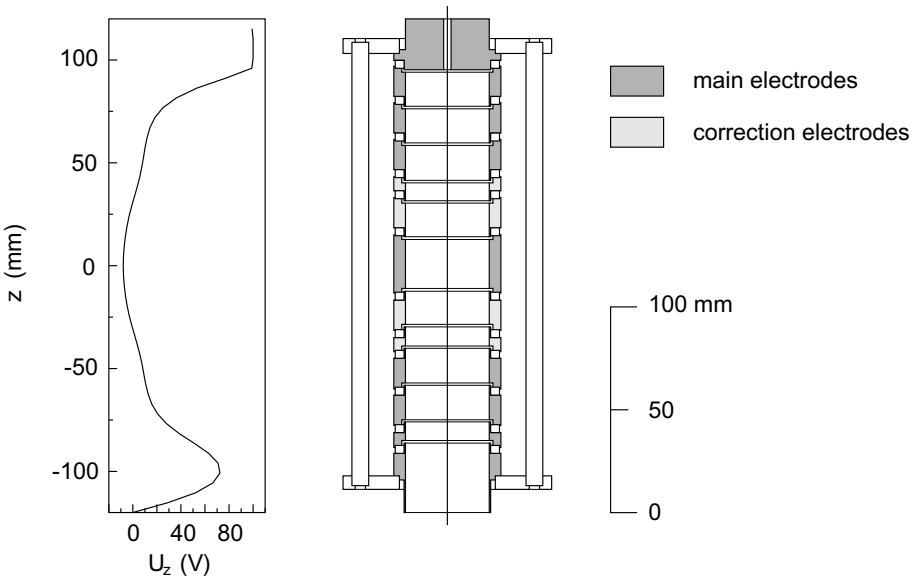

Figure 3.5: Detailed sketch of the cylindrical preparation Penning trap at ISOLTRAP [Raim1997]. The graph on the left shows the potential on axis which results from the voltages applied to the cylinder segments. A harmonic potential is created around $z = 0$ whereas the extended potential well is used for efficient capturing of injected ions. Similar to the RFQ trap helium gas is used in the preparation trap for mass-selective buffer-gas cooling (see Chap. 2). An eight-fold segmented ring electrode allow the manipulation of the ion motion by inducing dipolar and quadrupolar electrical driving fields.

source, which delivers the alkali ion species $^{39}K^+$, $^{85}Rb^+$, $^{87}Rb^+$, and $^{133}Cs^+$ for calibration purposes. They are produced via surface ionization. Except for ^{39}K, their masses have been measured with relative uncertainties at the 10^{-10} level [Brad1999]. For reference measurements the ions from the source, placed on the same high-voltage as the RFQ, are injected as short ion bunches into the RFQ, instead of the continuous ISOLDE ion beam. A timing scheme of the complete preparation procedure and measurement cycle is described in the next section. The mass determination including reference measurements is explained in Chap. 5, where actual mass measurements and the data evaluation are presented and discussed. One of the most important technical improvements at ISOLTRAP in the past years is the implementation of a carbon cluster reference ion source [Blau2002, Kell2003]. The carbon clusters are produced via laser-induced fragmentation and ionization either of a C_{60} sample or of a sigradur pellet. Carbon clusters allow an absolute mass measurement, since they have masses that are exact multiples of the unified atomic mass unit u [Qui1998].

3.1.3 Timing of the measurement cycle

The experimental procedure at ISOLTRAP is computer controlled by a LabVIEW based control system. Ion transport and preparation as well as the mass measurement itself

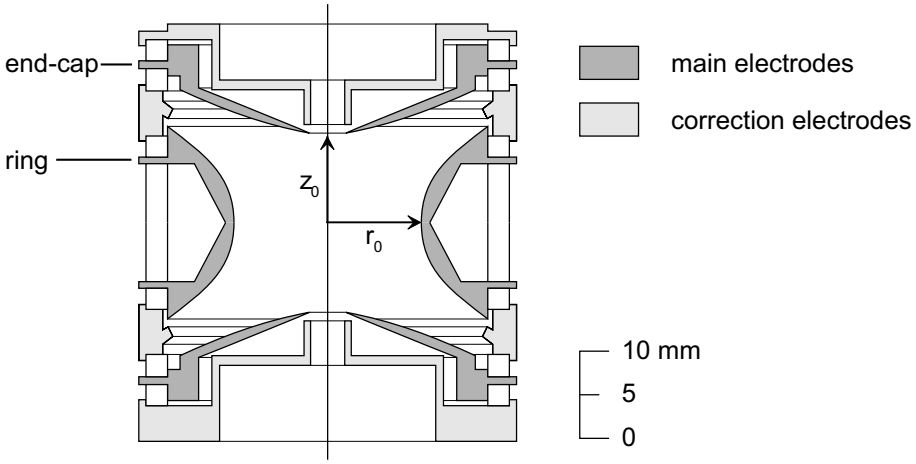

Figure 3.6: Schematic view of the hyperbolical precision Penning trap at ISOLTRAP with an inner diameter of $\rho_0 = 13$ mm and a distance from the center to the end-caps of $z_0 = 11.18$ mm. The correction electrodes (light gray) are designed such that deviations from the ideal quadrupole field are minimized [Boll1996]. Similar to the preparation trap is the ring electrode four-fold segmented allowing ion manipulation by electrical driving fields.

is triggered by a sequence of timings from a FPGA (Field Programmable Gate Array) card from National Instruments. A detailed timing diagram of the total measurement cycle including excitation times, waiting periods, and delay times is shown in Fig. 3.7. Two possibilities are typically used to start the measurement cycle. On the one hand the cycle is triggered by the proton impact (time step (1) in Fig. 3.7) on the ISOLDE target. The delay time between the ion production and capturing in the RFQ can be adjusted to the release properties and ionization process of the ion species in order to obtain a maximum yield (2). On the other hand the experiment start can be triggered by an artificial trigger from a frequency generator. This so called pseudo-proton trigger is mainly used for off-line test measurements or reference measurements with ions from the stable surface ion source. After the ions are trapped and bunched in the RFQ-trap (3) they are guided through the two pulsed drift tubes to the first Penning trap, which has already been introduced as the gas-filled cylindrical Penning trap. The ion extraction out of the buncher (4) as well as the energy reduction in the two pulsed cavities (5) are realized via a lowering of electrostatic potentials. The reduction of this potential lasts only a few μs and is controlled by three delay times, which are a function of the mass of the ions under investigation. In the preparation trap the first manipulation of a specific ion species takes place.

The capturing of the ions in the first Penning trap is controlled via a delay time with respect to the buncher ejection (6). All following time periods are not fixed and may vary for different ion species and for different required resolving powers. First, the ions remain in absence of external driving fields in the trap for usually 20 ms (7). During this time the ions' axial motion is cooled and they accumulate in the small potential minimum. Subsequently, a dipolar excitation at the magnetron frequency ν_- is applied to the ring

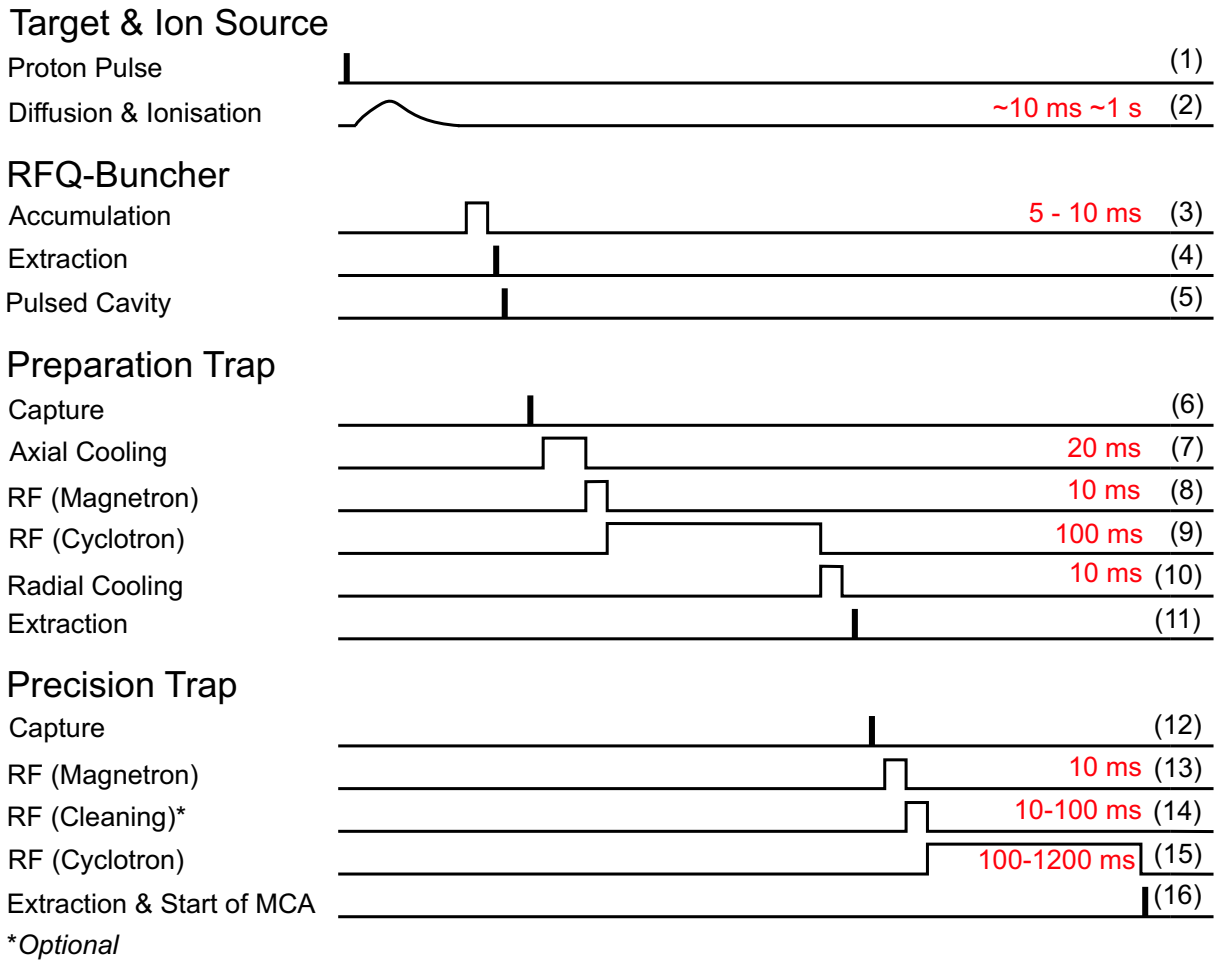

Figure 3.7: Timing diagram of the total measurement cycle. The scheme gives an chronological overview of the preparation and measurement process at ISOLTRAP and shows the timings of the individual steps of the experiment. The given time periods can vary depending on the nuclide under investigation. For more details see text.

electrode for about 10 ms (8). This mass-independent frequency enables the excitation of all ions simultaneously. Thereby, the ions' magnetron radius is enlarged to a size bigger than the exit hole in the end-cap of the trap. Afterwards the mass-dependent cyclotron frequency ν_c is applied for 100 ms (9) to cause a mass-selective centering by collisions with buffer-gas atoms (see Chap. 2). Due to the coupling of the magnetron mode and the cyclotron mode (see Chap. 2) the motion of the ions of interest is converted from pure magnetron motion into modified cyclotron motion. Since the cyclotron frequency is much higher this motion is damped faster than the magnetron motion and the motional radius shrinks towards the center of the trap. Depending on the buffer-gas pressure, the cyclotron-cooling time, and the amplitude of the quadrupolar radiofrequency field, a resolving power of up to 10^5 can be reached. A further waiting period of a few 10 ms (10) provides an additional cooling and centering. Thus, an isobaric clean ion cloud with well-defined staring conditions can be transferred from the preparation to the precision

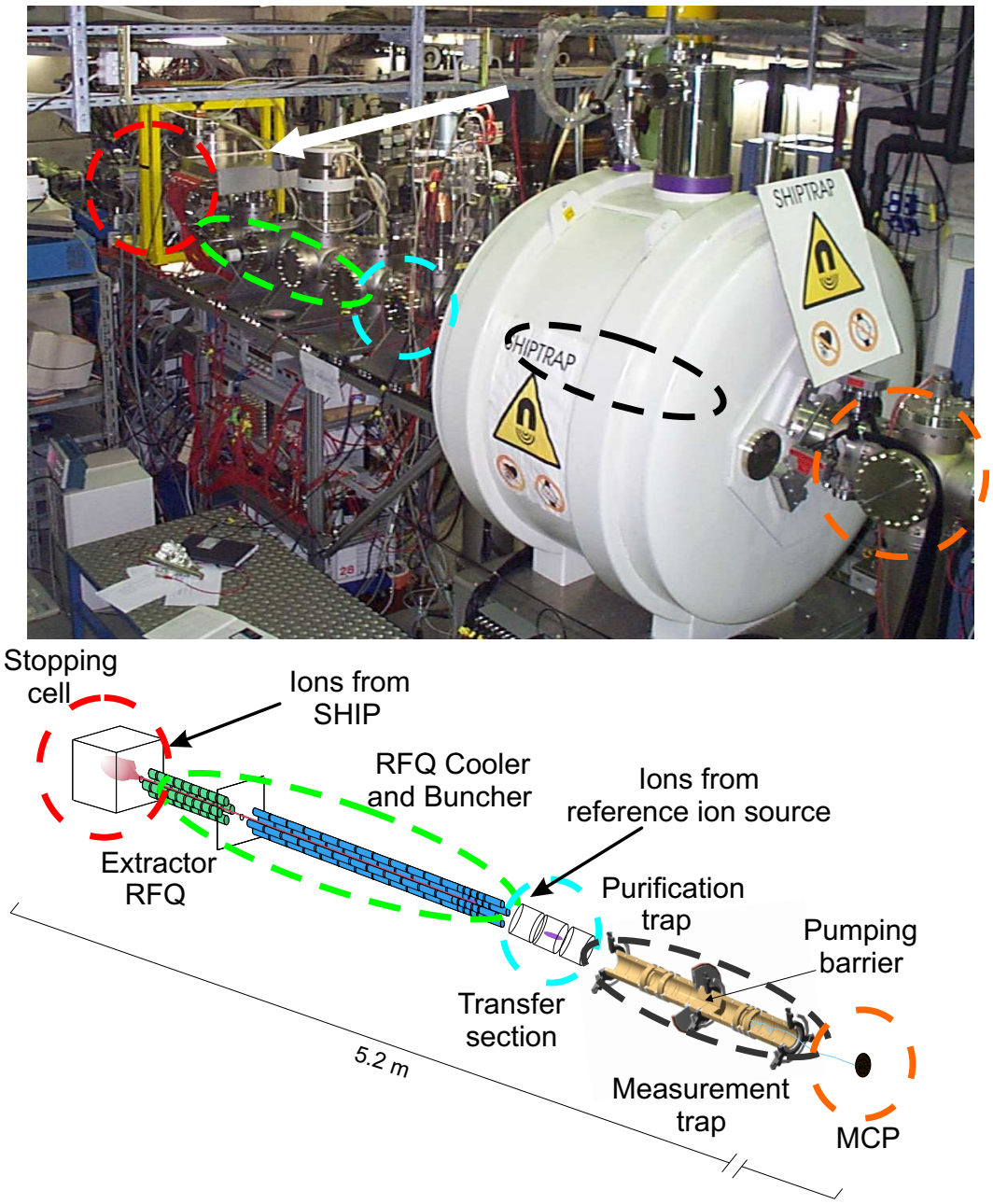

Figure 3.8: Overview of the SHIPTRAP setup at GSI/Darmstadt. Ions from the velocity filter SHIP are stopped in the gas cell, extracted by an extraction RFQ, and guided into the RFQ cooler and buncher. A low emittance bunch of ions is then transferred to the double Penning-trap system for further ion manipulation and the actual mass determination. Complementary, ions from the off-line surface ion source can be injected into setup after the second RFQ.

Penning trap (time steps 11 and 12).

The timing scheme of the precision trap starts with the capturing of the ions by changing the potential of the lower end-cap (12). The capture timing is a crucial parameter, since it defines the initial axial energy of the ions in the trap [Mari2008]. After trapping the

magnetron radius of all ions is increased analogous to the procedure in the preparation trap via a dipolar excitation at the magnetron frequency for 10 ms (13). If required, there is the possibility to remove remaining isobaric or even isomeric contaminations via mass-selective dipolar excitation at the reduced cyclotron frequency (14). Up to three different unwanted ion species can be removed simultaneously from the precision trap. Afterwards a quadrupolar excitation at a frequency near ν_c takes place with a duration between 100 ms and a few seconds (15) depending on the half-life of the ion under investigation and the resolving power $\Delta_\nu \propto \frac{1}{T_{rf}}$ and precision which should be achieved. After the cyclotron excitation the ions are ejected by ramping down the end-cap voltage (16) and their time of flight from the trap to the channeltron detector on top of the experiment (see Fig. 3.3) is measured. The frequency determination is performed by repeating the total timing sequence and varying the quadrupolar excitation frequency (time step (15) in Fig. 3.7) around the expected cyclotron frequency ν_c. All timings can be chosen with a precision of approximately 100 ns. They are synchronized to the start of the magnetron excitation in the upper trap (13). Thus, the magnetron mode can be excited in a phase-locked mode [Blau2003b]. A detailed description of this time-of-flight cyclotron resonance detection technique [Gräf1980, Köni1995] is given in Chap. 2.

3.2 The SHIPTRAP experiment

The SHIPTRAP experiment [Dill2000, Bloc2005], located at the velocity filter SHIP/GSI [Münz1979], is similar to ISOLTRAP a Penning trap mass spectrometer. It is dedicated to the study of fundamental properties of transactinides and superheavy nuclides. Of particular interest are investigations of transuranium species, which are not accessible at ISOL- or fragmentation facilities [Dill2001]. The reactions products from SHIP are delivered with 100 keV to the SHIPTRAP experiment. They are stopped in the first part of the experiment, a gas stopping cell [Neum2006] (see Fig. 3.8). From there the ions are extracted by electric fields. A first RFQ precools the ions and transfers them to an ion-beam cooler and buncher, itself a RFQ structure [Rodr2003]. Within a few ms the ions are cooled and subsequently ejected as an ion bunch of low emittance allowing for an efficient and well-defined injection into the Penning trap system [Sikl2003]. It consist of two cylindrical Penning traps in the same superconducting magnet of 7 T field strength. The first trap is used for isobaric separation and further cooling to provide well-known starting conditions for the precision trap. This trap is meant for high-precision mass measurements by use of the TOF-ICR technique. A stable alkali reference ion source is available for off-line tests and reference measurements. The ions from the off-line ion source are directly injected into the preparation trap. Within this thesis only off-line tests with the ion species ^{85}Rb and ^{133}Cs have been performed at SHIPTRAP.

Chapter 4

Damping effects in a Penning trap

In Chap. 2 the two important frequency measurement techniques in Penning trap mass spectrometry, TOF-ICR [Gräf1980] and FT-ICR [Comi1974, Comi1996], have been introduced. In the context of mass measurements and basic investigations presented in this work the TOF-ICR detection technique is of special importance, since both on-line Penning trap facilities ISOLTRAP as well as SHIPTRAP are so far using only this technique to determine the cyclotron frequency of the stored ions. Therefore, a resonance curve in the frequency domain is recorded, whose minimum can be identified with the desired free cyclotron frequency. To be able to extract this frequency very precisely it is indispensable to know the exact line shape of the resonance. The line shape depends on the excitation profile of the rf driving field. Primarily, a single, rectangular pulse of rf radiation was used to excite ion motion. Meanwhile line shapes for various excitation schemes have been calculated [Kret2007], discussed regarding their advantages, and experimentally tested within my diploma thesis and partly within in the work presented here [Geor2005, Geor2007a, Geor2007b]. Solely the Ramsey-type two-pulse excitation beside the conventional single pulse excitation (see Fig. 4.1) is discussed in this thesis, since the investigation in my diploma thesis pointed out that an excitation scheme with two pulses is most advantageous in respect to the precision of the derived cyclotron frequency. At that time only the ideal Penning trap neglecting any damping force due to rest gas atoms and molecules has been treated. Here, an extension accounting for damping effects due to ion collisions with residual gas atoms has been performed and experimentally proven.

4.1 Theoretical foundations

The understanding of the ion motion in an ideal Penning trap is of great relevance for the manipulation and control of the ion in high-precision experiments. In Chap. 2 dipolar and quadrupolar electric fields have been introduced for the excitation of the ion motion in general. Here, a more detailed description of the presence of external driving fields is given. Furthermore, the analytical description will be extended under consideration of a damping force due to ion collisions with residual gas atoms in a real Penning trap. The following theoretical derivations are partly based on the work of M. Kretzschmar [Kret2008].

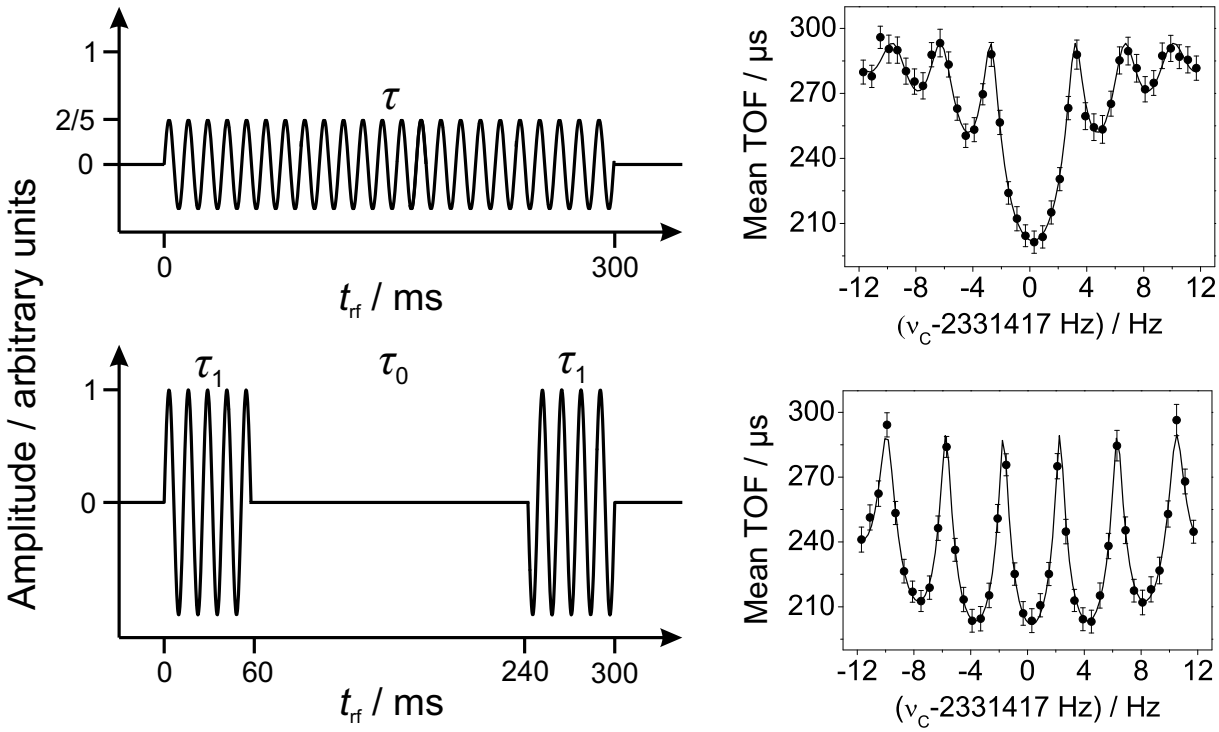

Figure 4.1: On the left side a continuous excitation (up) as well as a two-pulse excitation (down) scheme are shown. Examples of the corresponding TOF-ICR resonances are added on the right side.

4.1.1 Ideal Penning trap with damping force

The motion of the ion in an ideal Penning trap has been described by the Newtonian equations (2.7-2.9). With the introduction of the complex variable $u = x + iy$ the two equations of the radial modes (2.7, 2.8) have been simplified to a single complex equation (2.11). The general solution of (2.11) is:

$$u(t) \;=\; A_+ \exp(-i\omega_+ t) + A_- \exp(-i\omega_- t)\,. \tag{4.1}$$

In a real Penning trap ions do not move in perfect vacuum but in a neutral residual gas of low pressure. The ions are decelerated by an interaction of their Coulomb field with polarized gas atoms. In a good approximation the ions experience a viscous damping force [Ghos1995, Majo2005] as already introduced in Eq. (2.40) for the buffer-gas cooling. Considering the damping force the Newtonian equations of motion have to be extended to

$$\ddot{x} + 2\gamma\dot{x} - \omega_c\,\dot{y} - \frac{1}{2}\,\omega_z^2\,x \;=\; 0\,, \tag{4.2}$$

$$\ddot{y} + 2\gamma\dot{x} + \omega_c\,\dot{x} - \frac{1}{2}\,\omega_z^2\,y \;=\; 0\,, \tag{4.3}$$

$$\ddot{z} + \omega_z^2\,z \;=\; 0\,. \tag{4.4}$$

Important to note is that γ is a velocity-independent constant. Consequently, the differential equations still remain linear. Furthermore, the linearity with respect to velocity

keeps the axial and radial modes uncoupled. Simplifying Eqs. (4.2, 4.3) by introducing the complex variable $u = x + iy$ leads again to a single complex equation

$$\ddot{u} + i\,(\omega_c - 2i\gamma)\dot{u} - \frac{1}{2}\,\omega_z^2\,u \;=\; 0\,. \tag{4.5}$$

Comparing the equation of the undamped motion (see Eq. (2.11)) with the equation of motion including the damping force (4.5), the complex equation is obtained by replacing the real number ω_c by the complex number $\omega_c - 2i\gamma$. Thus, for the radial motions it is obvious to consider the cyclotron frequency as a complex parameter $\overline{\omega}_c$. In case of the undamped motion, $\overline{\omega}_c = \omega_c$ is a physically meaningful value on the positive real axis. If the motion is damped, $\overline{\omega}_c = \omega_c - 2i\gamma$ is in the complex plane below the positive real axis. Now it is possible to find the solution of Eq. (4.5) by an analytical continuation of Eq. (2.11). Since a damping force produces a new term in the equation of motion in case of the axial mode instead of varying an existing one, the analytical continuation can not be adopted.

Varying $\omega_c \to \overline{\omega}_c = \omega_c - 2i\gamma$ in the ideal Penning trap, the eigenvalues of the radial modes (see Eq. (2.13)) are changed to

$$\overline{\omega}_\pm \;=\; \frac{1}{2}\left(\overline{\omega}_c \pm \sqrt{\overline{\omega}_c^2 - 2\omega_z^2}\right) = \frac{1}{2}(\overline{\omega}_c \pm \overline{\omega}_1)\,. \tag{4.6}$$

These are complex numbers and the real parts are the eigenfrequencies and the imaginary parts represent decay constants of the damped motion:

$$\overline{\omega}_\pm \;=\; \Re(\overline{\omega}_\pm) + i\Im(\overline{\omega}_\pm) = \widetilde{\omega}_\pm - i\widetilde{\gamma}_\pm\,. \tag{4.7}$$

Calculating the expressions for $\widetilde{\omega}_\pm$ and $\widetilde{\gamma}_\pm$ leads to

$$\widetilde{\omega}_\pm \;=\; \frac{1}{2}(\omega_c \pm \widetilde{\omega}_1)\,, \tag{4.8}$$

$$\widetilde{\gamma}_\pm \;=\; \frac{1}{2}(2\gamma \pm \widetilde{\gamma}_1)\,, \tag{4.9}$$

with

$$\widetilde{\omega}_1 \;=\; \frac{1}{\sqrt{2}}\sqrt{\sqrt{(\omega_1^2 - 4\gamma^2)^2 + 16\gamma^2\omega_c^2} + (\omega_1^2 - 4\gamma^2)}\,, \tag{4.10}$$

$$\widetilde{\gamma}_1 \;=\; \frac{1}{\sqrt{2}}\sqrt{\sqrt{(\omega_1^2 - 4\gamma^2)^2 + 16\gamma^2\omega_c^2} - (\omega_1^2 - 4\gamma^2)}\,. \tag{4.11}$$

A conclusion from Eq. (4.10) is that damping causes small shifts in the modified cyclotron and magnetron frequencies. The modified cyclotron frequency increases while the magnetron frequency decreases such that the sum frequency $\widetilde{\omega}_+ + \widetilde{\omega}_- = \omega_c$ still holds. The so-called *Brown-Gabrielse Invariance Theorem* [Gabr2009] is valid in its complex form $\overline{\omega}_+^2 + \overline{\omega}_-^2 + \overline{\omega}_z^2 = \overline{\omega}_c^2$. In a real Penning trap ($\gamma \ll \omega_c$) the decay constant can be approximated by

$$\widetilde{\gamma}_\pm \approx \gamma\left(1 \pm \frac{\omega_c}{\sqrt{\omega_1^2 - 4\gamma^2}}\right) \approx \pm 2\gamma\frac{\omega_\pm}{\omega_1}\,. \tag{4.12}$$

An analytic evolution of the general solution of Eq. (2.11) is

$$\begin{aligned} u(t) &= A_+ \exp(-i\overline{\omega}_+ t) + A_+ \exp(-i\overline{\omega}_- t) \\ &= A_+ \exp(-\widetilde{\gamma}_+ t - i\widetilde{\omega}_+ t) + A_+ \exp(-\widetilde{\gamma}_- t - i\widetilde{\omega}_- t)\,. \end{aligned} \tag{4.13}$$

Since $\widetilde{\gamma}_+ > 0$ and $\widetilde{\gamma}_- > 0$ (see Eq. (4.12)) the radius of the cyclotron mode is decreasing while the radius of the magnetron mode is increasing.
In [Kret2007] it was shown that the introduction of "complex oscillator amplitudes" $\alpha_\pm(t)$ is very useful for the description of the ion motion in presence of external rf-fields. Following this line, Eq. (2.11) can be rewritten in the form

$$u(t) = \sqrt{2\hbar/(m\omega_1)}\,(\alpha_+(t) + \alpha_-^*(t))\,. \tag{4.14}$$

In terms of complex coordinates $u = x + iy$ and velocities $\dot{u} = \dot{x} + i\dot{y}$ the complex oscillator amplitudes are

$$\alpha_+ = \sqrt{\frac{m}{2\hbar\overline{\omega}_1}}(+i\dot{u} - \overline{\omega}_- u)\,, \tag{4.15}$$

$$\alpha_-^* = \sqrt{\frac{m}{2\hbar\overline{\omega}_1}}(-i\dot{u} + -\overline{\omega}_+ u)\,. \tag{4.16}$$

The inverse relations are

$$u = \sqrt{\frac{2\hbar}{m\overline{\omega}_1}}(\alpha_+ + \alpha_-^*)\,, \tag{4.17}$$

$$\dot{u} = -i\sqrt{\frac{2\hbar}{m\overline{\omega}_1}}(\overline{\omega}_+\alpha_+ + \overline{\omega}_-\alpha_-^*)\,. \tag{4.18}$$

The complex oscillator amplitudes satisfy the equation of motion

$$\dot{\alpha}_+(t) = -i\overline{\omega}_+\alpha_+(t)\,, \tag{4.19}$$

$$\dot{\alpha}_-(t) = +i\overline{\omega}_+^*\alpha_-(t)\,. \tag{4.20}$$

Explicit solutions are

$$\alpha_+(t) = \exp[-i\overline{\omega}_+ t]\alpha_+(0)\,, \tag{4.21}$$

$$\alpha_-(t) = \exp[+i\overline{\omega}_-^* t]\alpha_-(0)\,. \tag{4.22}$$

With respect to high precision experiments in Penning traps it is important to note that the radii of the cyclotron and magnetron motion can be described in terms of the complex oscillator amplitudes

$$R_\pm(t) = \sqrt{\frac{2\hbar}{m\,|\,\overline{\omega}_1|}}\,|\,\alpha_\pm(t)|\,. \tag{4.23}$$

For the undamped motion $\overline{\omega}_1$ has to be replaced by ω_1.

4.1.2 Dipolar excitation

In many Penning trap experiments the ring electrode is splitted into an even number of segments, which allows the application of external rf-fields for the manipulation of the motional modes [Boll1990, Blau2006]. An electric dipole field as described in Eq. (2.32) leads to a new inhomogeneous time-dependent term in the Newtonian equations of motion,

$$\ddot{x} + 2\gamma\dot{x} - \omega_c\,\dot{y} - \frac{1}{2}\,\omega_z^2\,x \;=\; (q/m)d_x\cos(\omega_d t + \Phi_d)\,, \tag{4.24}$$

$$\ddot{y} + 2\gamma\dot{x} + \omega_c\,\dot{x} - \frac{1}{2}\,\omega_z^2\,y \;=\; (q/m)d_y\cos(\omega_d t + \Phi_d)\,. \tag{4.25}$$

Replacing $d_x = d\cos\theta$ and $d_y = d\sin\theta$ leads again to a single complex equation

$$\ddot{u} + i\,(\omega_c - 2i\gamma)\dot{u} - \frac{1}{2}\,\omega_z^2\,u \;=\; (q/m)de^{i\theta}\cos(\omega_d t + \Phi_d)\,. \tag{4.26}$$

Thus, the equations of motion have to be modified into

$$\dot{\alpha}_+(t) \;=\; -i\overline{\omega}_+\alpha_+(t) + i2De^{i\theta}\cos(\omega_d t + \Phi_d)\,, \tag{4.27}$$

$$\dot{\alpha}_-(t) \;=\; +i\overline{\omega}_-^*\alpha_-(t) + i2D^*e^{-i\theta}\cos(\omega_d t + \Phi_d)\,, \tag{4.28}$$

with the constant $D = qd/(2\sqrt{2m\hbar\overline{\omega}_1})$. The general solutions of these equations, which are despite the external driving field still uncoupled, are:

$$\alpha_+(t) \;=\; A_+e^{-i\overline{\omega}_+t} - \frac{De^{-i(\omega_d t+\Phi_d-\theta)}}{\omega_d - \overline{\omega}_+} + \frac{De^{+i(\omega_d t+\Phi_d+\theta)}}{\omega_d + \overline{\omega}_+}\,, \tag{4.29}$$

$$\alpha_-(t) \;=\; A_-^*e^{+i\overline{\omega}_-^*t} + \frac{D^*e^{+i(\omega_d t+\Phi_d-\theta)}}{\omega_d - \overline{\omega}_-^*} - \frac{D^*e^{-i(\omega_d t+\Phi_d+\theta)}}{\omega_d + \overline{\omega}_-^*}\,. \tag{4.30}$$

$A_\pm$ are arbitrary complex constants. Neglecting the counterrotating third terms due the rotating wave approximation [West1984], leads to a good approximation for $\alpha_+(t)$, when $\omega_d \approx \widetilde{\omega}_+$, and for $\alpha_-(t)$, when $\omega_d \approx \widetilde{\omega}_-$, respectively. At time $t = 0$ the complex oscillator amplitudes with suitable chosen constants $A_\pm$ become $\alpha_\pm(0)$ and can be expressed as

$$\begin{aligned}\alpha_+(t) \;=\;& \alpha_+(0) + e^{-i\overline{\omega}_+t} - \frac{De^{-i(\Phi_d-\theta)}}{\omega_d - \overline{\omega}_+}(e^{-i\omega_d t} - e^{-i\overline{\omega}_+t}) \\ &+\frac{De^{+i(\Phi_d+\theta)}}{\omega_d + \overline{\omega}_+}(e^{+i\omega_d t} - e^{-i\overline{\omega}_+t})\,,\end{aligned} \tag{4.31}$$

$$\begin{aligned}\alpha_-(t) \;=\;& \alpha_-(0) + e^{+i\overline{\omega}_-^*t} - \frac{D^*e^{+i(\Phi_d-\theta)}}{\omega_d - \overline{\omega}_-^*}(e^{+i\omega_d t} - e^{+i\overline{\omega}_-^*t}) \\ &+\frac{D^*e^{-i(\Phi_d+\theta)}}{\omega_d + \overline{\omega}_-^*}(e^{-i\omega_d t} - e^{+i\overline{\omega}_-^*t})\,.\end{aligned} \tag{4.32}$$

With respect to the relevance in Penning trap mass spectrometry, the time-dependent developments of the radii $R_\pm(t)$ in the presence of the electric dipole field have to be studied. The detuning of the external field is described by

$$\overline{\delta}_\pm \;=\; \omega_d - \overline{\omega}_\pm = \omega_d - \widetilde{\omega}_\pm + i\widetilde{\gamma}_\pm = \widetilde{\delta}_\pm + i\widetilde{\gamma}_\pm\,. \tag{4.33}$$

Using Eq. (4.23) with $\alpha_\pm(0) = |\,\alpha_\pm(0)|\exp(\mp i\Phi_\pm)$ and the abbreviations $\Delta_\pm = \Phi_d - \Phi_\pm - \theta$ and $C_\pm = D/|\,\alpha_\pm(0)|$ results in

$$\frac{R_+(t)}{R_+(0)} = \left| e^{-\widetilde{\gamma}_+ t} - \frac{C_+ e^{-i\Delta_+}}{\widetilde{\delta}_+ + i\widetilde{\gamma}_+}(e^{-i\widetilde{\delta}_+ t} - e^{-\widetilde{\gamma}_+ t}) \right| , \tag{4.34}$$

$$\frac{R_-(t)}{R_-(0)} = \left| e^{-\widetilde{\gamma}_- t} + \frac{C_- e^{-i\Delta_-}}{\widetilde{\delta}_- + i\widetilde{\gamma}_-}(e^{-i\widetilde{\delta}_- t} - e^{-\widetilde{\gamma}_- t}) \right| . \tag{4.35}$$

Exactly on resonance a dipole rf-field effects a linear rise of the specific radius as far as the damping is negligible (see Fig. 2.5 (a,b)). The phase difference $\Delta_\pm$ defines the starting conditions at $t = 0$. If the value of the damping parameter is considerable large the rise of $R_+(t)$ is reduced due to $\widetilde{\gamma}_+ > 0$ and the rise of $R_-(t)$ is larger than in the undamped case, since $\widetilde{\gamma}_- < 0$. As already mentioned in Chap. 2, an excitation off resonance produces a periodic decrease and increase of the radii $R_\pm$. A damping force superimposes an exponential decay. Thus, $R_+(t)$ is approaching a constant radius, while the magnetron radius goes to infinity (see Fig. 2.7 (a,b)).

4.1.3 Quadrupolar excitation

More important in context of TOF-ICR mass spectrometry is the ion motion in presence of an external quadrupolar rf-field. As discussed in Chap. 2.4.2 a driving field matching exactly the cyclotron frequency of the stored ion $\omega_d = \omega_c$ leads to the periodic interconversion of the radial modes. A comprehensive theoretical description of this configuration has been carried out in the article of M. Kretschmar [Kret2007]. Here, a single pulse excitation as well as a two pulse Ramsey excitation pattern, both applied for high-precision mass measurements reported in the next chapters, shall be discussed in detail. In [Kret2008] the explicit analytical solutions for the complex oscillator amplitudes of the two radial modes have been derived to

$$\begin{aligned}\alpha_+(t) &= e^{-i(\omega_+ + \delta/2)t}\left[\left(\cos\frac{\omega_R t}{2} + i\frac{\delta}{\omega_R}\sin\frac{\omega_R t}{2}\right)\alpha_+(0)\right. \\ &\quad \left. -i\frac{2g}{\omega_R}\sin\frac{\omega_R t}{2}e^{-i\chi_d}\alpha_-(0)\right] , \end{aligned} \tag{4.36}$$

$$\begin{aligned}\alpha_-(t) &= e^{-i(\omega_- + \delta/2)t}\left[-i\frac{2g}{\omega_R}\sin\frac{\omega_R t}{2}e^{+i\chi_d}\alpha_+(0)\right. \\ &\quad \left.\left(\cos\frac{\omega_R t}{2} - i\frac{\delta}{\omega_R}\sin\frac{\omega_R t}{2}\right)\alpha_-(0)\right] . \end{aligned} \tag{4.37}$$

As introduced in Chap. 2, $\delta = \omega_{rf} - \omega_c$ is the frequency detuning, g the coupling constant, and $\omega_R = \sqrt{\delta^2 + 4g^2}$ the Rabi frequency of the interconversion. Furthermore, the identity $\omega_\pm + \delta/2 = (\omega_d \pm \omega_1)/2$ was used. Damping effects are again considered by the substitution of ω_c by $\overline{\omega}_c = \omega_c - 2i\gamma$. Additional to $\omega_\pm$ (see Eq. 4.7) $\delta \to \overline{\delta} = \delta + 2i\gamma$, $\omega_1 \to \overline{\omega}_1 = \widetilde{\omega}_1 - i\widetilde{\gamma}$, and $\omega_R \to \overline{\omega}_R = \sqrt{(\delta + 2i\gamma)^2 + 4g^2} = \widetilde{\omega}_R - i\widetilde{\gamma}_R$ has to be replaced. Here, the following abbreviations are used:

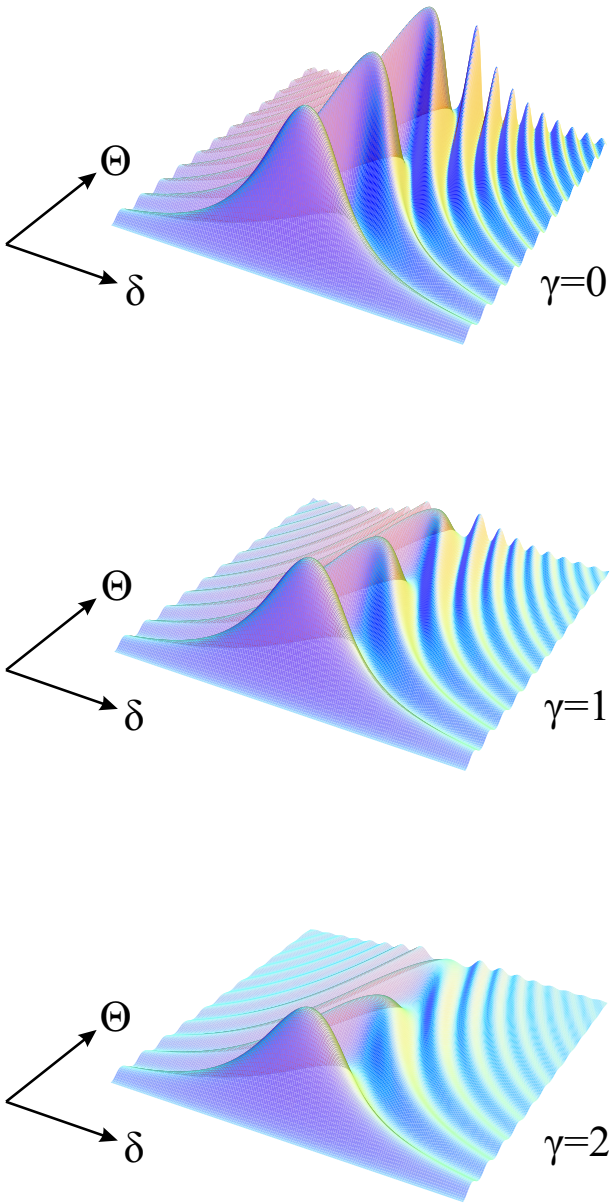

Figure 4.2: Degree of conversion as a function of the frequency detuning δ and the duration of the excitation pulse $\Theta = t/\tau_c(\gamma)$ measured in units of the conversion time. Without damping (top) a periodically full conversion and reconversion is observed. For $\gamma = 1$ (middle) and $\gamma = 2$ (bottom) two damped profiles are shown, illustrating the exponential loss of energy in time.

$$|\overline{\omega}_R^2| = \sqrt{(\omega_R^2 - 4\gamma^2)^2 + 16\gamma^2\delta^2}\,, \tag{4.38}$$

$$\widetilde{\omega}_R = \frac{1}{\sqrt{2}}\sqrt{|\overline{\omega}_R|^2 + \omega_R^2 - 4\gamma^2}\,, \tag{4.39}$$

$$\widetilde{\gamma}_R = -\frac{sign(\delta)}{\sqrt{2}}\sqrt{|\overline{\omega}_R|^2 - (\omega_R^2 - 4\gamma^2)}\,. \tag{4.40}$$

Thus, in the complex version of Eqs. (4.36,4.37) the following expressions can be substituted:

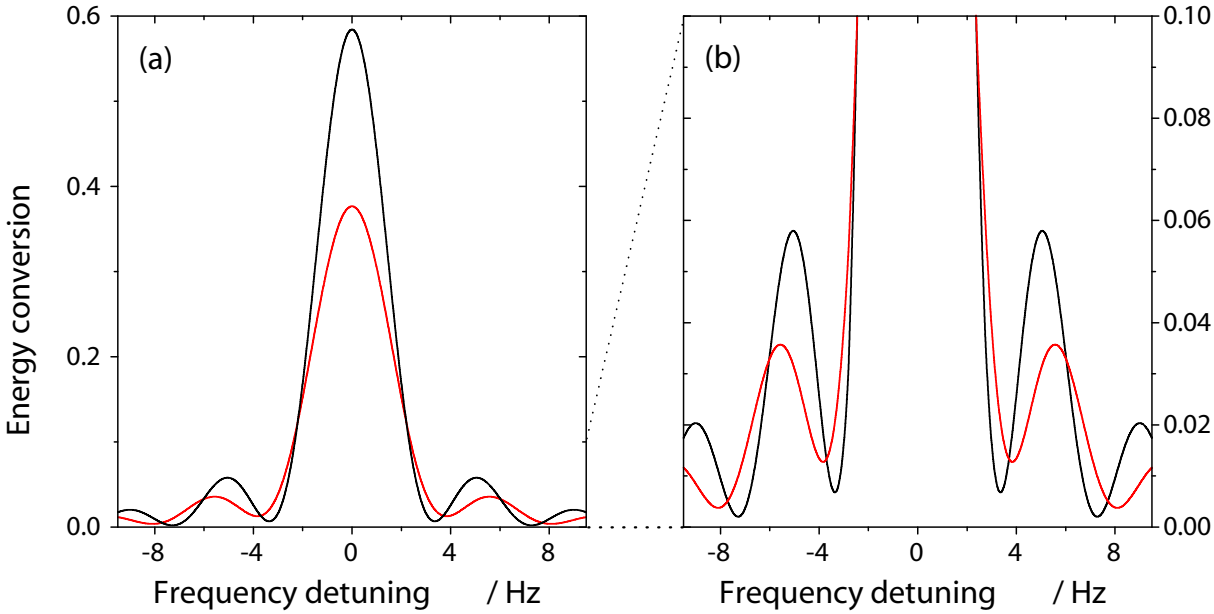

Figure 4.3: (a) Conversion line shapes in case of a single pulse of external radiofrequency radiation. They have been calculated for damping coefficients $\gamma = 1$ (black) and $\gamma = 2$ (red). The reduction of the conversion time due to damping effects has been considered for the best possible conversion. In (b) a zoom of the lower part of (a) is shown. Clearly, damping leads to a filling of the minima of the fringe pattern. Additionally, a line broadening of the curves is observed.

$$\cos\frac{\overline{\omega}_R t}{2} = \cos\frac{\widetilde{\omega}_R t}{2}\cosh\frac{\widetilde{\gamma}_R t}{2} + i\sin\frac{\widetilde{\omega}_R t}{2}\sinh\frac{\widetilde{\gamma}_R t}{2}\,, \tag{4.41}$$

$$\sin\frac{\overline{\omega}_R t}{2} = \sin\frac{\widetilde{\omega}_R t}{2}\cosh\frac{\widetilde{\gamma}_R t}{2} - i\cos\frac{\widetilde{\omega}_R t}{2}\sinh\frac{\widetilde{\gamma}_R t}{2}\,, \tag{4.42}$$

$$\frac{\overline{\delta}}{\overline{\omega}_R} = \frac{\overline{\delta}\overline{\omega}_R^*}{|\overline{\omega}_R|^2} = \frac{\delta\widetilde{\omega}_R - 2\gamma\widetilde{\gamma}_R + i(\delta\widetilde{\gamma} + 2\gamma\widetilde{\omega}_R)}{|\overline{\omega}_R|^2}\,. \tag{4.43}$$

This description of the damping effects can now be used to calculate the specific problems in TOF-ICR mass spectrometry. As a starting condition the ions are assumed to be prepared in a pure magnetron mode as already mentioned in Chap. 2. Thus, the values of Eqs. (4.36,4.37) are $\alpha_+(0) = 0$ and $\alpha_-(0) = \sqrt{m\overline{\omega}_1/(2\hbar)}R_-(0)$ with the initial magnetron radius $R_-(0)$. The time-dependent conversion from magnetron mode into cyclotron mode can then be written as

$$\left(\frac{R_+(t)}{R_-(0)}\right)^2 = e^{-\widetilde{\gamma}_1 t}\frac{4g^2}{|\overline{\omega}_R|^2}\left|\sin\frac{\overline{\omega}_R t}{2}\right|^2\,. \tag{4.44}$$

A full landscape of degree of conversion as a function of frequency detuning δ as well as of the duration of the excitation pulse $\Theta = t/\tau_c(\gamma)$ is shown in Fig. 4.2 for various damping coefficients. In resonance, *i.e.* $\delta = 0$, the conversion is most efficient. Consequently, this

leads to $\widetilde{\gamma}_R = 0$ and $\widetilde{\omega}_R = \sqrt{4g^2 + \delta^2}$, which simplifies the equation of conversion to

$$\left(\frac{R_+(t)}{R_-(0)}\right)^2 = \frac{e^{-\widetilde{\gamma}_1 t}}{1-(\gamma/g)^2}\sin^2\left(t\sqrt{g^2-\gamma^2}\right) . \tag{4.45}$$

Neglecting any damping force a complete conversion has been achieved after the so-called "conversion time" $\tau_c = \pi/(2g)$. Periodic Rabi cycles between the radial modes are shown in Fig. 2.9. A damping force requires an amplitude of the external driving field, which is strong enough to counteract the damping force. Therefore, the denominator in Eq. (4.45) has to be positive and leads to $(\gamma/g)^2 < 1$. With such an external driving field the degree of conversion still passes through minima and maxima as a function of time, but the damping force decreases the height of the maxima and extends the conversion time. The first maximum, which is now the highest possible degree of conversion, is reached after a conversion time of

$$\tau_c(\gamma) = \frac{2}{\sqrt{4g^2-4\gamma^2}}\,\mathrm{arccot}\left(\frac{\widetilde{\gamma}_1}{\sqrt{4g^2-4\gamma^2}}\right) . \tag{4.46}$$

For $\gamma = 0$ this equation is simply reduced to $\tau_c = \pi/(2g)$. With respect to TOF-ICR mass spectrometry it is most important to know in case of a resonant excitation, which means t=$\tau_c(\gamma)$, the line shape as a function of the frequency detuning δ. In Fig. 4.3 calculated line shapes of an excitation with a single, continuous pulse are shown. Black curves represent a damping coefficient of $\gamma = 1$ and red curves of $\gamma = 2$. The undamped conversion time with appropriate coupling strength g was chosen to be 300 ms. To calculate the profiles in Fig. 4.3 the eigenfrequencies $\nu_c = 1\,\mathrm{MHz}$ and $\nu_z = 44\,\mathrm{kHz}$ were used. Further line shapes for $\gamma = 1$ but different excitation durations are shown in the left column of Fig. 4.4.
In [Kret2007, Geor2007a, Geor2007b] a symmetric two-pulse Ramsey scheme has been introduced as an advantageous excitation pattern compared to the conventional one. Neglecting any damping force the time-dependent conversion from the magnetron into the cyclotron mode was determined to be

$$\begin{aligned} F_2(\delta,\tau_0,\tau_1,g) &= \frac{4g^2}{\omega_R^2}\cdot\sin^2\frac{\omega_R\tau_1}{2} \\ &\quad\cdot\left[2\cos\frac{\delta\tau_0}{2}\cdot\cos\frac{\omega_R\tau_1}{2} - 2\frac{\delta}{\omega_R}\sin\frac{\delta\tau_0}{2}\cdot\sin\frac{\omega_R\tau_1}{2}\right]^2 , \end{aligned} \tag{4.47}$$

with τ_1 being the duration of one excitation pulse and τ_0 being the duration of the waiting period. Introducing the damping force and replacing the excitation time t by $2\cdot\tau_1$ leads to

$$\begin{aligned} F_2(\delta,\tau_1,\tau_0,g,\gamma) &= e^{-\widetilde{\gamma_1}(2\tau_1+\tau_0)}\frac{4g^2}{|\,\overline{\omega}_R\,|^2} \\ &\quad\cdot\left|\cos\left(\frac{\overline{\delta}\tau_0}{2}\right)\sin\left(\overline{\omega}_R\tau_1\right)\right. \\ &\quad\left.+\left(\frac{\overline{\delta}}{\overline{\omega}_R}\right)\sin\left(\frac{\overline{\delta}\tau_0}{2}\right)\left(\cos(\overline{\omega}_R\tau_1)-1\right)\right|^2 , \end{aligned} \tag{4.48}$$

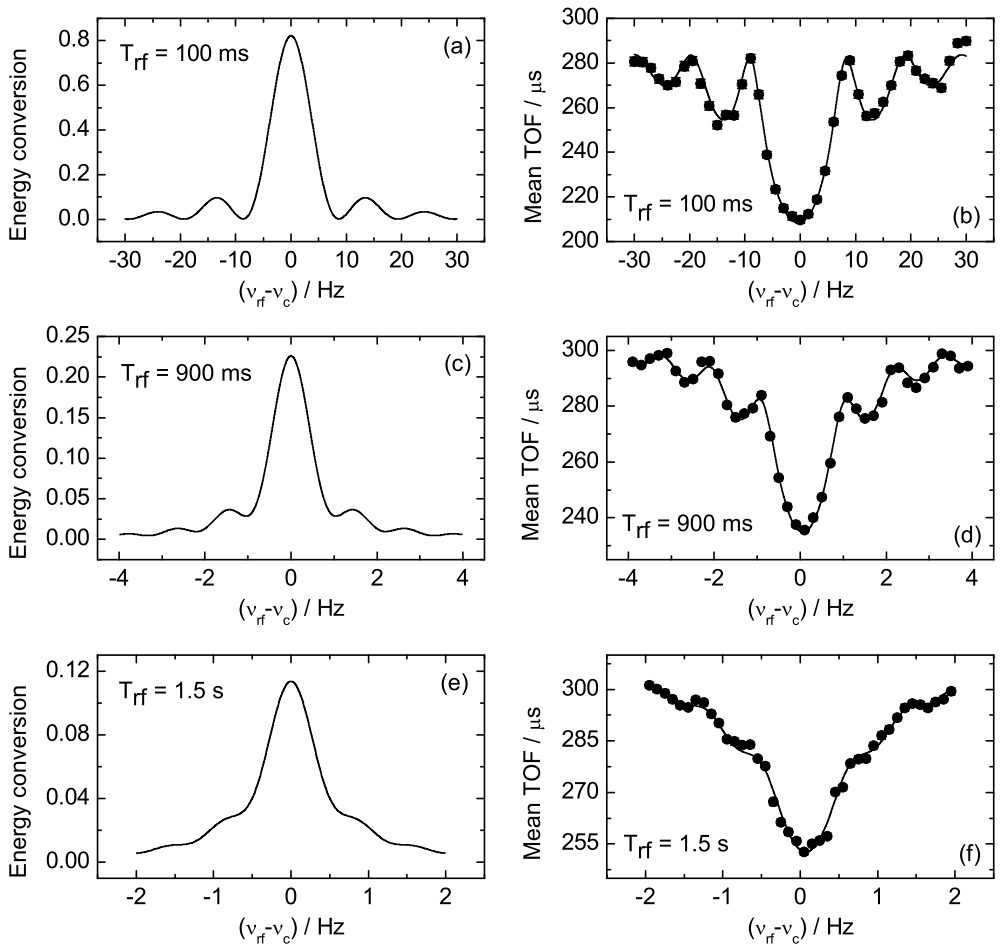

Figure 4.4: In the left column the calculated percentage of conversion from the initial magnetron mode into the cyclotron mode for a standard excitation is presented (a,c,e). The damping coefficient used for the calculations is γ=1. In the right column the corresponding time-of-flight spectra measured at ISOLTRAP are shown (b,d,f). In the first row (a,b) the excitation time is 100 ms, 700 ms in the second (c,d), and 1.5 s in the third (e,f), respectively. For this spectra $^{39}K^+$ as ion species was chosen. Since about 20000 ions have been taken for each resonance, the statistical uncertainties of the individual frequency points are smaller than the size of the data points itself. The solid lines are fits of the theoretical line shapes to the experimental data.

with the abbreviations

$$\begin{aligned}\cos\left(\frac{\bar{\delta}\tau_0}{2}\right) &= \cos\left(\frac{\delta\tau_0}{2} - i\gamma\tau_0\right) \\ &= \cos\left(\frac{\delta\tau_0}{2}\right)\cosh(\gamma\tau_0) + i\sin\left(\frac{\delta\tau_0}{2}\right)\sinh(\gamma\tau_0) \end{aligned} \tag{4.49}$$

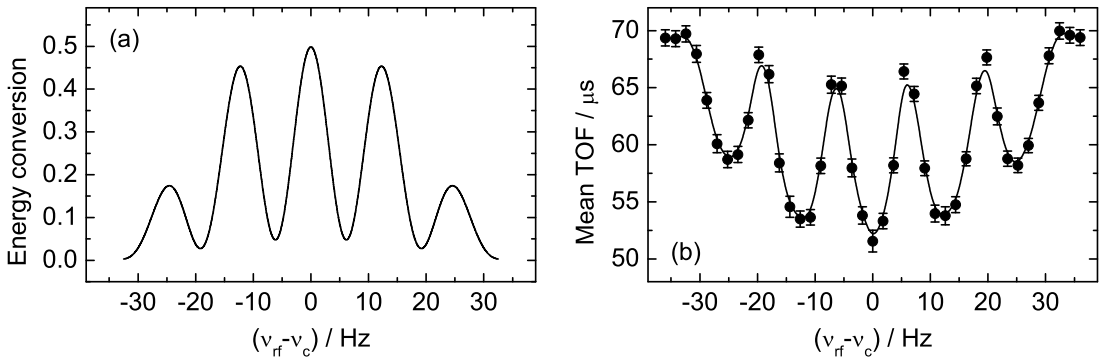

Figure 4.5: In (a) the energy conversion of a Ramsey pattern with two 25 ms excitation pulses interrupted by a 50 ms waiting period under shown. A damping coefficient of $\gamma = 3$ was used for the calculation. It was derived from the fit of the theoretical line shape derived within this thesis (solid line) to the data points in (b). Here, a time-of-flight curve for the excitation pattern described in (a) has been recorded at SHIPTRAP. ^{85}Rb ions were used.

$$\begin{aligned} \sin\left(\frac{\bar{\delta}\tau_0}{2}\right) &= \sin\left(\frac{\delta\tau_0}{2} - i\gamma\tau_0\right) \\ &= \left(\sin\frac{\delta\tau_0}{2}\right)\cosh(\gamma\tau_0) - i\left(cos\frac{\delta\tau_0}{2}\right)\sinh(\gamma\tau_0)\,. \end{aligned} \tag{4.50}$$

In Fig. 4.5 (a) the line shape of the energy conversion for a symmetric two-pulse Ramsey-type pattern with two 25 ms excitation pulses and a 50 ms waiting period is shown. The damping coefficient for the calculation has been chosen to be $\gamma = 3$. The theoretical calculations of this section will be experimentally proven in the following.

4.2 Experimental results

Two issues of the TOF-ICR mass spectrometry have been investigated extensively in context of damping effects within this thesis. They are of special importance for the high-precision mass measurements reported in Chap. 5. The first one is the interconversion of the magnetron and cyclotron mode due to an external quadrupolar rf-field. As described in Chap. 2 an excitation at exactly the sum frequency of the two radial motions $\nu_+ + \nu_- = \nu_c$ leads to the periodic conversion of energy from one mode into the other and vice versa. Thus, after twice the conversion time the energy is converted back into the initial state. A continuous excitation results in a Rabi-like oscillation between the two states. The time of conversion depends ideally only on the coupling strength of the external field, which is proportional to the rf-field amplitude. Under consideration of damping due to buffer gas this conversion time is reduced, see Eq. (4.46). Since the time scale of the damping in the

cyclotron mode is in the order of the conversion time a considerable loss in radial energy is expected. Second, the effects of damping on the line profiles for quadrupole excitation has been studied. In respect to high-precision mass spectrometry especially the adjustment of Eq. (4.45) to a measured line profile with strong damping has been tested [Geor2009a].

To prove these assumptions a series of measurements have been performed at the Penning trap mass spectrometers SHIPTRAP and ISOLTRAP. In order to investigate the inter-conversion of motional modes ^{133}Cs ions from the reference ions source of SHIPTRAP are stored in the precision trap and prepared in a pure magnetron mode. An external rf-field exactly at the resonance frequency is applied for a time t. The amplitude of the rf-field is chosen in a way that a full conversion is obtained within 100 ms. Then, the radial energy of the ions is probed via the time-of-flight detection method. This has been repeated for various excitation times between 0 and 600 ms. The background pressure in the precision trap, which is responsible for the damping of the ion motion, is mainly caused by the helium buffer-gas in the preparation trap. A small fraction (∼0.1-1%) of it is diffusing continuously from the preparation to the precision trap, although the gas flow is suppressed by a differential pumping barrier [Neid2008]. Since only this differential pumping takes place between the preparation and precision trap, the gas flow rate in the preparation trap can be used to effectively controll the pressure in the precision trap. The resulting Rabi oscillations of the conversion, calculated for three different gas flow rates, are shown in Fig. 4.6 (a). The damping coefficients have been extracted from fits of the theoretical line shapes to the data points in Fig. 4.6 (b). A gas flow rate of $4{\cdot}10^{-3}$ mbar·l/s, which is in the order of the normal flow rate during a mass measurement at SHIPTRAP, yields a damping coefficient of $\gamma = 0.7$ (black). Using gas flow rates of $1 \cdot 10^{-2}$ mbar·l/s and $2.5 \cdot 10^{-2}$ mbar·l/s result in damping coefficients of $\gamma = 1.0$ (green) and $\gamma = 2.0$ (red), respectively. The exponential decay of the radial energy in time is emerged. Even the less pronounced effect of the reduced conversion time for higher damping coefficients, here expressed in an occurrence of the maxima at larger $\theta = t/\tau_c(\gamma)$, is clearly observable and agrees with the predictions from Eq. (4.46). In the mass measurement process itself the excitation time is in general fixed to a desired value. To be able to work with the best possible degree of conversion, and thus yielding the strongest contrast in the time of flight, the amplitude of the rf field is adjusted in a way that it counteracts the shift of the conversion time. The background pressure in the environment of a Penning trap mass spectrometer is usually stable enough that such an adjustment has only to be performed once during a measurement period of a few days. More important in respect of mass measurements are the damping effects on the line profiles of quadrupole excitation. The frequency determination by using the TOF-ICR method yields characteristic resonance curves as described in Chap. 2. The line shape of the curve is a direct consequence of the applied excitation pattern. It can be calculated by a Fourier transformation of the particular profile. A damping force due to collisions of ions with residual gas atoms broadens the width of the resonance and reduces considerably the time of flight of the excited ions. Both effects increase the uncertainty of the frequency determination.

Among the conventional excitation with a single pulse of continuous rf radiation, Ramsey's method of separated oscillatory fields has recently been introduced for the excitation

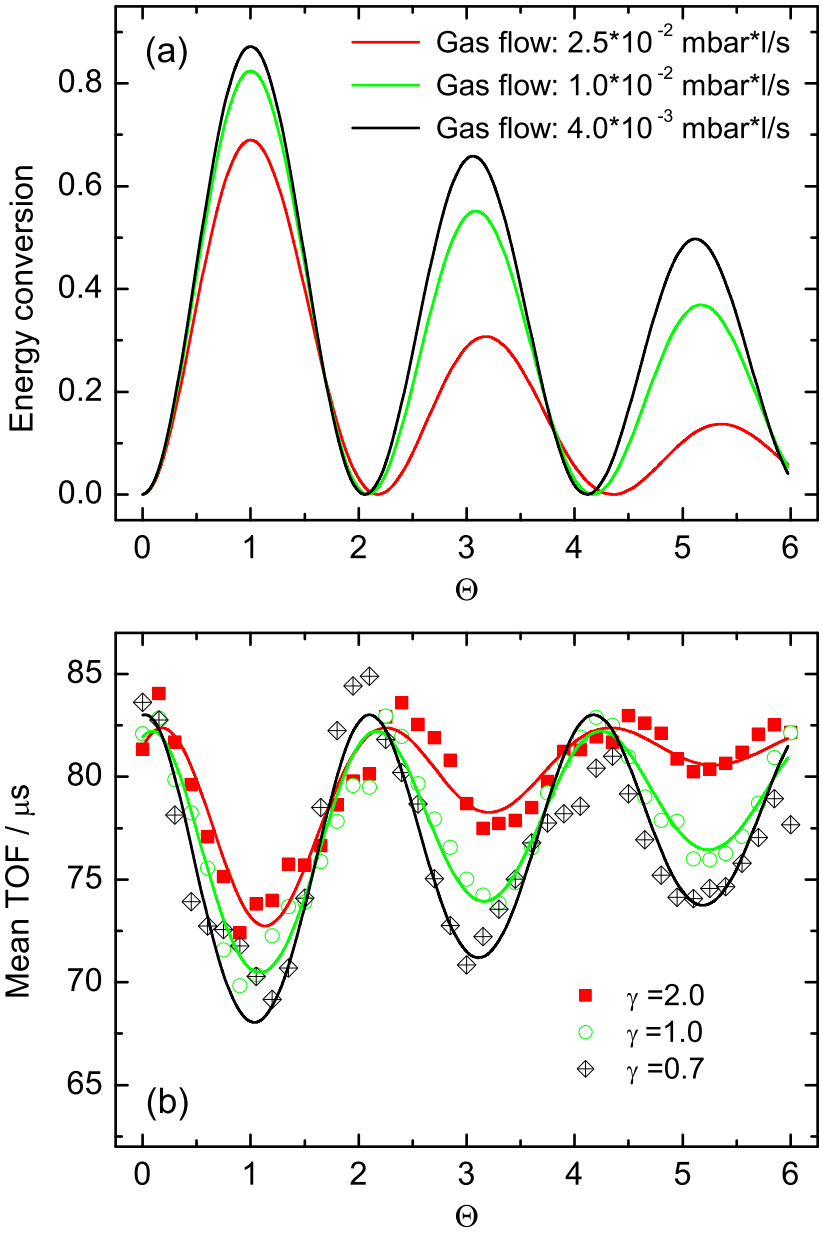

Figure 4.6: (a) Energy conversion of magnetron into modified cyclotron energy in resonance as a function of time in units of the conversion time $\theta = t/\tau_c(0)$, neglecting any damping force. The damping coefficients γ are corresponding to that one extracted from the experimental time-of-flight curves in (b). Here, the mean time of flight as a function of θ for different helium gas-flow rates in the preparation trap of SHIPTRAP are shown. The ion species used in this measurements was ^{133}Cs. The solid lines are best fits of the theoretical curves to the data.

of the ion motion. In [Kret2007, Geor2007a, Geor2007b] its adaption to Penning trap mass spectrometry has been analytically derived and experimentally demonstrated. To study the damping effects on the resonance line shapes and test the analytical descrip-

tion [Kret2008] TOF-ICR curves of $^{39}K^{+}$ ions in presence of an enhanced background pressure have been recorded at the ISOLTRAP experiment. The buffer-gas flow rate in the preparation trap of ISOLTRAP can not be used to control the background pressure in the precision trap as done at SHIPTRAP, since the long distance of close to two meters between the preparation and precision trap as well as an additional vacuum pump in between reduces the gas flow effectively. Instead, the pumping power in the setup was reduced in order to increase the pressure to 1.1-1.3·10^{-6} mbar from initially a few parts in 10^{-8} mbar for a measurement period of five days. Doing this it was not possible to vary the background pressure for different measurements as done at SHIPTRAP. Nevertheless, conventional TOF-ICR curves with various excitation times ranging from 100 ms up to 3 s with approximately 20000 recorded ions in each resonance have been measured. Three examples of such reference curves with 100 ms, 900 ms, and 1.5 s excitation time are shown in the right column of Fig. 4.4. The damping coefficients extracted from the fits to the experimental data are around $\gamma = 1$ and have been used to calculate the corresponding energy conversion profiles in the left column. Furthermore, all data have been evaluated twice: first, using the equations of motion found in König *et al.* [Köni1995], up to now used in the fitting routine; second, the equations described above have been used. So far, in the typical pressure regime of a Penning trap no difference in the extracted resonance frequency and its uncertainty has been found for all measured curves. However, the damping coefficient can now further be used to calculate the corresponding background pressure. These values can then be compared to the monitored pressure in the setup. Eq. (2.41) can be permuted to

$$p \;=\; A \cdot \frac{1}{0.48242} \cdot 10^{-12} \left[\frac{\mathrm{eVs}^2}{\mathrm{cm}^2}\right] \frac{K_0}{q} \left[\frac{\mathrm{cm}^2}{\mathrm{eVs}}\right] p_0 \cdot \gamma \,. \tag{4.51}$$

A is the mass of the ions in atomic units $u = 1.0364273 \cdot 10^{-12}\,\mathrm{eVs}^2/\mathrm{cm}^2$ and $K_0 \approx 16 \left[\frac{\mathrm{cm}^2}{\mathrm{eVs}}\right]$. This leads for the highest extracted damping coefficient $\gamma = 2.54$ (for 1 s excitation time) to a background pressure of 3.3·10^{-6} mbar. For the lowest extracted value of $\gamma = 1.24$ (for 3 s excitation) a background pressure of 1.6·10^{-6} mbar is obtained. These values are slightly higher than the experimental values measured by the full-range vacuum gauges of 1-2·10^{-6} mbar. The difference is not unexpected, since the gauges are not directly placed at the position of the precision trap. Furthermore, these full-range gauges have usually uncertainties of up to 30%.

An extended description of damping effects in context of Ramsey pattern has been tested at the SHIPTRAP facility. An excitation ´scheme of two 25 ms excitation periods interrupted by a 50 ms waiting time has been used to measure a time-of-flight resonance with relatively high background pressure (see Fig. 4.5 (b)). The extracted damping coefficient is $\gamma = 3$ and is used to calculate the corresponding conversion profile (Fig. 4.5 (a)). The theoretical line profile describes very well the experimental data. Thus, the understanding of the resonance line shape for Ramsey excitation schemes is now completed. This allowed the application of the Ramsey method for high-precision mass measurements as described in the next chapter.

Chapter 5

Mass measurements at ISOLTRAP

High-precision mass measurements on the nuclides ^{26,27}Al and ^{38,39}Ca have been performed with the Penning trap mass spectrometer ISOLTRAP. These are the first isotopes measured with the Ramsey method applied in a Penning trap. A general discussion about the evaluation procedure and the present accuracy of mass measurements with ISOLTRAP can be found in [Kell2003, Mukh2008a]. Starting with a summary in view of the data analysis within this work, the mass measurements itself will be discussed. Especially the advantage of the Ramsey method with respect to the precision of the derived cyclotron frequency will be emphasized.

5.1 Principle of a mass measurement

Knowledge about the magnetic field strength B is indispensable for the mass determination via a measurement of the cyclotron frequency ν_c. Any other measurement device or technique to determine B with a precision comparable or even better than a measurement via the cyclotron frequency is not possible. To this end, the cyclotron frequency of a reference ion $\nu_{c,ref}$ with well-known mass is measured before and after the cyclotron frequency of the ion of interest. A linear interpolation of the two reference frequencies to the time, where the frequency of the ion of interest is measured, allows one to quote a cyclotron frequency ratio. Assuming all ions to be singly-charged, the frequency ratio can be used to derive the desired mass of the ion of interest:

$$m = \frac{\nu_{ref}}{\nu_c}(m_{ref} - m_e) + m_e \,, \tag{5.1}$$

whereas the magnetic field strength B cancels out. The mass m is now referred to the mass m_{ref} of the reference ion as well as to the electron mass m_e of the missing electron, respectively. The binding energy of a few eV of the removed electron is negligible in context of mass measurements of short-lived radionuclides since a typical uncertainty of a few hundred eV is obtained. As reference ion species carbon clusters are preferable [Blau2002], since they provide masses all over the nuclear chart, which are at most six mass units away from any nuclide of interest. Furthermore, they are traced back to the unified atomic mass unit u, which is defined as 1/12 th part of the mass of ^{12}C.

The derived mean frequency ratios $r = \frac{\nu_{c,ref}}{\nu_c}$ are the final results of ISOLTRAP. Thus, the determination of the mass of interest can later be repeated using an up-to-date mass value of the reference ion. The mean frequency ratios will later be included in the Atomic-Mass Evaluation (AME) (see Chap. 6). Beside the mass value its uncertainty has to be declared. In general it is composed of the experimental standard deviation of the frequency measurements according to the law of uncertainty propagation as well as of various systematic uncertainties in the measurement procedure. In the following the mass evaluation under consideration of the attending uncertainties at ISOLTRAP is discussed.

5.1.1 Frequency determination

A typical experimental TOF resonance curve of $^{39}K^+$ from the alkali ion source at ISOLTRAP, later used as a reference ion for the mass measurements of calcium isotopes, is shown in Fig. 5.1 (a). For such a resonance curve the time of flights at 40 different frequency points around the expected cyclotron frequency are taken. The chosen scan range depends on the excitation duration and thus on the line-width. The frequency difference between two points is chosen to be equidistant. The average ion number in a single measurement is kept close to two in order to minimize ion-ion interaction. In order to accumulate enough statistics the full sequence of 40 frequency steps is repeated several times. For the resonance in Fig. 5.1 approximately 10000 ions are taken, the duration of the excitation was chosen to be 300 ms resulting in a line-width of $\Delta\nu \approx 1/T_{rf} \approx 3.3$ Hz. The shape of the resonance curve is described by Eq. (4.44). A least-square fit of this function to the experimental data points is added (black solid line). This fit determines the central frequency with its statistical uncertainty. The time-of-flight uncertainties of the individual data points (see Fig. 5.1) are depending on the number of ions and on the width of the TOF distribution of the detected ions in each frequency point. The width of a TOF distribution depends on the position of the frequency point within the resonance curve. This is demonstrated in the inset of Fig. 2.12, where the distributions for non-resonant (1) and resonant (2) excited ions are shown. The resonantly excited ions (2) are clearly shifted to a smaller time of flight compared to the non-resonant case (1). Additionally, the time-of-flight distribution is in (2) much narrower than in (1). With a sufficient number of detected ions the reduced χ^2 of the fit should be close to one.

Among some parameters of the magnetic and electric fields in the drift section from the trap to the particle detector, the most important parameters describing the ion motion in the trap shall be discussed. They are used as free parameters in the fitting routine. Their impact will be demonstrated in the following:

The cyclotron frequency ν_c: It represents the center frequency of the resonance and is the parameter of interest. Fixing ν_c to wrong value shifts the whole resonance in the frequency domain (Fig. 5.1 (b)). Thus, the cyclotron frequency is of course a free parameter.

Initial magnetron radius $\rho_-(0)$: The parameter $\rho_-(0)$ determines the radial energy in the magnetron mode after the dipolar excitation in the precision trap. Choosing $\rho_-(0)$ too small leads in general to longer time of flight (see red line in Fig. 5.1 (c)), whereas

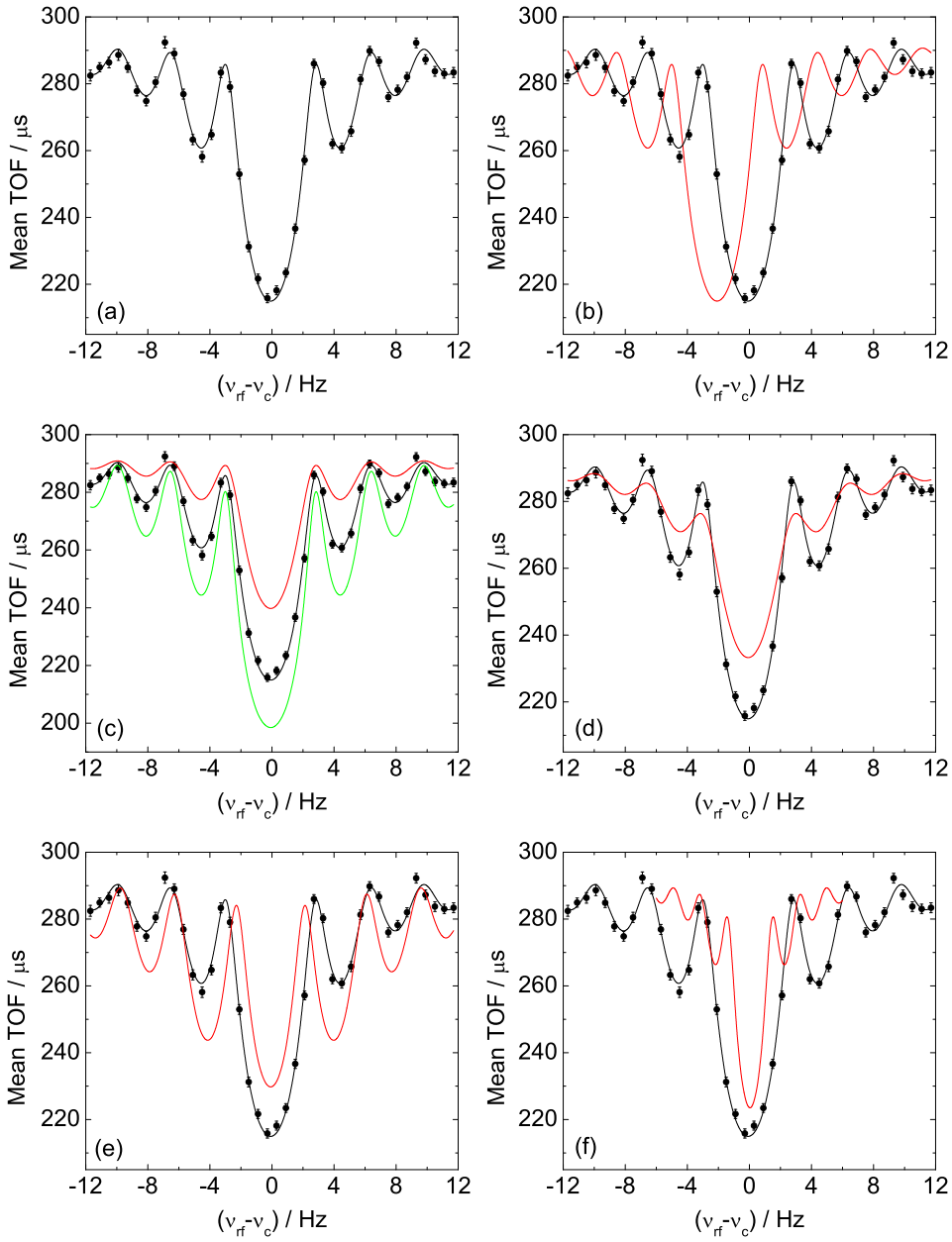

Figure 5.1: Influence of the main fitting parameters for the frequency determination. (a) shows the best possible least-square fit with a reduced χ^2 of 1.1. Fixing the resonance frequency to a smaller value leads to the red curve in (b). In (c) the magnetron radius $\rho_-(0)$ is either reduced (green line) or enhanced (red line). An increased damping coefficient smears the resonance (d). The effect of an on purpose wrongly chosen degree of conversion or excitation time T_{rf} is shown in (e) and (f), respectively.

a value of $\rho_-(0)$, which is too big, results in a reduced time of flight (see green line in Fig. 5.1 (c)). For non-resonant ions this shift is linear to ρ_-, for resonant excited ions the effect is amplified due to the energy gain via the quadrupolar excitation. The effect of

$\rho_+(0)$ is identical to the one of $\rho_-(0)$. Since $\rho_+(0)$ is expected to be zero it is not used as a free parameter.

Damping coefficient γ: This parameter describes the effect of a damping force due to collisions of ions with residual gas atoms or buffer-gas and is extensively studied in Chap. 4. Choosing a higher value for γ leads to the red damped curve in Fig. 5.1 (d).

Degree of conversion: Amplitude and duration of the rf excitation shall be chosen in a way that the degree of conversion equals one. Deviations from that may indicate wrong excitation settings and change the shape of the resonance (see Fig. 5.1 (e)).

Excitation time T_{rf}: The excitation time defines the width of the resonance, which is given by the Fourier limit $\Delta\nu = 1/T_{rf}$. It is not treated as a free parameter, since the duration of the excitation pulse is exactly given. Nevertheless, a wrong excitation time would result in a wrong FWHM of the resonance, as it can be seen in Fig. 5.1 (f), where the excitation time is increased on purpose to 600 ms (red curve).

The same parameters are used to fit Ramsey-type profiles to the corresponding sets of data. Only, the excitation time T_{rf} has to be replaced by the duration of one excitation pulse. Additionally, the waiting time between the two excitation pulses has to be introduced. But all of them are not regarded as free parameters. The fitting procedure delivers the desired cyclotron frequency ν_c and its statistical uncertainty σ_ν. Further evaluation and error propagation will be discussed in the following. The quantifiable effects that contribute to the uncertainty of the mean cyclotron ratio $r = \frac{\nu_{c,ref}}{\nu_c}$ will be presented and an upper limit on the unknown systematic uncertainties given.

5.1.2 Statistical uncertainty

The experimental standard deviation σ_ν of the extracted cyclotron frequency ν_c depends on two experimental quantities: (1) The resolving power of the trap, which is Fourier limited by the duration of the excitation time T_{rf} of the external quadrupole field, and (2) the number of recorded ions N. Introducing a dimensionless constant c leads to the empirical description [Boll2001]

$$\frac{\sigma_\nu}{\nu_c} = \frac{1}{\nu_c}\frac{c}{\sqrt{N}\cdot T_{rf}}\,. \tag{5.2}$$

The line width of a resonance at ISOLTRAP, called $\Delta\nu_c$, can be approximately described by $\Delta\nu_c \approx 0.8/T_{rf}$ [Boll1990]. In an extensive series of measurements with carbon clusters at ISOLTRAP the constant was determined to be $c = 0.898(8)$ [Kell2003]. A typical number of recorded ions in the reported measurements of short-lived radionuclides is approximately 2500 ions per resonance.

5.1.3 Contaminations

A mass separation takes place in all three traps of ISOLTRAP. The lowest resolving power offers the RFQ cooler and buncher in combination with the first pulsed drift tube. It is high enough to distinguish the reference ion species $^{39}K^+$, $^{85,87}Rb^+$, and $^{133}Cs^+$ from the alkali reference ion source. But is not sufficient to separate $^{85}Rb^+$ and $^{87}Rb^+$. This is

done in the preparation trap via a mass-selective buffer gas cooling (see Chap. 2) with a resolving power of up to 10^5. Nevertheless, unresolved isobaric or isomeric impurities in the radioactive ion beam cocktail of ISOLDE, decay products of short-lived radionuclides or products of charge exchange reactions with residual gas in the ISOLTRAP setup have to be expected. They may even not be resolvable in the precision trap with $m/\Delta m = 10^6$. A progress in cleaning of radioactive ion beam cocktails have recently been made by the successful application of a dipolar Ramsey-type excitation pattern, where the resolution has almost been doubled [Eron2008a]. The effects of the presence of contaminations in the precision trap have been studied carefully in case of a conventional quadrupolar excitation [Köni1995, Boll1992a] and are already mentioned in Chap. 2. From now on I will concentrate only on the most frequently case, where beside the ions of interest only one species of contaminations appears. If at maximum a single ion is stored in the trap in each measurement cycle, two separate resonance curves appear, assuming sufficient resolving power. Of course, one of the two resonances can be out of the scanning range of the quadrupolar excitation frequency. In this case the positions of the resonances are not affected, but the contrast in the time of flight between ions in resonance and off resonance is decreased. This is due to the calculated average time of flight of all ions excited with the same driving frequency. Increasing the number of ions in the trap will not change the frequency as long as space charge effects can be neglected and only one ion species is present. Having stored two ion species at the time in the trap their interaction effects a gradual approach of the two resonance peaks, while the centroid is shifted to a lower frequency.

However, it is possible to correct the shift originating from contaminations. Therefor, all recorded ions have to be divided into different count rate classes, *i.e.* different number of ions stored simultaneously in the precision trap. Then the cyclotron frequency is determined for all count rate classes, also called z-classes. Subsequently, the centroid frequencies of all classes are plotted as a function of the center of gravity of the specific count-rate distribution. A linear least-squares fit is then applied to the data points. With a detection efficiency of approximately 100% for a channeltron detector the data points are linear extrapolated to ion number one. Using an MCP detector with only 25(10)% efficiency at an energy of about 2 keV requires an extrapolation to 0.25. The uncertainty of this value is correlated to the uncertainty of the efficiency. Introducing the upper ν_{max} and lower ν_{min} values of the extrapolated cyclotron frequency leads to the corrected frequency and its uncertainty

$$\nu_c = \frac{\nu_{max} + \nu_{min}}{2} \tag{5.3}$$

and

$$s(\nu_c) = \frac{\nu_{max} - \nu_{min}}{2}\,. \tag{5.4}$$

This is the standard procedure for contaminated ion ensembles and described in more detail in [Kell2003]. Even though for all online experiments in this thesis the presence of possible contaminations can be excluded due to very clean molecular beams and careful investigations during the data taking period, the z-class analysis has been consequently performed. This conservative approach increased for a certain set of data the

uncertainty of the extracted frequency by factor 2-3 compared to an evaluation without z-class analysis. At ISOLTRAP high-precision mass measurements hampered by isobaric as well as by isomeric contaminations have already been performed successfully [Boll1992a, Roos2004, Webe2005].

5.1.4 Ramsey-type excitation of contaminated ion ensembles

Especially in the case of a mixture of isomeric states in the radioactive ion beam cocktail delivered by ISOLDE, the different cleaning processes at ISOLTRAP are often not sufficient. Hence, the determination of a mass is more difficult and the uncertainty of the derived value will increase. If the duration of the quadrupolar excitation is not long enough to reach a sufficient resolving power for two neighboring ion species, a single resonance line at the center of mass is observed (see Fig. 5.2 (a)). Its line width is narrower than expected from a linear superposition [Boll1992a]. Increasing the duration of the rf-excitation results in an improved sepration of the two states, see Fig. 5.2 (b,c). In case the mixing ratio R of the isomeric population N_{is} to the ground state population N_{gr} as well as the excitation energy E of the isomer are known [Audi2003a], the ground state mass m_{gr} can be deduced from the averaged mass of the mixed system m_{mix} by [Webe2005]

$$m_{mix} = m_{gr} + \frac{R}{R+1}E\,. \tag{5.5}$$

In the history of ISOLTRAP a number of mass measurements of isomeric states have been performed. Often, it was not possible to isolate a single state for a dedicated measurement. Examples can be found in [Boll1992a, Roos2004, Webe2005]. All these experiments have been performed with a single, rectangular pulse of rf-radiation. Thus, the shape of the resonance in the frequency domain, which is originated by the Fourier transformation of the excitation pulse, is similar to a sinc-function. Accordingly, the sidebands are strongly suppressed. Thus, two resonances could be distinguished as soon as the separation is large enough that the center peak of the first resonance is not overlapping any more with the center peak of the second resonance. For illustration see Fig. 5.2 (b). Employing a Ramsey-type excitation pattern will change this situation completely. In the theoretical limit two peaks of a δ-function serve as excitation. The resulting resonance in the frequency domain would evolve from the Fourier transformation of two δ-functions, which is a sinus-function. Thus, a resonance of equally peaks covering the whole frequency space would appear. Even in a real experiment, where the two excitation peaks are not shaped like a δ-function, but having a rectangular profile of short length, the resonance could cover most likely an area in the frequency domain, which is larger than the separation of the two resonances itself. To investigate the applicability of the in general advantageous Ramsey excitation pattern to contaminated ion clouds, a mixture of the ground and isomeric state of $^{121}In^{+}$ delivered by ISOLDE has been used. The indium isotopes were produced by bombarding an uranium carbide target with $3 \cdot 10^{13}$ 1.4-GeV protons per pulse from the CERN proton synchrotron booster. Isotopic separation was performed with the high-resolution separator HRS of ISOLDE. The half-lives of the ground state ^{121}In and of the isomeric state ^{121m}In are $T_{1/2} = 23.1\,\mathrm{s}$ and $T_{1/2} = 3.88\,\mathrm{min}$, respectively. Since the total measurement

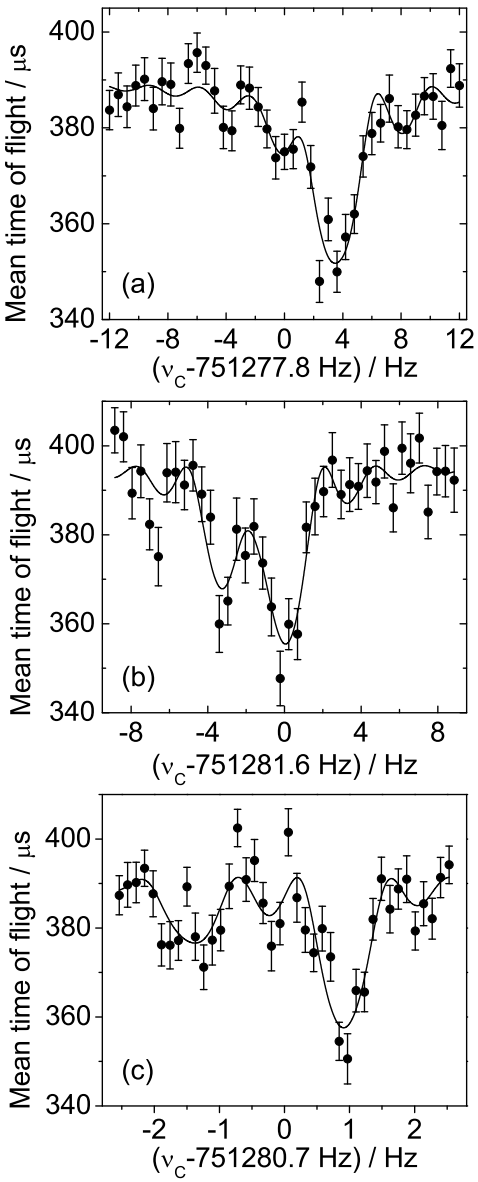

Figure 5.2: Conventional resonance curves of $^{121}In^{+}$, where both the ground state as well as the isomeric state are present with a mixing ratio $N_{gs}/N_{is} \approx 2$. The mass difference is 313 keV [Audi2003a], corresponding to 1.7 Hz difference in the precision trap. Thus, the required resolving power to separate the two states is $5{\cdot}10^5$. In (a) the excitation time was chosen to be $T_{rf} = 300$ ms with a resolving power of $2 \cdot 10^5$, not enough to resolve the two states. With an excitation time of 600 ms ($m/\Delta m \approx 4 \cdot 10^5$) the resonances are still not completely separated, although the two states are now clearly observable. An excitation time of 1.2 s ($m/\Delta m \approx 10^6$) is long enough to resolve the two states sufficiently.

cycle in the precision trap is not longer than 2 s, additional contaminations due to in-trap decay products can be neglected. The excitation energy is 313 keV [Audi2003a], which corresponds to 1.7 Hz frequency difference in the precision trap. This is usually sufficient to remove one of the ion species by an excitation at the mass-selective modified cyclotron

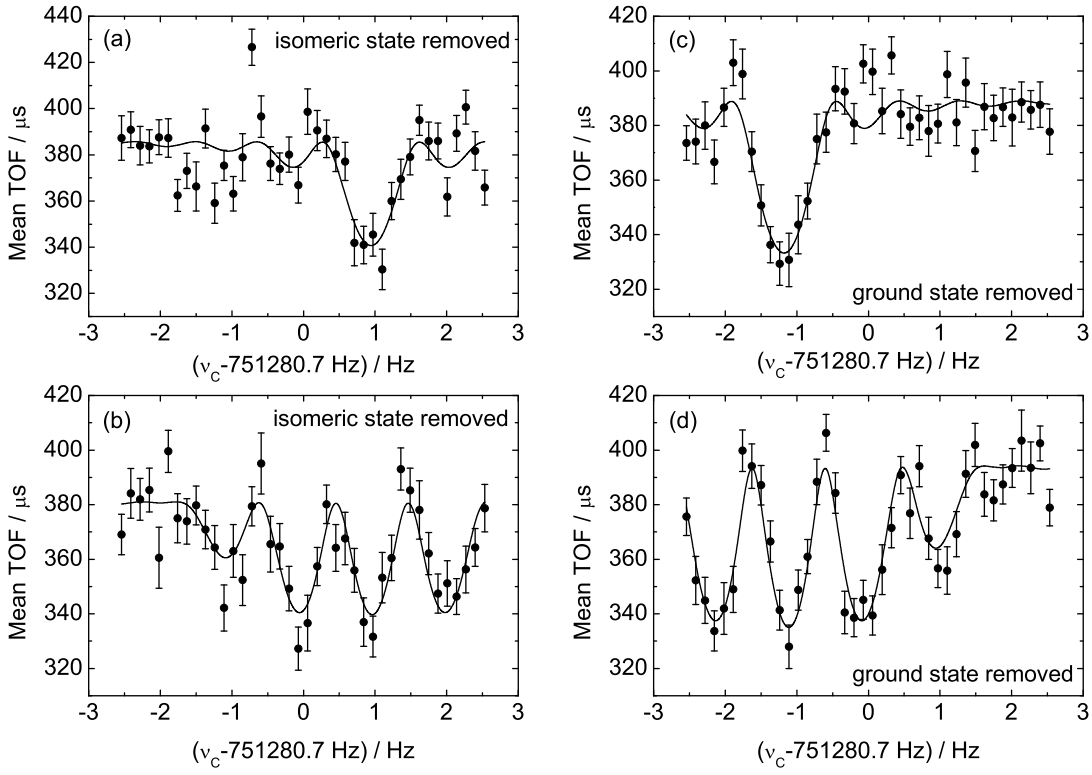

Figure 5.3: A dipolar cleaning is first applied either to remove the isomeric state (a,b) or the ground state (c,d) of ^{121}In in order to provide a clean ions ensemble. The purified ion ensemble has than been excited with a conventional one-pulse excitation (a,c) of 1.2 s or with a Ramsey-type excitation of two 300 ms excitation pulses interrupted by waiting period of 600 ms (b,d).

frequency. For the two states of ^{121}In this is demonstrated in Fig. 5.3, where either the isomeric state (a,b) or the ground state (c,d) is removed. It is further shown that beside the conventional one-pulse excitation (a,c) a Ramsey-type excitation scheme (b,d) can be used to determine the cyclotron frequency of one of the two states. In contradiction to the conventional excitation, where a frequency determination even with two simultaneously stored ion species is possible, a Ramsey-type excitation pattern is therefor not suited. A resonance curve of such a situation is shown in Fig. 5.4. Both states of ^{121}In with a mixing ratio of $N_{gs}/N_{is} \approx 2$ are stored in the trap, and subsequently all ions have been excited with a pattern of two 100 ms excitation pulses interrupted by a waiting period of 1 s. The expected resonance frequencies of the isomeric state (dashed line) and of the ground state (solid line), respectively, are indicated. Obviously the structure of the resonance is very complex due to the reduced width of the peaks as well as the enhanced depth of the sidebands. Certainly, a two resonance fit to the data would require a high statistical significance of the data points. This is counteracting to the principle idea of

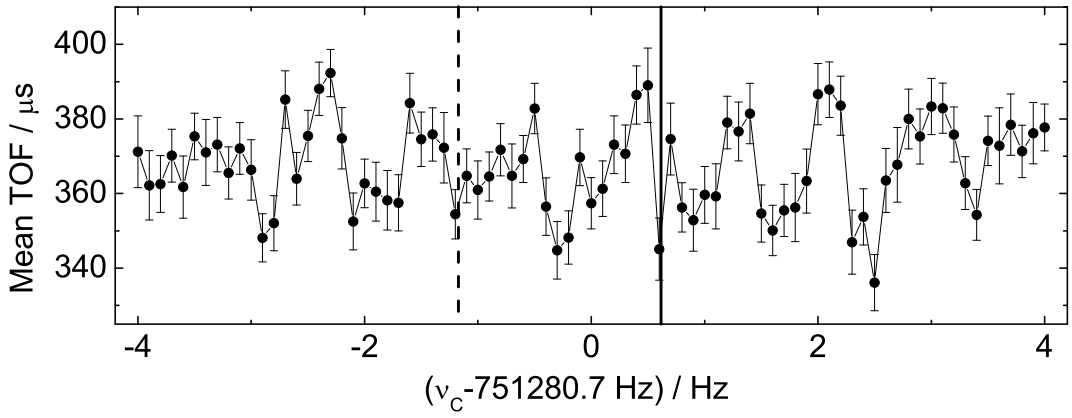

Figure 5.4: The ion ensemble at the mass of ^{121}In is not further cleaned in the precision trap of ISOLTRAP. Thus, both the ground as well as the isomeric state are present with a ratio of $N_{gs}/N_{is} \approx 2$. As excitation pattern a Ramsey-type excitation with two 100 ms long pulses and a waiting period of 1 s was chosen. The overlaping of the two resonance curves leads to a destructive interference, where no clear resonance structure is found in order to make a fit to the data points. The expected cyclotron frequency of the isomeric state, extracted from Fig. 5.3 is marked with a dashed line and the one of the ground state with a solid line, respectively.

the Ramsey-type excitation, which should reduce the needed number of recorded ions to reach a certain statistic as demonstrated in [Geor2007b, Geor2008]. Furthermore, if the cyclotron frequency of the contaminating species would differ by a multiple of the frequency distance between the center peak and a sideband of the ion species of interest, the presence of the contamination would be almost undetectable. These studies have a direct impact on the mass measurements described later. Since the Ramsey technique will be applied for the first time on high-precision mass measurements in a Penning trap, one has to carefully exclude any possible contamination prior the measurement.

5.1.5 Systematic uncertainties

Beside the statistical uncertainty of a frequency determination a couple of systematic uncertainties limit the precision of Penning trap mass spectrometry. The known uncertainties shall be discussed in the following paragraphs and an upper limit of unknown errors shall be assigned.

Time-dependent systematic uncertainties

In Sec. 5.1 the procedure to use a reference ion for calibration of the magnetic field has been introduced. The calibration procedure has to be performed regularly, since the magnitude of the magnetic field in the precision Penning trap varies by a couple of reasons as a function of time. Different mechanisms for this phenomenon have been identified. First, the current in the superconducting coils of the magnet decreases continuously with time due to the so called *flux creep* phenomena, which is extensively described in Chap. 2. The second reason for a change in the magnetic field is originated by environmental influences. Any ferromagnetic or paramagnetic material within a short distance around the magnet distorts the magnetic field lines and thus the homogeneity. To minimize this effect the use of such materials in the surrounding of the experiments has been constrained. Furthermore, the movement of remaining ferromagnetic or paramagnetic materials, as for example the crane in the ISOLDE hall, should be avoided.
Third, temperature and pressure fluctuations should be minimized in general for the following reasons: if the pressure on the recovery line for evaporated gaseous helium is subjected to fluctuations, the boiling point of the liquid helium changes. Thereby, the temperature of the helium and accordingly of the whole system alters. The temperature dependence of the magnetic permeability of the included materials then causes fluctuations in the magnitude of the magnetic field inside the trap [Dyck1992]. Additionally, the temperature of the experimental hall determines the temperature in the warm bore of the superconducting magnet. Thus, temperature fluctuations will change magnetic permeabilities of all surrounding materials and varies the magnetic field amplitude [Blau2005c]. Recently a temperature and pressure stabilization system has been developed in order to reduce the temperature variations of the precision trap setup to a few 10 mK over a time period of several hours [Mari2008]. In the future the stabilization system will allow for a more accurate determination of the magnetic field within calibration measurements. In the case of ISOLTRAP the magnet of the precision trap showed over a measurement period of 40 days a linear decay of [Kell2003]

$$\frac{\delta B}{\delta t}\frac{1}{B} = -2.30(3) \times 10^{-9}/h\,. \tag{5.6}$$

Thus, the actual magnetic field strength has to be interpolated by two reference measurements to the time, where the ion species of interest is measured. They should be performed shortly as possible prior and after the actual measurement of the dedicated ion species, since the reliability of this interpolation obviously decreases with an increased time window between the two reference measurements [Kell2003, Mukh2008a]. A careful investigation at ISOLTRAP shows a relative standard deviation of the reference cyclotron frequency of

$$\frac{\sigma_B(\nu_{ref})}{\nu_{ref}} = 6.35(45) \times 10^{-11}/\mathrm{min} \times \Delta T\,, \tag{5.7}$$

with ΔT being the time interval between the frequency measurement of the reference ion and the ion of interest.

Impact on the frequency ratio

As mentioned above, the frequency ratio at ISOLTRAP is the basic result of the measurements. It is not obtained by a single measurement cycle of reference ion - ion of interest - reference ion, but by a series of such measurements. Thus, a weighted mean $\bar{r}$ of all frequency ratios has to be calculated according to

$$\bar{r} = \frac{\sum_i \frac{r^i}{\sigma_c^2(r^i)}}{\sum_i \frac{1}{\sigma_c^2(r^i)}}\,, \tag{5.8}$$

whereas $\sigma_c(r^i)$ is the uncertainty of the i-th determination of the cyclotron frequency ratio. The relative standard uncertainty due to the magnetic-field drift is already included, such that the uncertainty calculated by Eq. (5.7) is added quadratically to the relative standard uncertainty in the cyclotron determination for the reference mass. The uncertainty of the weighted mean ratio $\bar{r}$ is accordingly

$$\frac{\sigma(\bar{r})}{\bar{r}} = \frac{1}{\bar{r}\sqrt{\sum_i \frac{1}{\sigma_c^2(r^i)}}}\,. \tag{5.9}$$

Mass-dependent systematic effect

Imperfections of the electrostatic quadrupole field and misalignment of the electrostatic potential with respect to the magnetic field axis can lead to a new origin of uncertainties: a mass dependent frequency ratio shift. It has been experimentally investigated at ISOLTRAP by use of carbon cluster ions of different size [Blau2002, Kell2003], whereas in the first order a linear dependence was observed:

$$\frac{\epsilon_m(r)}{r} = -1.6(4) \times 10^{-10}/u \times (m - m_{ref})\,. \tag{5.10}$$

Here, $(m - m_{ref})$ is the mass difference in atomic units between the ion of interest and the reference ion.

Residual systematic uncertainty of ISOLTRAP

After discussing the well-known sources of errors an estimation about the residual systematic uncertainty of ISOLTRAP is needed. Long-term measurements using carbon clusters have been used not only to determine time- and mass-dependent uncertainties, but also to assign an upper limit on unknown systematic uncertainties, which marks the present limit of mass accuracy of ISOLTRAP. Such tests have been performed in 2003 and an upper limit of

$$\frac{\sigma(r)}{r} = 8 \times 10^{-9} \tag{5.11}$$

has been reported [Kell2003]. The error due to the magnetic field drift is added already quadratically to the statistical uncertainty of the corresponding frequency ratio. In contradiction, the mass-dependent uncertainty as well as the residual systematic uncertainty of ISOLTRAP are entering the error budget at the end of the evaluation, when they are added in quadrature to the uncertainty of the mean ratio of all single measurements.

5.2 High-precision mass measurements at ISOLTRAP

After having discussed the evaluation procedure of mass measurements at ISOLTRAP under consideration of the statistical as well as the manifold systematic uncertainties, the results of high-precision mass measurements on the stable nuclide ^{27}Al as well as on the radionuclides ^{26}Al and ^{38,39}Ca will be presented. Thereby, Ramsey's method of separated oscillatory fields has been applied for the first time for the excitation of the cyclotron motion of short-lived ions in a Penning trap to improve the precision of their measured mass values in an on-line experiment. A further discussion of the obtained mass values in context of the Atomic-Mass Evaluation AME [Audi2003a] as well as their application in different fields of research will follow in Chap. 6. The results have already been published in scientific journals [Geor2007a, Geor2007b, Geor2008].

5.2.1 Ion production

All data presented here have been taken during two on-line beam times at ISOLTRAP in May and June 2006. In the first run the calcium isotopes have been addressed. They were produced by bombarding a heated titanium foil target with 1.4-GeV protons from the CERN proton-synchrotron-booster accelerator. Surface ionization with a hot tungsten surface of the released atoms were done. In order to suppress isobaric contaminations by $^{38}K^+$ ions, CF_4 was added and the ions of interest were delivered to ISOLTRAP in form of the molecular sideband $Ca^{19}F^+$. The ions were extracted from the ISOLDE ion source and subsequently accelerated to 30 keV, mass separated in the high-resolution separator HRS of ISOLDE, and injected into the ISOLTRAP apparatus. From that point the usual cleaning and measurement procedures described in Chap. 3 have been applied. In a second beam time aluminium isotopes were produced in a silicon carbide target. The number of protons per pulse and their energies were similar to the calcium experiments. A hot plasma source ionized the released atoms. Isotopic separation was performed with the general purpose separator GPS.

5.2.2 Measurements and results

After successfully testing off-line the application of Ramsey's method of separated oscillatory fields in order to excite the ion motion in a Penning trap [Boll1992b, Kret2007, Geor2007a], the first on-line application has been done at ISOLTRAP. TOF-ICR mass measurements of the isotopes $^{26,27}Al^+$ as well as $^{38,39}Ca^{19}F^+$ have been performed employing both Ramsey's method of separated oscillatory fields and the conventional one-pulse excitation in order to compare both methods in respect to the achievable precision for a given measurement time. In addition, the feasibility of separated oscillatory fields for the ion motion excitation under on-line conditions shall be demonstrated. Theoretical calculations and off-line tests showed the great advantage of smaller statistical uncertainties for a fixed number of recorded ions [Geor2007b]. This shall be profen in on-line

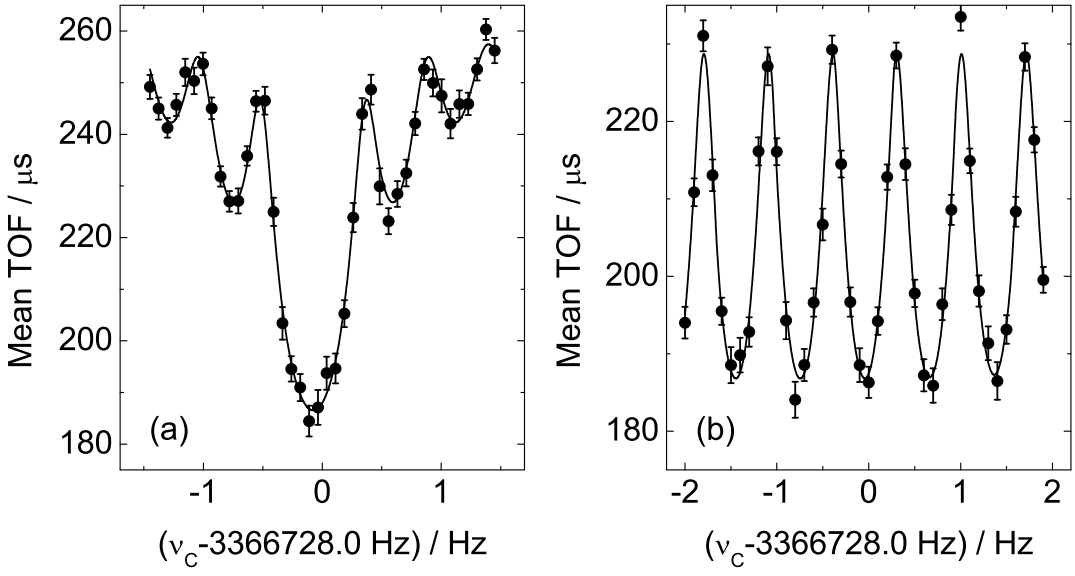

Figure 5.5: Time-of-flight ion-cyclotron resonance curves of ^{27}Al are shown. In (a) a conventional excitation with one pulse of 1.5 s duration has been used, while the Ramsey excitation applied in (b) has two 100 ms excitation pulses interrupted by a waiting period of 1.3 s.

measurements.

The number of recorded ions per resonance was kept constant at approximately 3000. Thus, the statistical uncertainties of both methods can be directly compared. In case of the aluminium isotopes the duration of the conventional one-pulse excitation pulse was chosen to be 1.5 s. For the Ramsey-type pattern two 100 ms excitation pulses were interrupted by a 1.3 s waiting period, such that the total duration of the excitation cycles is identical. In Fig. 5.5 resonances of ^{27}Al are illustrated, one for the conventional (a) and one for the Ramsey-type pattern (b).

Altogether five TOF-ICR measurements of each isotope have been recorded, two using the conventional method and three using the Ramsey-type pattern. As a reference ion species ^{23}Na, as well delivered by ISOLDE, was used. The derived frequency ratios including their uncertainties are shown in Fig. 5.6 (a,b). For a better illustration the average ratio R_{ave} has always been subtracted. The full dots in (a) denote the frequency ratios of ^{26}Al$^+$ to ^{23}Na$^+$ obtained by the conventional excitation, the empty circles mark data points according to Ramsey-type excitation. In (b) the filled squares are frequency ratios of ^{27}Al$^+$ to ^{23}Na$^+$ measured by the conventional excitation. For the data points shown as empty squares again the Ramsey pattern have been used. The gray bands indicate the uncertainties of the weighted mean ratios.

Five measurements, two using conventional and three using Ramsey-type excitation, have

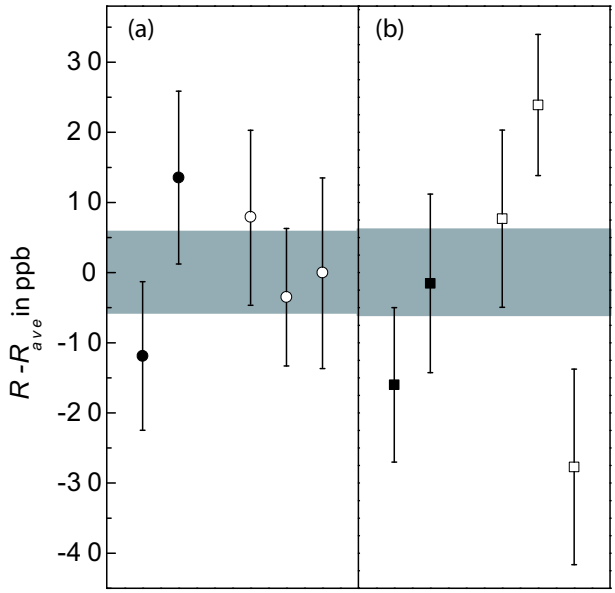

Figure 5.6: Difference between the measured cyclotron frequency ratios R and their average value R_{ave}. Each data point contains approximately the same number of recorded ions. Data points with filled symbols have been taken using the conventional excitation method, while empty symbols denote data points where the Ramsey method was applied. In (a) the difference R-R_{ave} for the ratio for $^{26}Al^+$ to $^{23}Na^+$ is shown. In (b) the same is plotted for the ratio of $^{26}Al^+$ compared to $^{23}Na^+$. The individual error bars include statistical as well as systematic uncertainties. The gray band indicates the uncertainty of the average ratio.

been performed in case of the molecular sideband $^{39}Ca^{19}F^+$ in comparison to the reference ion $^{39}K^+$ (see Fig. 5.7 (a)). In case of $^{38}Ca^{19}F^+$ eight resonance have been taken in total, six of Ramsey-type and two conventional ones. The frequency ratios including their uncertainties are shown in Fig. 5.7 (b). Due to the short half-life of ^{39}Ca ($T_{1/2}$ = 859.6(1.4) ms) the excitation time was reduced to 1.2 s and for ^{38}Ca ($T_{1/2}$ = 440(8) ms) to 900 ms, respectively. As before the duration of the Ramsey excitation pulses was 100 ms and the total cycle length has been kept identical to the conventional measurements.
No significant difference of the frequency ratios between conventional and Ramsey-type excitation has been observed. The weighted mean ratios of all measurements (see Table 5.1) were then used to derive the so called mass excess values, which is defined as

$$D = (m[\mathrm{in}u] - A)[\text{in keV}]\,, \tag{5.12}$$

where u is the atomic mass unit, defined as the twelfth part of the mass of ^{12}C and A the atomic number, respectively. Additionally to the overall mass excess values including both types of measurements, the individual mass excess values derived separately from both types of excitation are shown. Important to note are the small error bars next to the data points, which represent solely the statistical uncertainties of the different types of measurements and thus the tremendous benefit of the Ramsey-type excitation. In case of the ^{38,39}Ca the mean statistical uncertainty of the Ramsey-type excitation is less than

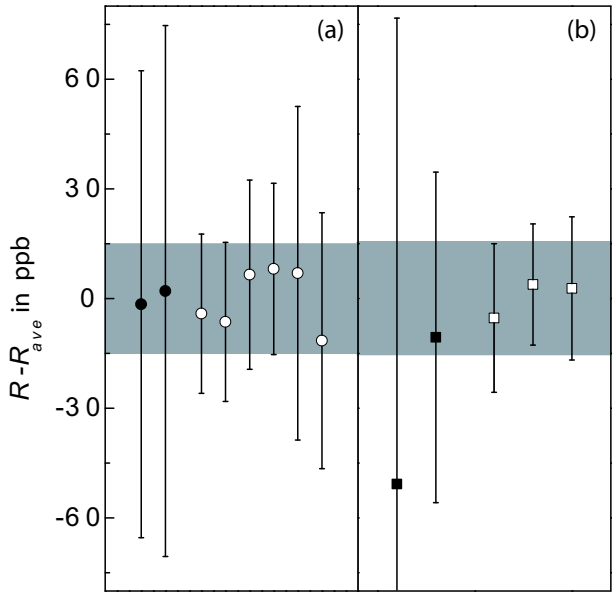

Figure 5.7: Same as Fig. 5.6, but now for $^{38,39}Ca^{19}F^{+}$ using $^{39}K^{+}$ as reference ions.

Table 5.1: Ratios of the cyclotron frequencies and the derived mass excess values of the isotopes investigated in this work.

Ion	$T_{1/2}$	Ref.	$\frac{\nu_{ion}}{\nu_{ref}}$	Mass excess / keV
$^{26}Al^{+}$	717 (24) ky	$^{23}Na^{+}$	1.1303707761(104)	-12210.18(22)
$^{27}Al^{+}$	stable	$^{23}Na^{+}$	1.1736365541(108)	-17196.92(23)
$^{38}Ca^{19}F^{+}$	440 (8) ms	$^{39}K^{+}$	1.4622576087(162)	-22058.01(60)
$^{39}Ca^{19}F^{+}$	859.6 (1.4) ms	$^{39}K^{+}$	1.4877789303(165)	-27282.59(61)

$2{\cdot}10^{-9}$, the lowest uncertainty ever achieved for a short-lived nuclide with $T_{1/2} < 1\,\mathrm{s}$. Here, only ISOLTRAPs unknown systematic uncertainties of $8 \cdot 10^{-9}$ are limiting the precision of the mass values [Kell2003, Mukh2008a]. In comparison the statistical uncertainty of the resonances, where the ions have been excited conventionally, is of the order of $1 \cdot 10^{-8}$. Of course one has to consider that there are six Ramsey-type resonances and only two of conventional type, respectively. Comparing the statistical uncertainty of any Ramsey-type resonance with a standard one, the uncertainty of the Ramsey-type resonance is decreased by approximately a factor of three to four. This agrees with the results of the extensive studies using stable reference ions [Geor2007a, Geor2007b].

However, for an excitation duration of 1.5 s the observed statistical uncertainty using the Ramsey-type excitation is only a factor of 1.8 smaller than for the conventional excitation, as seen for the Al isotopes. This effect is not yet understood and further detailed investigation is ongoing. The following assumption reveals the present status of the discussion: The statistical uncertainty of the frequency determination depends on two criteria. First,

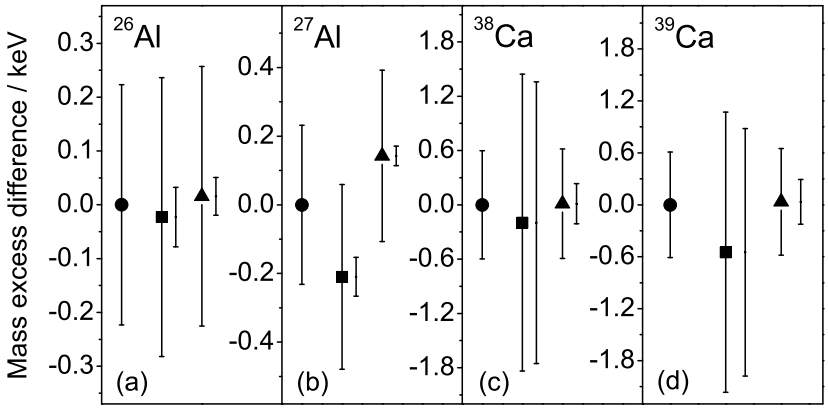

Figure 5.8: Mass excesses of all four radionucides derived from the ISOLTRAP measurements (full dots). In addition the mass excesses derived from measurements using the conventional excitation method (squares) as well as using the Ramsey excitation (triangles) are presented. The error bars next to the data points represent the statistical uncertainties.

the line width of the recorded resonance and second, the uncertainty of the measured mean time of flight of each frequency point. For a high number of collected ions compared to a broad line width, obtained from a short excitation cycle, the line width hampers the frequency determination. But for longer excitation cycles the uncertainty of the frequency determination is more and more dominated by the uncertainty of the measured mean time of flight of each frequency point, when the number of recorded ions is kept constant. Thus a further reduction of the line width will not improve the frequency determination unless the number of collected ions is increased.
Nevertheless, the Ramsey-type excitation is still favorable not only for shorter excitation cycles but also for larger ones: It allows, *e.g.*, for a 900 ms excitation a frequency determination which is more than three times more precise or vice versa it is about ten times faster to reach the same statistical uncertainty than using the conventional excitation. This gain in precision has been observed for a constant number of collected ions, comparable to the data of the mass measurements presented here. The Ramsey method has meanwhile been successfully adopted by the Penning trap experiments SMILETRAP [Suho2007], JYFLTRAP [Eron2008b], and CPT [Scie2009]. The final mass excess values derived from the new atomic-mass evaluation including the ISOLTRAP measurements will be shown in the next chapter accompanied by a discussion of their various applications.

Chapter 6

Discussion

In principle, the mass value excesses presented in Table 5.1 can simply be announced as the final result of the experiments. In some ways this is not advantageous. First of all, future changes in the mass values of the reference species would not be considered any more. This problem can be overcome by publishing the frequency ratios (see Table 5.1). Thus, at any time the frequency ratio combined with the latest mass value of the reference species will create an updated mass value. The second problem is that the masses of most nuclides have not been determined only once in the past, but many times over some decades. For example, mass values of the stable nucide ^{27}Al have been extracted from more than 50 individual measurements. Different experimental techniques such as decay spectroscopy, reaction measurements and Penning trap mass spectrometry have been applied. The achieved precision differed sometimes by orders of magnitude. Clearly, the mass values are often not agreeing within their uncertainties. Thus, the idea came to evaluate all the different measurements and calculate a weighted mean value of all input data. Subsequently, the first evaluation of atomic masses has been reported in 1960 at the First International Conference on Atomic Masses by A. Wapstra. The latest official Atomic-Mass Evaluation (AME) has been published by G. Audi and coworkers in 2003 [Audi2003b]. The Atomic-Mass Evaluation is important in the sense that it allows in principle all scientist to refer to the same mass value.

6.1 The Atomic-Mass Evaluation

Consequently, a new Atomic-Mass Evaluation incorporating the new ISOLTRAP values for ^{26,27}Al and ^{38,39}Ca has been performed in collaboration with G. Audi. A comprised version of the results have already been published in [Geor2008]. In the following the evaluation of the four measured nuclides will be discussed.

6.1.1 The mass of ^{26}Al

The mass value of ^{26}Al in the last Atomic-Mass Evaluation from 2003 was obtained by five measurements of four different types of reactions. They are shown in Fig. 6.1 (a). The highest impact derives from two independent measurements of the

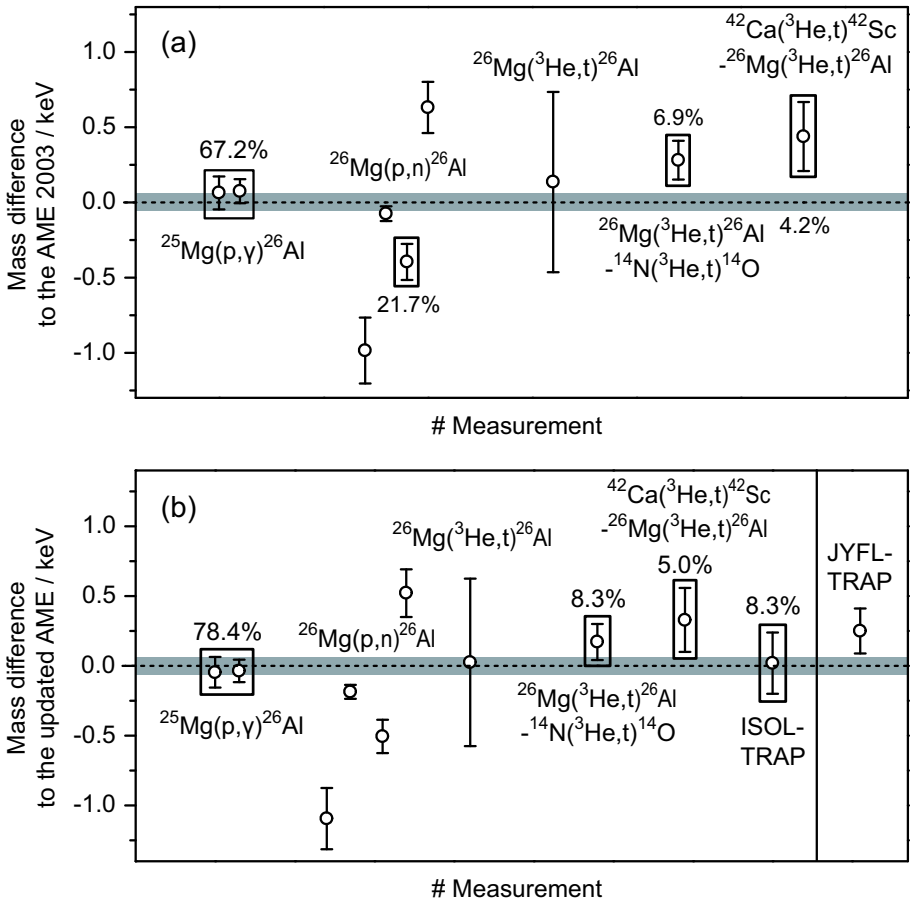

Figure 6.1: (a) Differences between ^{26}Al mass values derived from various reaction experiments and the average value of the atomic-mass evaluation from 2003 [Audi2003a], here denoted as zero line. The uncertainty of the atomic-mass evaluation is indicated as a gray band. The boxes mark the measurements which contribute to the accepted value at that time, whereas the impact of the individual type of measurements is reflected by the percentage of the contribution to the final value. (b) Same as graph (a) but including the ISOLTRAP measurement and a recently published Penning trap measurement of JYFLTRAP, which has not yet been included in the latest Atomic-Mass Evaluation. The zero line is slightly shifted due to the new average value in the new Atomic-Mass Evaluation.

reaction ^{25}Mg(p,γ)^{26}Al [Berg1985, Kiks1991]. In addition Q-values of the reactions ^{26}Mg(p,n)^{26}Al [Brin1994], ^{26}Mg(^{3}He,t)^{26}Al-^{14}N()^{14}O [Kosl1987], and ^{42}Ca(^{3}He,t)^{42}Sc-^{26}Mg()^{26}Al [Kosl1987] contribute to the mass of ^{26}Al, each of them with an individual weight. The value derived from the reaction ^{26}Mg(p,n)^{26}Al [Brin1994] disagrees with former measurements of the same group [Bark1984, Bark1992], but also with the four other measurements by more than three standard deviations. After the new evaluation this value is not taken into account any longer. Instead the ISOLTRAP value [Geor2008] is now contributing with 8.3%, whereas the reaction Q-values of ^{26}Mg(p,n)^{26}Al, ^{26}Mg(^{3}He,t)^{26}Al-^{14}N(^{3}He,t)^{14}O, and ^{42}Ca(^{3}He,t)^{42}Sc-^{26}Mg(^{3}He,t)^{26}Al are contributing with 78.4%, 8.3%,

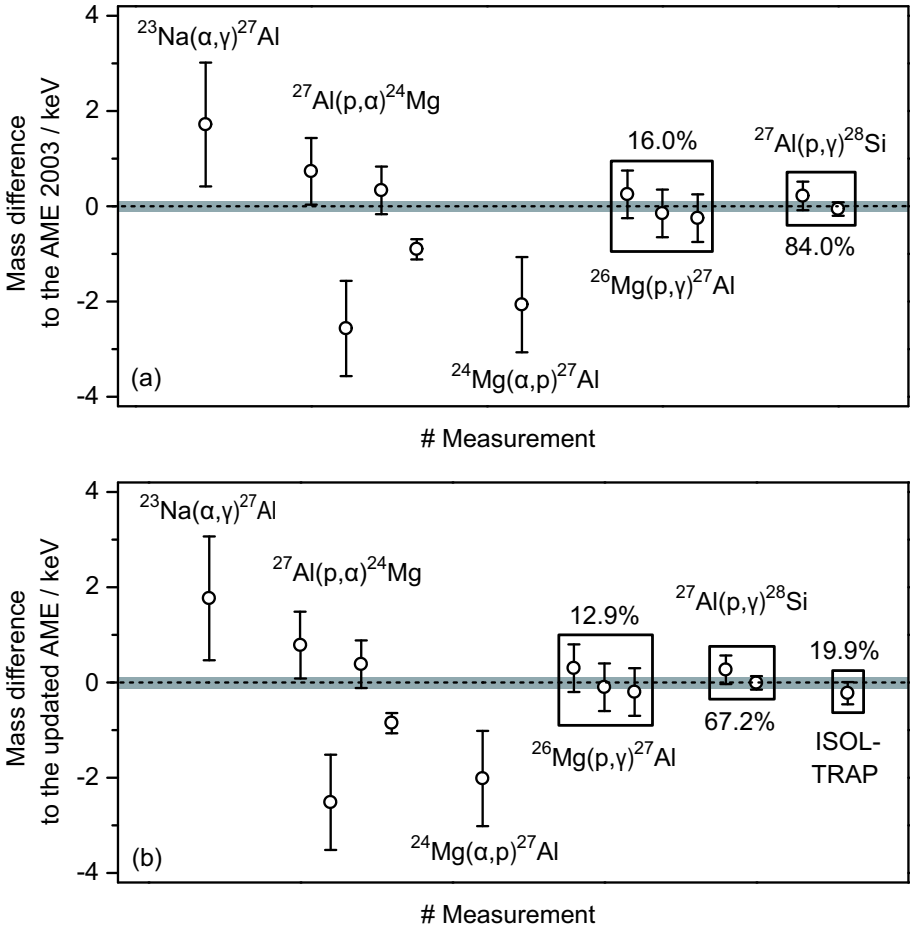

Figure 6.2: Same as fig. 6.1 but for ^{27}Al.

and 5.0%, respectively (see Fig. 6.1 (b)). Recently the Penning trap experiment JYFLTRAP published a mass excess value of -12209.95(16) keV [Eron2006a], which agrees very well with our value of -12210.18(22) keV, but is not yet included in the Atomic-Mass Evaluation. They did not measure the ground state mass of ^{26}Al directly, but the mass of the isomeric state ^{26m}Al. The well-known excitation energy can be used to derive the ground state mass. Altogether the new value for ^{26}Al has changed by 110 eV, which are almost 2 standard deviations. Additional, all data are listed with the corresponding references in Table A.1 in the addendum. Here, the order is identical to Fig. 6.1 (b). The deviations are related to the updated evaluation.

6.1.2 The mass of ^{27}Al

Five Q-value measurements of the reactions ^{26}Mg(p,γ)^{27}Al [Ande1959, Vand1963, Maas1978b] and ^{27}Al(p,γ)^{28}Si [Maas1978a] contributed to the mass value of ^{27}Al given in the AME2003. Together with some other reactions Q-values they are displayed in Fig. 6.2 (a) and are listed with the corresponding references in Table A.2. The three independent data points of the reaction ^{26}Mg(p,γ)^{27}Al and the two measurements of the

reaction ^{27}Al(p,γ)^{28}Si contributed 16.0% and 84.0%, respectively, to the mass value. Including the new mass measurement of ISOLTRAP [Geor2008], which is the first Penning trap measurement on ^{27}Al, the recent mass value of the AME shifts by 0.05 keV to a lower value. The ISOLTRAP measurements contributes now 19.9% to the new value. Therefore the influences of the reaction measurements of ^{26}Mg(p,γ)^{27}Al and ^{27}Al(p,γ)^{28}Si are reduced to 12.9% and 67.2%, respectively. All the contributing data points agree within the given uncertainties. Important to note is the fact that no Q-value measurement of the reaction ^{27}Al(p,α)^{24}Mg contributes at all to the mass value, even though the most precise data point has an uncertainty of only 0.21 keV [Maas1978a]. But this measurement has been rejected due to inconsistent data of the same group. The different Q-value measurements of this reactions, published by the same group, disagree with each other, although one has to consider the different level of precision with which they have been performed. Furthermore, it deviates by more than four standard deviations from the accepted mean value.

6.1.3 The mass of ^{38}Ca

The mass of ^{38}Ca was determined from the most precise of three Q-value measurements of the reaction ^{40}Ca(p,t)^{38}Ca [Hard1966, Padd1972, Seth1974], before Bollen and coworkers performed a mass measurement with the Penning trap mass spectrometer LEBIT [Boll2006]. Due to their large error bars the Q-value measurements of the reactions ^{36}Ar(^{13}He,n)^{38}Ca [Shap1969] and ^{24}Mg(^{16}O,2n)^{38}Ca [Zion1972] did not contribute to the mass of ^{38}Ca. The uncertainty of the mass value of ^{38}Ca was 5 keV (see Fig. 6.3 (a)). The Penning trap measurement reduced the uncertainty by more than one order of magntitude to 0.28 keV and lowered the value by 3.3 keV. At ISOLTRAP this new value has been confirmed [Geor2007a]. Here, the achieved uncertainty has been determined to 0.59 keV. Both values from Penning traps differ only by 0.43 keV. In the new evaluation of the AME the ISOLTRAP value contributes 17.7%. The main contribution of 82.3% still comes from the LEBIT measurement. Including the ISOLTRAP value the mass value is only shifted by 0.08 keV compared to the LEBIT value (Fig. 6.3 (b) and Table A.3 in the addendum).

6.1.4 The mass of ^{39}Ca

Up to now five Q-value measurements of different reactions are available to determine the mass of ^{39}Ca. Beside two measurements of the reaction ^{40}Ca(^{3}He,α)^{38}Ca [Rapa1971, Hind1966] and one Q-value measurement of the β^+-decay ^{39}Ca(β^+)^{39}K [Kist1958], where the uncertainty is on a level of a few ten keV, the lowest uncertainties have been obtained by two measurements of the reaction ^{39}K(p,γ)^{39}Ca (see Fig. 6.4 (a)). Despite their relative small uncertainties of 1.8 keV [Rao1978] and 6 keV [Kemp1970], respectively, they differ by more than 12 keV. In the paper of Rao and coworkers an explanation for this deviation is given. They mention a recalibration of the ^{27}Al(p,n)^{27}Si reaction Q-value, but this reaction was never used as a calibrant for the measurement of Kemper and coworkers. Kemper and coworkers only checked their calibration with the reaction

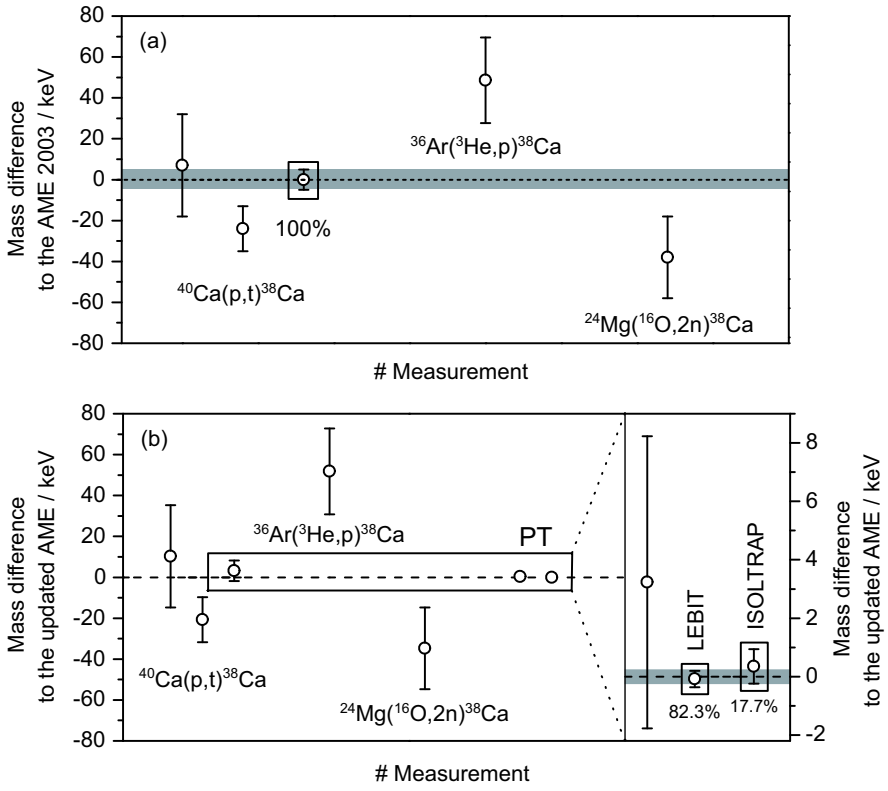

Figure 6.3: (a) Mass differences of ^{38}Ca derived from Q-value and Penning trap measurements compared to the previous value of the AME 2003, here denoted as zero line, in keV. In this case the value is derived up to 100% from the most precise Q-value measurement of the reaction ^{40}Ca(p,t)^{38}Ca. Its uncertainty is indicated by the gray band. In (b) the same is shown now including the result of ISOLTRAP. The new value is a weighted average of the two Penning trap measurements.

energy of ^{27}Al(p,n)^{27}Si. Until now the value of Rao *et al.* [Rao1978] was used as the AME value. The new ISOLTRAP value presented in this work disagrees with this value by more than four standard deviations. But it is in perfect agreement with the value of Kemper *et al.* [Kemp1970]. Since their uncertainty is one order of magnitude higher than the ISOLTRAP one, solely the new ISOLTRAP value is used for the AME, as shown in Fig. 6.4 (b). All data are listed in Table A.4.

6.2 Mass surface in the region of light nuclei

In Fig. 6.5 the nuclear chart of ^{26,27}Al, ^{25,26}Mg, and ^{28}Si including their connecting reactions is shown. Especially due to the stable nuclides ^{27}Al, ^{25,26}Mg, and ^{28}Si this system can be addressed easily and an over-determination of masses is obtained. Furthermore, the measurements have been performed with very high precision. Thus, small shifts in the data lead easily to disagreements. This occurs in the case of ^{26,27}Al, where the different types of reaction measurements do not agree with each other [Waps2003]. The

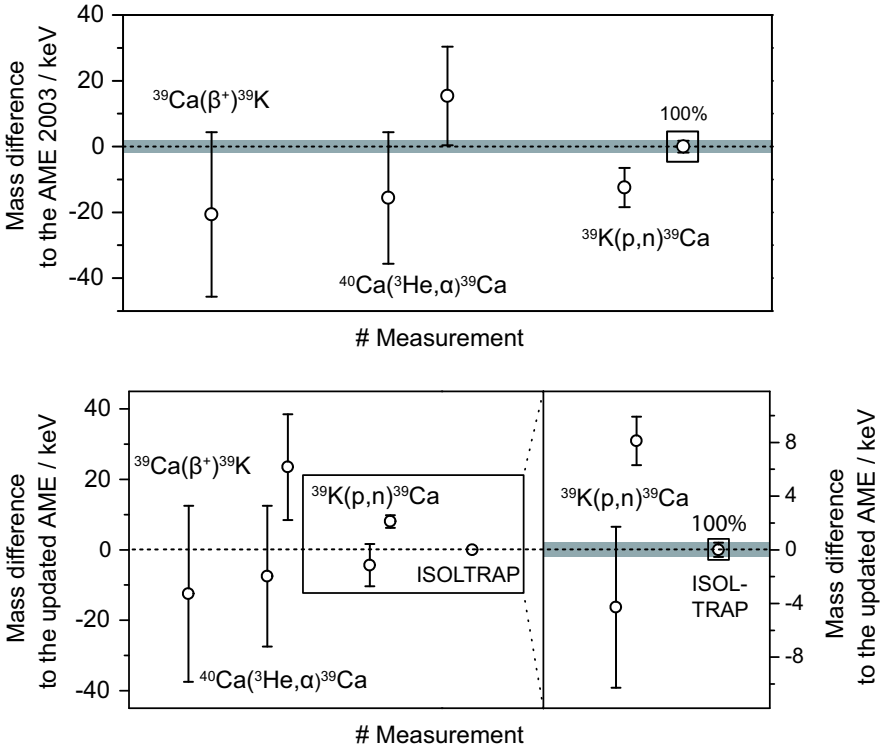

Figure 6.4: Mass differences of ^{39}Ca derived from Q-value measurements compared to the AME 2003 (a), here denoted as zero line, in keV. The value of the AME 2003 is identical with the latest Q-value measurement of the reaction ^{39}K(p,γ)^{39}Ca. Considering the most precise mass determination by ISOLTRAP a disagreement with the former value appears (b) and the ISOLTRAP value contributes after the readjustment 100%.

masses of the stable nuclides ^{24,26}Mg [Berg2003] and ^{28}Si [DiFi1994, Jert1993] have all been measured with Penning trap experiments. Furthermore, they are also related via reaction Q-values, namely ^{24,26}Mg by a pair of (n,γ) reactions through the stable isotopes ^{25}Mg and ^{26}Mg, and ^{28}Si by a pair of (p,γ) reactions via the isotope ^{27}Al. The masses of ^{25}Mg and ^{26}Mg are related by a sequence of a (p,γ) reaction and a (p,n) reaction via the isotope ^{26}Al (see fig. 6.5). The two most precise values of the ^{25}Mg(n,γ)^{26}Mg reaction agree neither with each other nor with the results from the combined ^{25}Mg(p,γ)^{26}Al and ^{26}Mg(p,n)^{26}Al reactions. A similar inconsistency occurs for the nuclide ^{27}Al in relation to the magnesium isotopes and ^{28}Si. This unsatisfactory situation is now resolved in the new Atomic-Mass Evaluation, when the ISOLTRAP values are included in the atomic-mass evaluation and the mass values derived from the ^{26}Mg(p,n)^{26}Al reaction are rejected due to inconsistency.

6.3 Test of the Standard Model

In Chap. 1 the importance and applications of nuclear masses were briefly discussed. Among tests of different mass models and reliable calculations of the stellar nucleosythe-

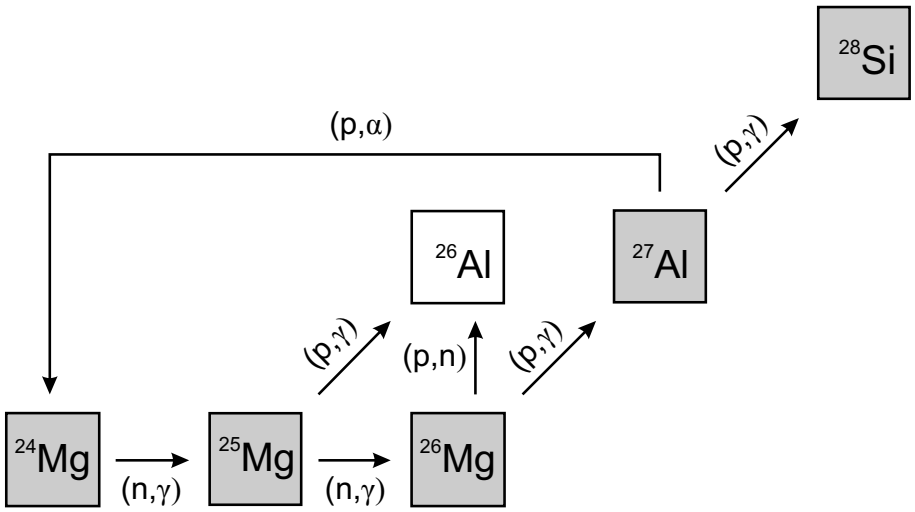

Figure 6.5: Section of the nuclear chart in the region of interest for the Al mass measurements indicating the reactions connecting the nuclides. Gray boxes denote stable isotopes.

sis are contributions to the verification of the Standard Model of particle physics an active research field of Penning trap mass spectrometry, which requires the highest precision of nuclear masses in context of short-lived radionucides. With respect to the mass measurements of ^{26}Al and ^{38}Ca within this thesis tests of the Standard Model will be discussed more extensively. The Standard Model itself is a theory including three of the four known fundamental interactions and the elementary particles that are effected by these interactions. It is a gauge theory of the strong, weak, and electromagnetic interactions with the gauge group $SU(3) \times SU(2) \times U(1)$. Still, the Standard Model is not a complete theory of fundamental interactions, since it does not include gravity. Furthermore, it can not explain observations of the neutrino oscillations. Due to its wide extension the Standard Model can be probed with many particle systems. Up to now, all experimental tests of the Standard Model have agreed with its predictions. The high-precision mass measurements presented in this thesis contributed to tests of fundamental concepts of the Standard Model.

Quarks, the constituents of hadrons, are the only particles in the Standard Model which experience all four fundamental forces. Their weak interaction is described by the so called Cabibbo-Kobayashi-Maskawa (CKM) quark-mixing matrix [Koba1973], which transforms the basis from quark weak-interaction eigenstates to quark-mass eigenstates. Recently, Kobayashi and Maskawa have been awarded with the Nobel Prize in physics 2008 for their theory. The Standard Model does not predict the matrix elements, but asks as a fundamental concept for the unitarity of the CKM matrix itself. The matrix elements can be experimentally derived from weak decays of the related quarks. The first element V_{ud}, which is the largest and most prominent one, is among others accessible via high-precision mass measurements.

Nuclear transitions between analog states of isospin, called superallowed $0^+ \rightarrow 0^+$ β-decays can be successfully described by the comparative half-life ft, where f is the statis-

tical rate function and t the partial half-life. The strongest contribution to the comparative half-life comes from the Q-value of the superallowed transition, which enters to the fifth power [Hard2005a]. Furthermore, it depends on the half-life $T_{1/2}$, the branching ratio b, and the electron capture fraction P_{EC} of the decay [Bamb1977], all of them experimentally accessible data. Additional, various theoretical correction terms have to be considered. Accordingly to the Standard Model all $0^+ \rightarrow 0^+$ β-decays are depending solely on the vector part of the weak interaction.
The conserved vector current (CVC) hypothesis claims identical ft values for all of these decays. Vice versa variations in the ft values of different nuclei may be hints for possible scalar parts in the weak interaction. The mean ft value of all transitions can be used to derive the vector coupling constant G_V. This is related via the Fermi coupling constant of the myon decay G_μ to the up-down matrix element V_{ud}. Supplementary, V_{ud} can be derived by other experimental approaches, such as measurements of the half-life [Nico2005] and asymmetry [Abel2002] of the neutron decay, the pion decay [Poca2004], or from nuclear mirror transitions [Navi2008]. This will not be discussed in detail, but all results will be compared to that one obtained by superallowed β-decays.
The comparative half-life ft can be written as

$$ft = \frac{K}{G_V^2 \left|M_F\right|^2} = const., \tag{6.1}$$

where K is a numerical constant and M_F is the Fermi matrix element, which has for isospin $T = 1$ states the value $M_F = \sqrt{2}$.
Unfortunately, some theoretical corrections have to be applied [Town2002, Town2008]. Since isospin is not an exact symmetry in nuclei a correction term has to be added to the nuclear matrix element M_F resulting in $\left|M_F\right|^2 = 2(1 - \delta_C)$. Furthermore, radiative corrections have to be added. Consequently, a "corrected" ft is expressed by

$$\mathcal{F}t \equiv ft(1 + \delta_R)(1 - \delta_C) = \frac{K}{2G_V^2(1 + \Delta_R^V)} = const.. \tag{6.2}$$

δ_C is the isospin-symmetry-breaking correction. δ_R and Δ_R^V are denoting the parts of the radiative correction, which are transition-dependent and transition-independent, respectively. The contribution of all corrections is at the order of 1%. Another way to distinguish the correction terms is to separate them concerning their dependency on the nuclear structure. Thus, the transition-dependent radiative corrections splits up into $\delta_R = \delta_R' + \delta_{NS}$. δ_{NS} depends like δ_C on the structure of the specific nuclei, whereas δ_R' is only a function of the electron's energy and the charge Z of the daughter nucleus. Thus, $\mathcal{F}t$ can be rewritten as

$$\mathcal{F}t \equiv ft(1 + \delta_R')(1 + \delta_{NS} - \delta_C)\,. \tag{6.3}$$

Incorporation of these theoretical corrections should result in identical $\mathcal{F}t$ values for all superallowed $0^+ \rightarrow 0^+$ transitions.
In 2005 J.C. Hardy and I.S. Towner published a comprehensive summary about the actual status of superallowed $0^+ \rightarrow 0^+$ β-decays, including all available experimental data as well as theoretical calculations [Hard2005a]. In their survey they addressed 20 of such

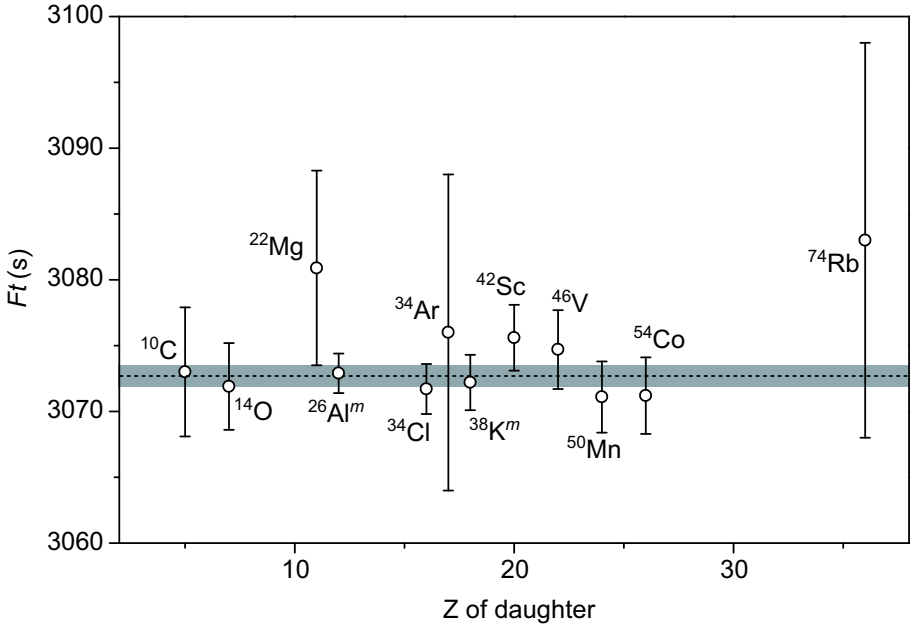

Figure 6.6: $\mathcal{F}t$ values plotted as a function of the charge on the daughter nucleus, Z (status 2004). The horizontal band gives the standard uncertainty of the average $\overline{\mathcal{F}t}$ value [Hard2005a].

decays covering the nuclear chart from ^{10}C to ^{74}Rb. They were able to confirm the CVC hypothesis, test the unitarity of the CKM matrix under consideration of the newest data for V_{us} and V_{ub}, and set an upper limit on any possible scalar interaction. In their evaluation Hardy and Towner considered all experimental data published before November 2004. ISOLTRAP contributed here with mass measurements for Q-value determinations on the nuclides ^{22}Mg [Mukh2004], ^{34}Ar [Herf2002], and ^{74}Rb [Kell2004a]. Experimental data of half-lifes $t_{1/2}$ and branching ratios b are used to determine the partial half-life

$$t = \frac{t_{1/2}}{b}(1 + P_{EC})\,. \tag{6.4}$$

Due to large differences in the uncertainties of the available experimental data only the 12 most precise measured transitions were contributing significantly to a weighted average value. These nuclides are shown in Fig. 6.6. Their average has been determined to

$$\overline{\mathcal{F}t} = 3072.7 \pm 0.8\,\mathrm{s}\,, \tag{6.5}$$

whereas the uncertainty is pure statistically. Important to note from the point of view of mass spectrometry is that only the $\mathcal{F}t$ values of ^{14}O and ^{46}V were so far limited by the precision of the Q-value. In all other cases the accuracies were limited by the half-life, the branching ratio or the various theoretical correction terms.
The presented set of data verified the CVC hypothesis at the level of 3×10^{-4}. Accounting for systematic uncertainties of the theoretical calculations by different models leads to

$$\overline{\mathcal{F}t} \;=\; 3073.5 \pm 0.8_{stat}\,\mathrm{s} \pm 0.9_{syst}\,\mathrm{s}\,. \tag{6.6}$$

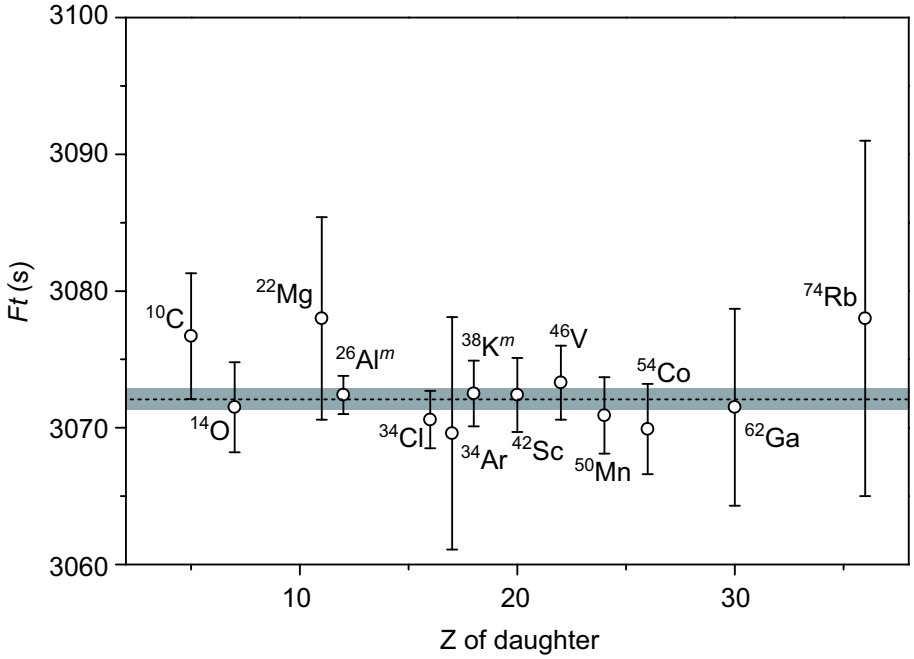

Figure 6.7: $\mathcal{F}t$ values plotted as a function of the charge on the daughter nucleus, Z (status 2008). The horizontal band gives the standard deviation around the average $\overline{\mathcal{F}t}$ value [Hard2008].

The mean $\overline{\mathcal{F}t}$ value of a consistent set of data can now be used to derive the up-down matrix element V_{ud} of the CKM matrix. This is linked to the vector coupling constant G_V and to the Fermi coupling constant of the myon decay G_μ via $G_V = G_\mu V_{ud}$. Using Eq. 6.2 leads to

$$V_{ud}^2 = \frac{K}{2G_\mu^2(1+\Delta_R^V)\overline{\mathcal{F}t}}\,. \tag{6.7}$$

The recent value of G_μ was obtained from the Particle Data Group (PDG) [Eide2004]. Thus, a final value for V_{ud} could be stated to

$$|V_{ud}| = 0.9738 \pm 0.0004\,. \tag{6.8}$$

A matrix is unitary, if the sum of the squares of elements in all rows or columns is equal one. Currently, the most demanding available test in case of the CKM matrix is obtained by the top-row with its elements V_{ud}, V_{us}, ad V_{ub}. Referring to the recommended values of the PDG 2004 [Eide2004], $|V_{us}| = 0.2200 \pm 0.0026$ and $|V_{ub}| = 0.00367 \pm 0.00047$, yielded

$$|V_{ud}|^2 + |V_{us}|^2 + |V_{ub}|^2 = 0.9966 \pm 0.0014\,, \tag{6.9}$$

which failed by 2.4 standard deviations. The values for V_{us} and V_{ub} were derived from measurements of the kaon-decay and from measurements of the B-meson-decay, respectively. But at the time of the review of Hardy and Towner [Hard2005a] already two new measurements of the kaon-decay existed, which both disagreed with the value of the

PDG [Sher2003, Alex2004]. Calculating a weighted average value of these two measurements leads to $|V_{us}| = 0.2259 \pm 0.0018$. This would change Eq. (6.9) to

$$|V_{ud}|^2 + |V_{us}|^2 + |V_{ub}|^2 = 0.9993 \pm 0.0011\,, \tag{6.10}$$

now satisfying the unitarity. Despite the fact, that V_{ud} has already been determined very precisely by the 12 best known transition, there is a strong demand to add more transitions to that collection. They would allow one in addition to test the theoretical calculations of the correction terms, which are often unconfident in their predictive power at the required level of accuracy. After November 2004, a number of new measurements related to half-lives, decay-energies and branching-ratios have been performed. Here, Penning trap facilities have strongly contributed with mass measurements for the superallowed transitions of ^{22}Mg [Mukh2004, Sava2004, Mukh2008b], ^{38}Ca [Boll2006, Geor2007a, Geor2008], ^{26}Al^m [Eron2006a, Geor2008], ^{42}Sc [Eron2006a], ^{46}V [Sava2005, Eron2006a], ^{50}Mn [Eron2008b], and ^{54}Co [Eron2008b]. Thereby the set of available data has been extended considerably. Very recently an updated survey of superallowed β-transitions has been published [Hard2008] including all new measurements until September 2008. In this line the high-precision mass measurements of ^{26}Al and ^{38}Ca reported in this thesis are included in the new evaluation. The most important modification with respect to the last survey is its extension to 13 very precisely measured transitions by consideration of the decay of ^{62}Ga. Their $\mathcal{F}t$ values are shown in Fig. 6.7 and their mean value with its statistical uncertainty is now determined to

$$\overline{\mathcal{F}t} = 3072.08 \pm 0.79\,\mathrm{s}\,. \tag{6.11}$$

Although this value is shifted by almost one standard deviation compared to 2005 [Hard2005a], it is still verifying the CVC hypothesis at the level of 3×10^{-4}. The shift is originated by a significant change of the isospin-symmetry-breaking correction δ_C due to improved shell-model calculations [Town2008]. Consideration of the systematic uncertainties as well leads to

$$\overline{\mathcal{F}t} \;=\; 3071.87 \pm 0.79_{stat}\,\mathrm{s} \pm 0.27_{syst}\,\mathrm{s} = 3071.87 \pm 0.83\,\mathrm{s}\,. \tag{6.12}$$

Nevertheless, the mean $\mathcal{F}t$ value showed a remarkable consistency in the past two decades. This is clearly a consequence of the large number of measurements contributing, which provide a robust set of data, not subjected to fluctuations caused by new measurements. But furthermore, it shows that $\mathcal{F}t$ and subsequently V_{ud} are very sensitive to changes of the theoretical correction terms. Thus, these theoretical calculations have further to be improved and tested. Especially ^{34}Ar [Herf2002] an ^{38}Ca (within this thesis) are suited for such tests, since these transitions have remarkable large corrections terms. The corresponding V_{ud} value is

$$|V_{ud}| = 0.97425 \pm 0.00022\,. \tag{6.13}$$

In comparison to (6.11) this value is shifted as well by one standard deviation. As mentioned before, V_{ud} can not only be determined by superallowed β transitions, but also by neutron and pion decay as well as by the mean $\mathcal{F}t^{mirror}$ value of nuclear mirror

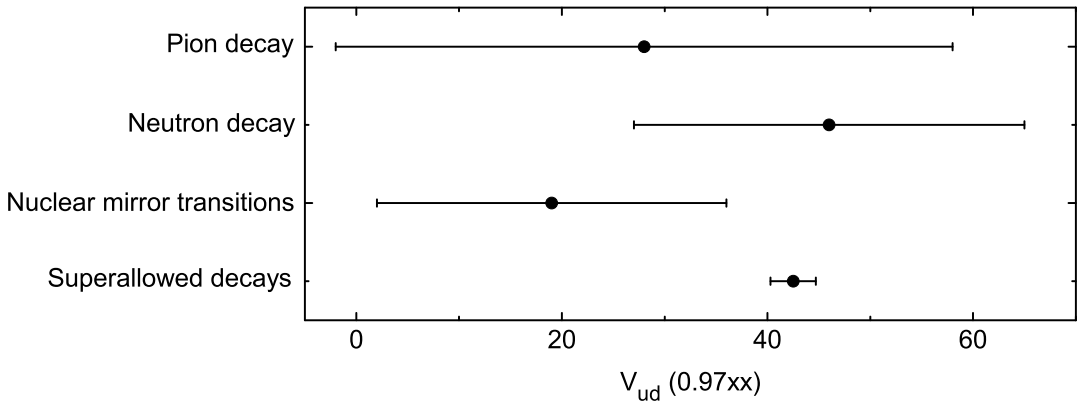

Figure 6.8: V_{ud} values derived from different experimental approaches are compared. The highest precision is by far obtained from measurements of superallowed β-decays.

transitions [Seve2008]. The most recent V_{ud} value derived from the neutron decay is the compilation of the Particle Data Group 2008 (PDG 2008) [Amsl2008]:

$$|V_{ud}| = 0.9728 \pm 0.0030\,. \tag{6.14}$$

The pion decay, which is in analogy to superallowed β decays a pure vector transition between two spin-zero members of an isospin triplet, yields

$$|V_{ud}| = 0.9746 \pm 0.0019\,. \tag{6.15}$$

The three investigated mirror transitions of ^{19}Ne, ^{21}Na, and ^{35}Ar deliver

$$|V_{ud}| = 0.9719 \pm 0.0017\,. \tag{6.16}$$

All four values of V_{ud} are illustrated in Fig. 6.8. They agree very well with each other, whereas the uncertainty of the value obtained from the superallowered β decays is more than an order of magnitude smaller than the uncertainties of the other values. Thus, superallowed transitions allow up to now the most stringent tests of the CKM unitarity. In the history of surveys of superallowed β decays the uncertainties of the published V_{ud} value steadily decreases, but the value itself showed a remarkable consistency within these data [Hard1990, Town1995, Town1999, Hard2005a, Hard2008]. An overview of $\mathcal{F}t$, V_{ud}, V_{us}, and the CKM unitarity for the past two decades is shown in Fig. 6.9. Important to note is the new assignment of V_{us} due to improved kaon decay measurements. Taking the recent values of V_{us} and V_{ub} from the PDG [Amsl2008] a test of the unitarity of the CKM matrix yields:

$$|V_{ud}|^2 + |V_{us}|^2 + |V_{ub}|^2 = 0.99995 \pm 0.00061\,. \tag{6.17}$$

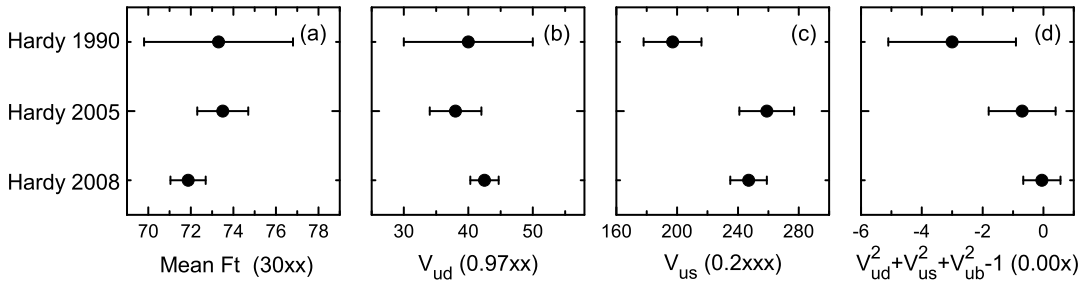

Figure 6.9: The history of some important constants to test the weak interaction are shown. The mean $\mathcal{F}t$ of superallowed β-decays (a) and the corresponding value of V_{ud} (b) showed a remarkable consistency in the past, although their values recently changed by almost one standard deviation due to improved calculations of the isospin-symmetry-breaking corrections δ_C. A significant change of V_{us} (c) a few years ago in combination with the shifted value of V_{ud} restored the unitarity sum of the first row of the CKM matrix (d).

Aside from incorporation of the first row of the CKM matrix, the unitarity can of course be tested in different ways. They are in described in detail in [Char2005].
Beside tests of the unitarity of the CKM matrix more concepts of the Standard Model can be proven. In general, the weak interaction is described by vector and axial-vector interactions, called $V-A$ theory, that maximizes parity violation. Until now no scalar or tensor interactions have been found in experiments, despite the fact of a steadily increasing accuracy. Thus, there is a strong interest of setting upper limits on the contribution of the latter two interactions to the weak interaction. Assuming that scalar and vector currents are time-reversal invariant and that the scalar current is maximally parity violating a tight limit on possible scalar contribution C_S with respect to the vector part C_V can be set. In the recent summary of Hardy and Towner [Hard2008] they claimed an upper limit of

$$\frac{C_S}{C_V} = 0.0011 \pm 0.0013\,, \tag{6.18}$$

which is consistent with zero.

Chapter 7

PENTATRAP project

Coming from mass measurements of short-lived radionuclides at the level of 10^{-8} I will report now on a new project dedicated to high-precision mass measurements at the level of 10^{-11}. As mentioned in the introduction, only a few mass measurements on stable and very long-lived nuclides at the level of better than $\delta m/m = 10^{-10}$ or even down to $\delta m/m = 10^{-11}$ have been performed so far [Rain2004, VanD2004, Shi2005, Reds2007, Reds2009]. Improvements of the most precise test of Charge, Parity, and Time Reversal (CPT) symmetry on the baryonic sector, which is presently the mass comparison of the proton and the antiproton at the level of $9{\cdot}10^{-11}$ [Gabr1999], or tests of the QED theory in extreme fields can be done by mass measurements of highly-charged, stable nuclides at the level of below $\delta m/m = 10^{-11}$. This corresponds for ^{208}Pb to a mass uncertainty of $\delta m \approx 2\,\mathrm{eV}$, which would allow to determine the binding energy of the last remaining (1s) electron in highly-charged Pb by measuring the mass difference of $m(\mathrm{Pb}^{81+})$ - $m(\mathrm{Pb}^{82+}) = m_e$ - E_B. It would be more precise than presently achieved by X-ray spectroscopy [Stöh2006]. Thus, a stringent test of quantum electrodynamics in the little explored regime of extreme electromagnetic fields could be performed.
For these purposes a new cryogenic Penning trap project dedicated to high-precision mass measurements on highly-charged ions has been developed and partly designed and constructed within this thesis. It is currently built up at the Max-Planck-Institute for Nuclear Physics in Heidelberg, Germany. An arrangement of three compensated and orthogonalized Penning traps for simultaneous ion preparation and mass measurement in combination with two monitoring traps for continuous B-field observation will provide a unique tool for mass measurements of isolated and cooled, highly-charged ions. In this chapter the design studies of the project are discussed and the status is presented.

7.1 Motivation

In order to motivate the need for a new ultra-high-precision Penning trap experiment the existing experiments and techniques are briefly discussed under consideration of their advantages and limitations. In principle two types of experiments can be distinguished:
(1) In open systems the ions of interest are produced outside the setup and then transferred into the Penning trap. This technique is generally used for mass measurements on short-

lived radionuclides [Sava2005, Boll2006, Eron2006a, Geor2007a, Ryjk2008] at radioactive ion-beam facilities. All of these setups are using so far the TOF-ICR detection technique and reach routinely a relative mass precision at the order of $\delta m/m = 10^{-8}$. Such mass measurements have been extensively presented and discussed in the previous chapters.

(2) In closed systems ions are directly produced inside the trap. This technique is mainly used to perform mass measurements on atomic or molecular ions of stable isotopes. Here, a non-destructive FT-ICR measurement technique is employed where the image current induced in the Penning trap electrodes by the ion motion is detected.

An enormous potential for an increase in precision, so far only used by the SMILETRAP experiment in Stockholm [Berg2002], is the use of highly-charged ions. Due to the relation between cyclotron frequency and charge state, the relative cyclotron frequency uncertainty $\delta\nu_c/\nu_c$ decreases linearly with the charge state. Unfortunately, in the environment of a tiny Penning trap setup dedicated to high-precision mass measurements, in-trap creation of highly-charged ions such as $^{208}Pb^{82+}$ is so far not possible. Thus, one has to design an open setup attached either to an electron beam ion trap (EBIT) source or an accelerator facility such as the HITRAP project at GSI [Klug2008]. The concept of using an EBIT as an ion source for a Penning trap was already demonstrated at the Livermore EBIT facility using RETRAP with charge states up to Th^{80+} [Schn1994]. The first mass spectrometer using routinely highly-charged ions was, as mentioned above, SMILETRAP. It explores the TOF-ICR detection with a mass precision down to a few parts in 10^{-10} [Nagy2006]. It was so far connected to a 50-kV electron beam ion source (EBIS) named CRYSIS for the production and delivery of highly-charged ions. The future SMILETRAP-II setup will be connected to a Super-EBIT. The TITAN experiment [Delh2006] at TRIUMF/Vancouver is presently commissioning a 60 kV EBIT [Froe2006] for stable and unstable nuclei.

As mentioned earlier, the achievable precision with Penning trap mass spectrometers is in general limited by unobserved magnetic field fluctuations during the measurement process. Advanced magnetic field stabilization techniques, such as a feedback control of the magnetic field [VanD1999] as well as a stabilization of the ambient temperature and the gas pressure in the helium dewar of the superconducting magnet [Berg2002, Mari2008] have been developed over the years. In cause of the TOF-ICR technique a minimum of 30 minutes of measurement time is typically needed during which the magnetic field remains unobserved. In order to reduce this limitations the SMILETRAP experiment interchanges the ion of interest and the reference ion after two frequency scans, *i.e.* within about two minutes. But at least 15 of such cycles are required to record sufficient ion events to obtain the resonance curves of the two ion species. Thus, a frequency comparison still requires about 30 minutes of measurement time [Berg2002] and limits the precision of the frequency determination. The advantage of the TOF-ICR technique is its applicability to very short-lived radionuclides with half-lives well below 100 ms [Kell2004a, Smit2008]. Unfortunately, the required number of ions hampers its use for mass measurements of ions species which are rarely produced (<1 ion/s) at radioactive ion beam facilities although recently a mass measurement on ^{252}No at SHIPTRAP with a production rate of 0.6 ions/s was reported [M. Block, *private communication*]. Altogether we can conclude that the long measurement cycle as well as the high number of required ions make the TOF-ICR

detection technique inefficient for our purpose to perform mass measurements of highly-charged ions at the level of $\delta m/m = 10^{-11}$ or even below.

Thus we have to concentrate on the image current detection. This is mainly used in closed systems, where all three eigenfrequencies of the ion motion in the Penning trap can be measured to obtain ν_c via Eq. (2.27). A coupling of the eigenmodes allows the determination of all frequencies of a single ion via its axial oscillation. These experiments are typically hampered by the time for the production, isolation, and preparation of a single ion in the trap.

Although in these experiments all three eigenfrequencies are commonly measured by using the image current technique, they have slightly different measurement principles. In 1992 E. Cornell *et al.* at MIT developed a technique to measure two ions of different species with nearly identical masses simultaneously stored on a common magnetron radius in the trap [Corn1992]. A detailed description of the technique can be found in [Rain2003, Thom2003]. It allows for mass measurements at the level of 10^{-11} for low charge states where the ion-ion perturbation of the Coulomb-force is well understood [Rain2004]. A similar approach of two ions in a trap has been performed by Gabrielse *et al.* [Gabr1999]: While one ion was measured in the center of the trap, the second one was stored on a big cyclotron radius to suppress ion-ion interaction. This technique was also implemented for mass measurements by M. Redshaw *et al.* [Reds2009] after the MIT-TRAP moved to Floria State University.

The two-ion techniques of these two groups, which allowed for the first mass measurements at the level of 10^{-11}, are not suitable for ions in high charge states as the project proposed here aims for. At their level of precision the experiments of the MIT group were limited by ion-ion interactions in the trap [Thom2003]: two singly-charged ions, separated by 1 mm, experience an additional electric field of $14.4\,\mu$V/cm due to the Coulomb force, compared to the radial trap electric field of approximately 1.2 V/cm. Using two ions with charge state 82+ and 81+, respectively, would increase the perturbation of the Coulomb interaction by more than 3 orders of magnitude and thus increases the systematic uncertainty, which is not acceptable for our purpose. Consequently, one has to further separate the highly-charged ions of different species or even store them in different traps by fast ion exchange.

7.2 The PENTATRAP project

Aiming for a relative mass precision of highly-charged ions at a level of 10^{-11} and below a completely new experimental setup and measurement procedure has to be developed overcoming the limitations of in-trap ion creation and Coulomb interaction mentioned above. To address the latter problem, beside the precision trap an additional trapping region, well enough separated from the precision trap, has to be established for storage of the second ion. This allows on the one hand unperturbed measurements in the precision trap and on the other hand a much shorter duration of a complete measurement process including magnetic field calibration.

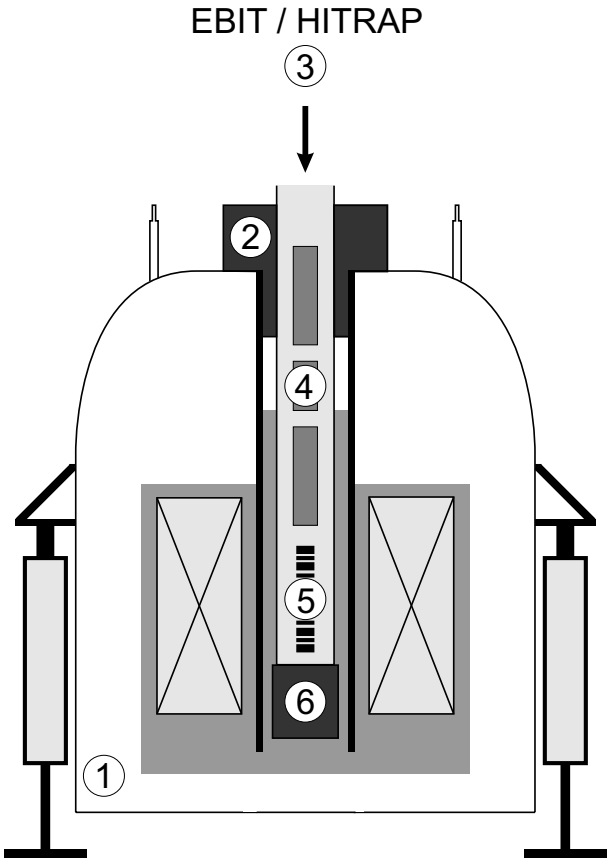

Figure 7.1: Sketch of the planned experimental setup: A superconducting magnet (1) contains a liquid helium cryostat, which cools the vacuum chamber as well as the superconducting coils of the magnet. A holder (2) keeps the vacuum chamber in a fixed position within the bore of the magnet. Ions are entering the experiment from top. They are delivered by an external ion source, an EBIT, or the HITRAP facility (3). They are guided via ion optic elements (4) to the Penning traps (5), which are placed in the homogeneous center of the magnet. Some parts of the cryogenic electronics are placed below (6) the chamber for the traps.

7.2.1 Experimental setup

A novel trap system will be placed in a vibration stabilized superconducting magnet with a field strength of approximately 7 T (see Fig. 7.1). It shall guarantee high-precision frequency measurements, fast measurement cycles, and a continuous B-field observation. A trap system with five five-pole cylindrical Penning trap regions (see Fig. 7.2) has been designed in the context of this thesis work. The three centered traps are compensated and orthogonalized and have identical electrode configurations. They are meant for ion storage, cooling, manipulation as well as for high-precision frequency measurements. Due to the fact that both ion species, the ion of interest and the reference ion, can be stored at the beginning of the experiment in the traps, a fast (but adiabatic) exchange between preparation and the measurement trap during the experimental cycle is possible, without any loss of time due to ion creation processes. At the bottom as well as on top of the

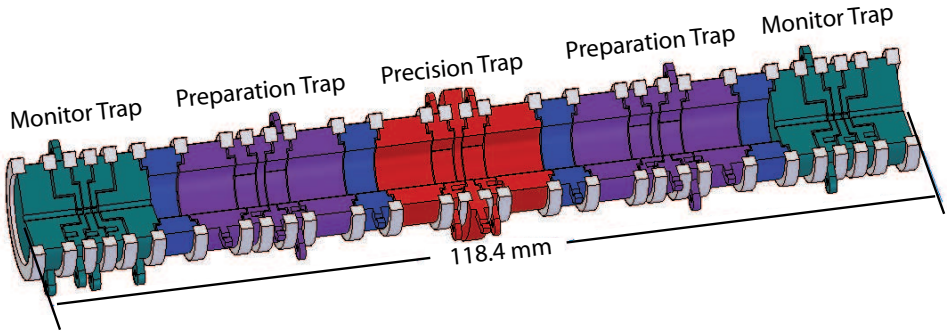

Figure 7.2: Sketch of the open traptower. The electrodes are made of oxygen free copper, covered with a 10 μm thick layer of silver and 2 μm thick layer of gold. Insulators between the electrodes are made of sapphire.

trap tower, two traps with an inner radius of only r_0=0.5 mm serve as so called "monitor traps" for a continuous observation of the magnetic field. This will allow for a correction of magnetic field fluctuations between two measurements of the reference ion. Thus, a further reduction of the uncertainty may be feasible. All frequencies will be measured by a well-established resonant detection method, which is routinely applied in different Penning trap experiments of our group, using high quality narrow-band resonance circuits connected either to cryogenic amplifiers or to superconducting quantum interference devices (SQUID). The trap-tower as well as the detection electronics will be surrounded by a 4.2 K environment of a helium cryostat. Highly-charged ions will enter the setup from the top. Furthermore, stable and well-controlled environmental conditions are needed to ensure highest precision measurements. Therefore, the complete setup will be placed in a separated temperature and pressure controlled room, in which the temperature stability will be 0.1 K or even below. In addition, a pressure regulation for the cryostat of the trap as well as of the magnet shall further stabilize the magnetic field. In the following the subsystems like trap design and detection systems will be addressed in more detail.

7.2.2 Measurement procedure

Two measurement schemes are foreseen for the PENTATRAP project, both illustrated in Fig. 7.3. Two ions are permanently studied in the monitor traps to observe the magnetic field. In the first scheme (see Fig. 7.3 (a)) the ion of interest as well as the reference ion are alternately measured in the central trap. At time t_1 the reference ion is measured and the ion of interest is being prepared in the right trap. Later, both ions are transferred one trap further and the ion of interest is precisely measured (t_2). At time t_3 the ions are moved back to the initial positions and the reference ion is measured again. This cycle can be performed within a few 10 seconds. It will be redone until the desired statistical precision is achieved. A second possible measurement scheme employs two of the precision

traps to measure simultaneously the reference ion and the ion of interest. Exchanging the ions between two measurements (see Fig. 7.3 (b)) reduces systematic uncertainties such as different field strengths B in the traps.

In Fig. 7.4 the use and advantage of the monitor traps is illustrated. The usual way of determining the frequency ratio is illustrated in Fig. 7.4 (b) and can be summarized as follows: A reference ion with well-known mass is stored in the precision trap and its cyclotron frequency is measured at a time t_1. Then the ion is exchanged with the ion of interest and its frequency is determined at t_2 (Fig 7.4 a). Afterwards again the reference ion is measured at a time t_3. Now the two frequency measurements of the reference ion are used to interpolate the frequency linearly to the time t_2, when the ion of interest was measured. Unfortunately, but unavoidable, this interpolation increases the uncertainty of the frequency determination of the reference ion at time t_2 (see the light gray frequency point in Fig. 7.4 (b)) as studied extensively at ISOLTRAP [Kell2003] and described previously.

The first improvement in this direction is achieved by the use of the two preparation traps for ion storage in the PENTATRAP setup. One single ion of each species can be stored and initially prepared in the experiment simultaneously. Thus, during the experiment a fast exchange of both ions is possible. This reduces the time period between t_1 and t_3 significantly (see Fig. 7.4 (c)). Note, that the time-axis is not to scale. But still there is a time period during the measurement of the ion of interest, in which the magnetic field is not observed. At this point the monitor traps are considered to overcome this limitation. In both traps an ion with a large q/m-ratio (about 0.5) will be stored, which permanently monitors the magnetic field at the position of the monitor traps by measuring ν_+. Magnetic field shifts, which arise from the magnet itself, are assumed to be present along the complete traptower. Thereby, relative shifts in the monitor traps can be scaled to shifts in the precision trap (see Fig. 7.4 (d)). Thus, the uncertainty about the frequency of the reference ion at time t_2 can further be reduced. This has to be of course extensively investigated prior to mass measurements with the PENTATRAP apparatus.

7.2.3 Limitations

Still, the achievable precision of the measurement is limited due to several reasons. The residual gas pressure leads to collisions between rest gas molecules and stored ions, resulting in a charge exchange with the highly-charged ions as well as in a damping of the eigenmotions. The damping is typically accompanied by a frequency shift of the eigenmotions. Furthermore, they will be disturbed by the induced image charges as mentioned before.

In the context of the measurement cycle it is important to consider especially the storage time of the trapped ions, which is limited by charge exchange with residual gas atoms. Since the environment is cooled to 4.2 K He and H_2 are the only neutral particles which will not adhere to the cold surfaces. In the following we approximate that mainly H_2 molecules are present. The probability for a charge exchange depends on the mean free path of the ion and the charge exchange cross section. Here, a maximum pressure of

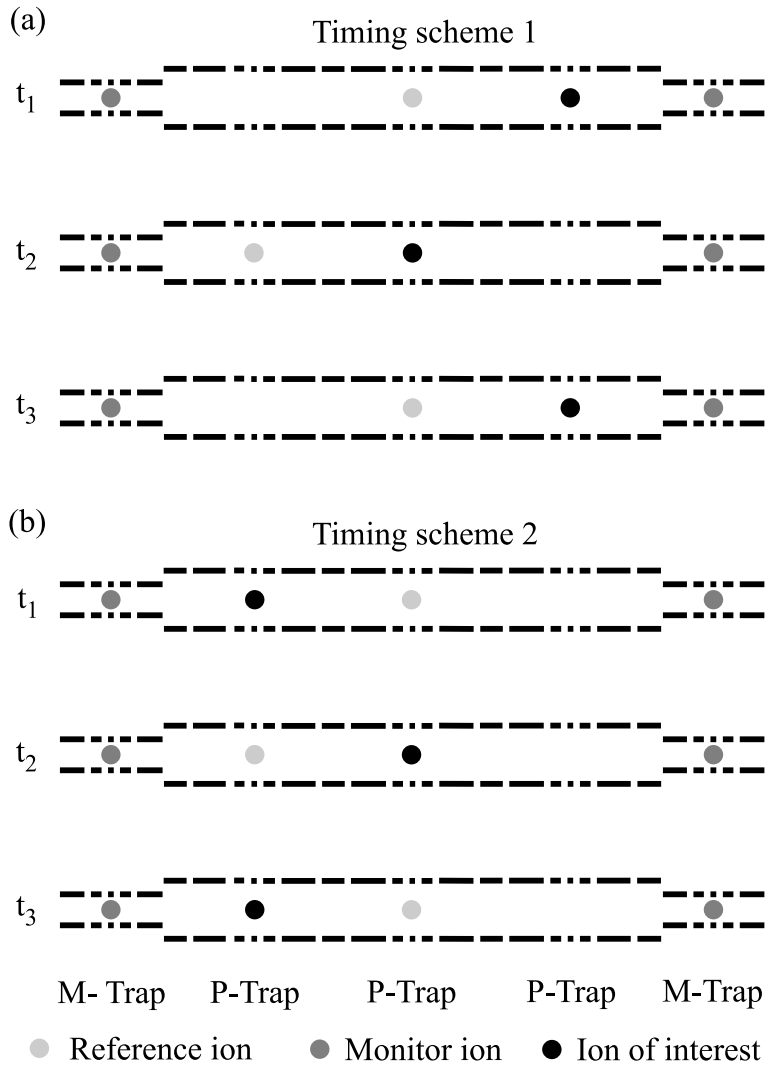

Figure 7.3: A cartoon of possible measurement cycles in PENTATRAP. In (a) the frequency of the reference ion is measured in the central trap at t_1, while the ion of interest is prepared in the right preparation trap. At t_2 both ions are transferred one trap further and the ion of interest is measured in the central trap. Afterwards both ions are moved back to the initial positions and the reference measurement is performed again. In parallel the B field is monitored via the two ions in the monitor traps to the left and to the right. The measurement scheme in (b) differs such that the frequency ratio of both ions is determined directly by a parallel frequency measurement in two of the three traps. An exchange of the ions between two measurements shall minimize the uncertainties due to the different localization of the ions.

10^{-14} mbar is aspired for the experiment. The mean free path $x(t) = \hat{v} \cdot \tau$, with τ the mean time between two collisions and $\hat{v}$ the mean thermal velocity, is given as:

$$\hat{v} = \sqrt{< v_{H_2}^2 > + < v_{ion}^2 >} = \sqrt{3kT \left(\frac{1}{m_{H_2}} + \frac{1}{m_{ion}} \right)}. \tag{7.1}$$

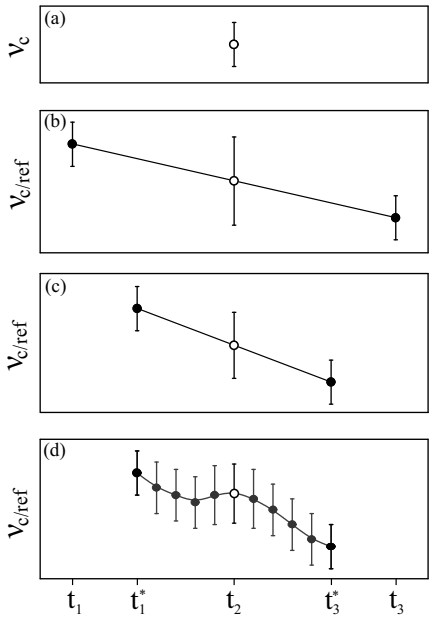

Figure 7.4: A measurement cycle of the new trap setup. Before (t_1) and after (t_3) a frequency measurement of the ion of interest at time t_2 (a), a reference ion is used to calibrate the magnetic field (b). The required linear extrapolation to the desired time increases the uncertainty (empty data point in the middle). This time period is significantly reduced, when both ion species are stored simultaneously in the trap setup. To avoid ion-ion interactions they are spatially separated and prepared in different trapping regions. Thus, they can be exchanged quickly during the measurement cycle (time t_1^* and t_3^*) (c). A further reduction of the uncertainty can be achieved by a continuous B-field observation in the so called monitor traps. The relative magnetic field shifts are adopted to shifts in the precision trap (d).

The pressure is given by

$$p = nkT = \frac{kT}{\sigma \hat{v} \tau}\,, \tag{7.2}$$

where σ is the charge exchange cross section. It can be described by $\sigma = \pi \cdot R_c^2$, where R_c is estimated using the classical over-barrier model to be $R_c = \frac{2\sqrt{q}+1}{I_p}$. Here, q is the charge state of the ion and I_p the ionization potential of the atom [Mann1986, Herm1999]. R_c is given in atomic units. Using these equations one can calculate the mean storage time of $^{208}Pb^{82+}$ to be approximately 25 minutes, which is at least acceptable for some measurement cycles. To overcome the problem of limited storage time of the ion species in the monitor traps, $^4He^+$ or $^4He^{2+}$ are foreseen as monitor ions.

7.3 Trap design

The traps have been designed such that the electrostatic potential is as harmonic as possible and magnetic field inhomogeneities due to the electrode material in the strong

magnetic field are minimized. First, the electrostatic potential will be considered: Confining a particle in a desired volume by electric fields implies that the mean value of the electric field with respect to time vanishes:

$$\left\langle \vec{E}(r,z,\Theta;t) \right\rangle_t = \left\langle \vec{\nabla} \cdot \Phi(r,z,\Theta\ t) \right\rangle_t = 0\,. \tag{7.3}$$

The potential of the electrostatic field $\vec{E} \neq \vec{E}(\mathrm{t})$ with cylindrical symmetry $\Phi \neq \Phi(\Theta)$ has to fulfill the Laplace equation:

$$\Delta\Phi(r,z) = 0\,, \tag{7.4}$$

neglecting any free charges and the confined ion itself in the trap volume. A general solution of the problem can be written in terms of a Taylor expansion [Verd2003]:

$$\begin{aligned} \Phi(r,z) &= \sum_{j=0}^{\infty}\left[\sum_{i=0}^{j}\frac{1}{j!}\begin{pmatrix} k \\ i \end{pmatrix}\left.\frac{\partial^j\Phi}{\partial r^i\cdot\partial z^{j-i}}\right|_{(0,0)}\cdot r^i\cdot z^{j-i}\right] \\ &= \sum_{j=0}^{\infty}\left(\sum_{i=0}^{j}\frac{1}{j!}C_{i,j}\cdot r^i\cdot z^{j-i}\right)\,. \end{aligned} \tag{7.5}$$

Compensated, cylindrical five-pole Penning traps as tools for precision experiments have been discussed extensively by Gabrielse and Mackintosh [Gabr1984]. Compensation of the Penning trap means that the electrostatic potential is as much harmonic as possible. Thus, in principle all coefficients $C_{i,j}$ $(i,j \geq 4)$ in Eq. (7.4) have to vanish. In real Penning traps only $C_{0,4}$ and $C_{0,6}$, the most important disturbing terms, cancel out. In the five-pole Penning trap two additional correction electrodes are added between the end-caps and the ring electrode to consort the electrostatic potential. An analytical solution and discussion of the potential can be found in [Verd2001, Verd2003]. In Fig. 7.5 such a five-pole trap configuration is shown. It has a symmetry axis in the z-direction and a symmetry plane at z=0. Thus the potential is rotationally symmetric and the odd terms of the Taylor expansion $(C_{i,j}, \forall(i,j) i+j = 2n-1)$ vanish. Since the magnetic field confines the particle in the radial plane, we define the z-direction in which the particle is trapped electrostatically. From now on the relevant coefficients $C_{0,j}$ are labeled C_j. The determination of the potential $\Phi(r,z)$ is a well-known electrostatic boundary value problem. With the conditions and parameters shown in Fig. 7.5 the solution is [Verd2001, Verd2003]:

$$\begin{aligned} \Phi(r,z) &= \sum_m \left\{ \frac{8U_0}{l\cdot d\cdot k_m^2\cdot I_0(k_m R_0)}\sin\left(\frac{k_m d}{2}\right)\left[\sin\left(\frac{k_m(d+l_r)}{2}\right)+\cdots\right.\right. \\ &\quad \left. +2\,T\sin\left(\frac{k_m(d+l_c)}{2}\right)\cos\left(\frac{k_m(2d+l_r+l_c)}{2}\right)\right] \\ &\quad \left. I_0(k_m r)\cos(k_m z)\right\}, \end{aligned} \tag{7.6}$$

where $k_m = m\pi/l$ $(m = 2n-1,\ n \in \mathbb{N})$ and $l = 4d + 2l_e + 2l_c + l_r$ is the total length of the trap. $T = U_c/U_0$ is the tuning ratio with U_c being the correction voltage and U_0

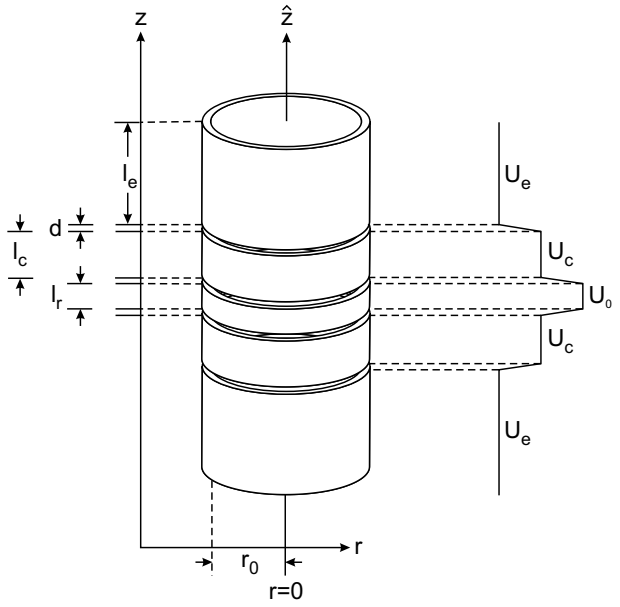

Figure 7.5: Five-pole cylindrical Penning trap. Symmetry axis is the $\hat{z}$-axis and a symmetry plane is perpendicular to $\hat{z}$ at $z = 0$. On the right side the potential on the surface of the electrodes is shown. Here, l_e, l_c, and l_r denote the lengths of the end-cap electrode, the correction electrode, and the ring electrode, respectively. d is the distance between the electrodes. U_0 is the voltage difference between the end-cap electrode and the ring electrode, U_c is the voltage applied to the correction electrode, and U_e the one applied to the end-cap electrode.

the voltage difference between ring electrode and end-cap electrodes. $I_0(x) = 1 + x^2/2^2 + x^4/(2^2 \cdot 4^4) + \cdots$ is the modified Bessel function of first kind, zeroth order, whereas $\Phi(r, z)$ is defined $\forall\ r \in [0, R_0], \Theta \in [0, 2\pi]$, and $z \in [-l/2, l/2]$. Dividing $\Phi(r, z)$ by the ring voltage U_0 normalizes the potential and the coefficients

$$c_j = \frac{C_j}{U_0} = c_j(l_e, l_c, l_r, d, R_0, T) \tag{7.7}$$

depend only on geometric parameters and the tuning ratio T. Defining the coefficients

$$\begin{aligned} A_m &= \frac{8}{l \cdot d \cdot k_m^2 \cdot I_0(k_m R_0)} \sin\left(\frac{k_m d}{2}\right) \sin\left(\frac{k_m (d + l_r)}{2}\right), \\ B_m &= \frac{16}{l \cdot d \cdot k_m^2 \cdot I_0(k_m R_0)} \sin\left(\frac{k_m d}{2}\right) \sin\left(\frac{k_m (d + l_r)}{2}\right) \end{aligned} \tag{7.8}$$

leads by considering $I_0(0) = 1$ to

$$\begin{aligned} c_j &= \frac{1}{j!} \cdot \frac{1}{U_0} \frac{\partial^j \Phi}{\partial z^j}\bigg|_{(0,0)} \\ &= \frac{1}{j!} \sum_m \left[A_m + T\, B_m\right] I_0(k_m r) \cos(k_m z) \left[\frac{\partial^j}{\partial z^j} \cos(k_m z)\right]. \end{aligned} \tag{7.9}$$

As mentioned before, all c_j with $(j \geq 4)$ have to vanish to obtain a harmonic potential. Additionally, the trap should be orthogonalized, which means that c_2 should be indepen-

Table 7.1: Parameters of the compensated and orthogonalized precision traps. All mechanical tolerances are well below $\pm 10\,\mu$m.

r_0	z_0	l_{cor}	l_e	T
3.57 mm	4.06 mm	2.76 mm	7.44 mm	0.881
d_2	d_4	c_2	c_4	c_6
$-4.87\cdot10^{-5}$	$-3.23\cdot10^{-3}$	$2.9\cdot10^{-2}$	$5.1\cdot10^{-7}$	$1.2\cdot10^{-7}$

dent of the applied voltage at the correction electrode. Therefore, the d_j-parameters are defined as follows:

$$d_j = \frac{\partial c_j}{\partial T}. \tag{7.10}$$

It is obvious that $c_2 = \text{const.}$ calls for $d_2 = 0$, but to be able to compensate the potential with the correction electrode $d_4 \neq 0$ is required.

Before starting to calculate the optimal trap geometry some boundary conditions have to be considered. The larger the trap dimensions, the more harmonic is the electrostatic potential in the center region. However, the trap system has to be placed in the homogeneous part of the magnetic field. Thus, the total length of the trap system is limited to 120 mm. Another boundary condition is that the gaps between two electrodes should not be smaller than $150\,\mu m$ for reasons of construction. Thus, three out of six free parameters are already fixed (see Eq. (7.7)). Two of the remaining three can be calculated such that c_4 and d_2 are equal to zero as required for compensation and orthogonalization of the Penning trap. The last one can be used to bring c_6, the next order perturbation of the harmonic potential, to zero as well. Since the perturbation scales with z^6, its impact is much less than the one of c_4 for ions with small motional amplitudes.

Table 7.1 lists all trap parameters. These values are used to calculate the coefficients of the electrostatic potential. In Fig. 7.6 the coefficient c_4 is shown as a function of the tuning ratio T, and the tuning ratio for a compensated Penning trap is indicated. The orthogonalization of the trap is realized by the d_2-term, which is close to 0.

Furthermore, one has to consider the homogeneity of the magnetic field, which will be disturbed by the susceptibilities of the trap materials, here oxygen free copper for the electrodes and sapphire for the insulators. This is of special concern for the central trap, where the actual frequency measurement takes place in case of the measurement scheme shown in Fig. 7.3 (a). The magnetic field here should be as homogeneous as possible. In this scheme the outer two traps are dedicated for ion cooling and storage. Therefore we added additional material to the outer side of the ring electrode of the central to counteract the distortion of the homogeneous magnetic field (see Fig. 7.7) [Brow1986]. Thus, the electrostatic potential in the trap is not affected. Doing this properly one can flatten the inhomogeneous part of the magnetic field. Expressing the magnetic field in a

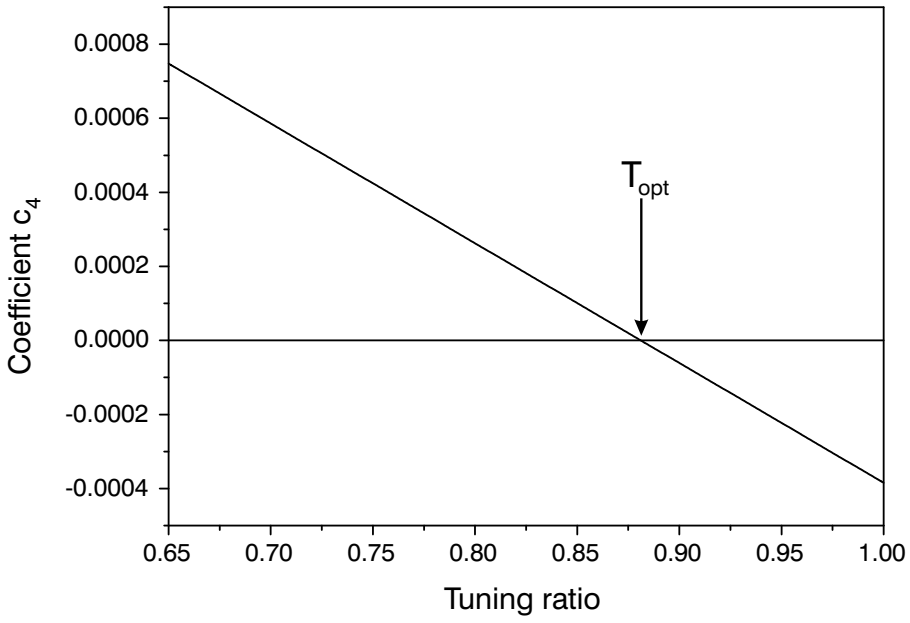

Figure 7.6: The coefficient c_4 as a function of the tuning ratio $T = U_c/U_0$. The optimal tuning ratio of $T_{opt} = 0.881$ leads for our given geometry to a compensated trap.

Taylor expansion, the β_2-term is the most important perturbation, since

$$B_z \approx B_0 \cdot \left[1 + \beta_2 \left(z^2 - \frac{\rho^2}{2}\right)\right]. \tag{7.11}$$

To calculate the additional field inhomogeneities the molar susceptibilities of copper ($\chi_A = -5.45 \cdot 10^{-6}\,\mathrm{cm}^3/\mathrm{mol}$ [Boll1989]) and sapphire ($\chi_A = -2.5 \cdot 10^{-7}\,\mathrm{cm}^3/\mathrm{mol}$ [Huss1989]) are used. The calculations have been done with the program SUSZI [Schw1993]. Table 7.2 shows the coefficients of β_2 obtained from fits to the data points, which are shown in Fig. 7.7. The inhomogeneities in the precision trap have been reduced significantly below 10^{-8} within a fit curve of 3 mm, which is below the homogeneity guaranteed by the supplier of the commercial superconducting magnet.

7.4 Ion manipulation and detection

To simplify the manipulation and detection of the ion motion in all five trapping regions mode coupling is applied. Thus, all frequencies could be measured via the axial oscillation. The required trap circuitry is shown in Fig. 7.8. In order to detect the ions non-destructively, the trapping regions will be connected to highly sensitive resonant detection systems, consisting of a tuned circuit followed by a high impedance amplifier or a SQUID system. The detectors will be operated at liquid helium temperature, which results in an increase of the signal-to-noise ratio since thermal noise is reduced and low-loss superconducting circuits can be applied.
In order to decouple the trap from disturbing rf signals, the dc lines are connected to the electrodes via RC-filters. To manipulate the eigenmotions of the stored ions, each trap

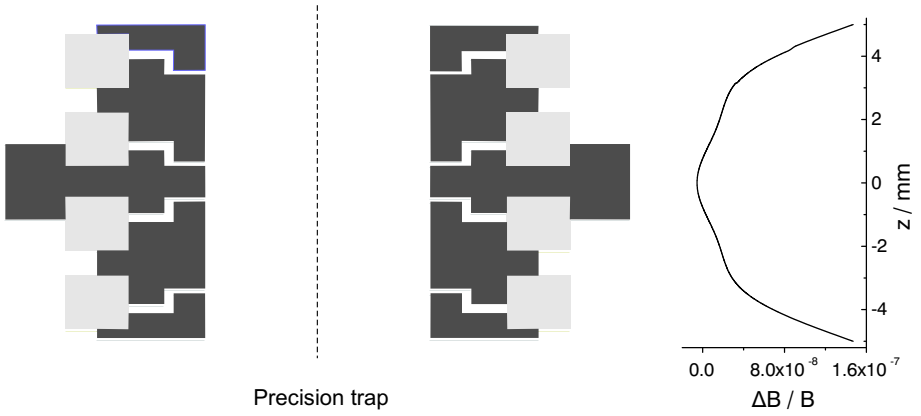

Figure 7.7: Precision trap, here pictured with truncated end-cap electrodes. The copper electrodes are indicated dark gray, while the sapphire insulators are light gray. At the outer side of the ring electrode copper material is added to flatten the curve on the right side, where $\Delta B/B$ on the $\hat{z}$-axis is plotted. ΔB denotes only magnetic field inhomogeneities which arise from the trap material and does not include the intrinsic inhomogeneities of the superconducting magnet itself.

Table 7.2: The β_2-coefficients of the magnetic field for different fit lengths on axis in the central as well as in the outer precision traps.

trap	fit length / mm	β_2 / 10^{-8}
central	1	0.32
	2	0.82
	3	0.45
outer	1	2.5
	2	3.7
	3	4.5

is connected to an axial and a radial excitation line. Since the radial excitation is not performed via the ring electrode but via the correction electrodes, the latter ones could be additionally used for mode coupling. In order to protect the detection systems care is needed to separate excitation signals and detection signals spatially.

To achieve maximum signal in the precision trap one of the correction electrodes will be connected to a high inductance LC-circuit for detection of the axial motion of the ion. Additionally, the central trap is connected to a cyclotron detection system. Another tuned circuit will be used to detect the axial motion of the two outer precision traps. Both traps will be connected to the same LC-circuit. As well as in the case of the cental trap the detection will be picked up from the correction electrodes. In the monitor traps the cyclotron frequency of a reference ion will be detected directly as explained in the next section. In all traps resistive cooling is applied, which is fast and efficient in the case

of highly-charged ions. Thus, each trap will be equipped with its own cyclotron detection system. As performed for the two outer precision traps, the axial signal of the monitor traps will be picked up with one common LC-circuit connected to both traps.

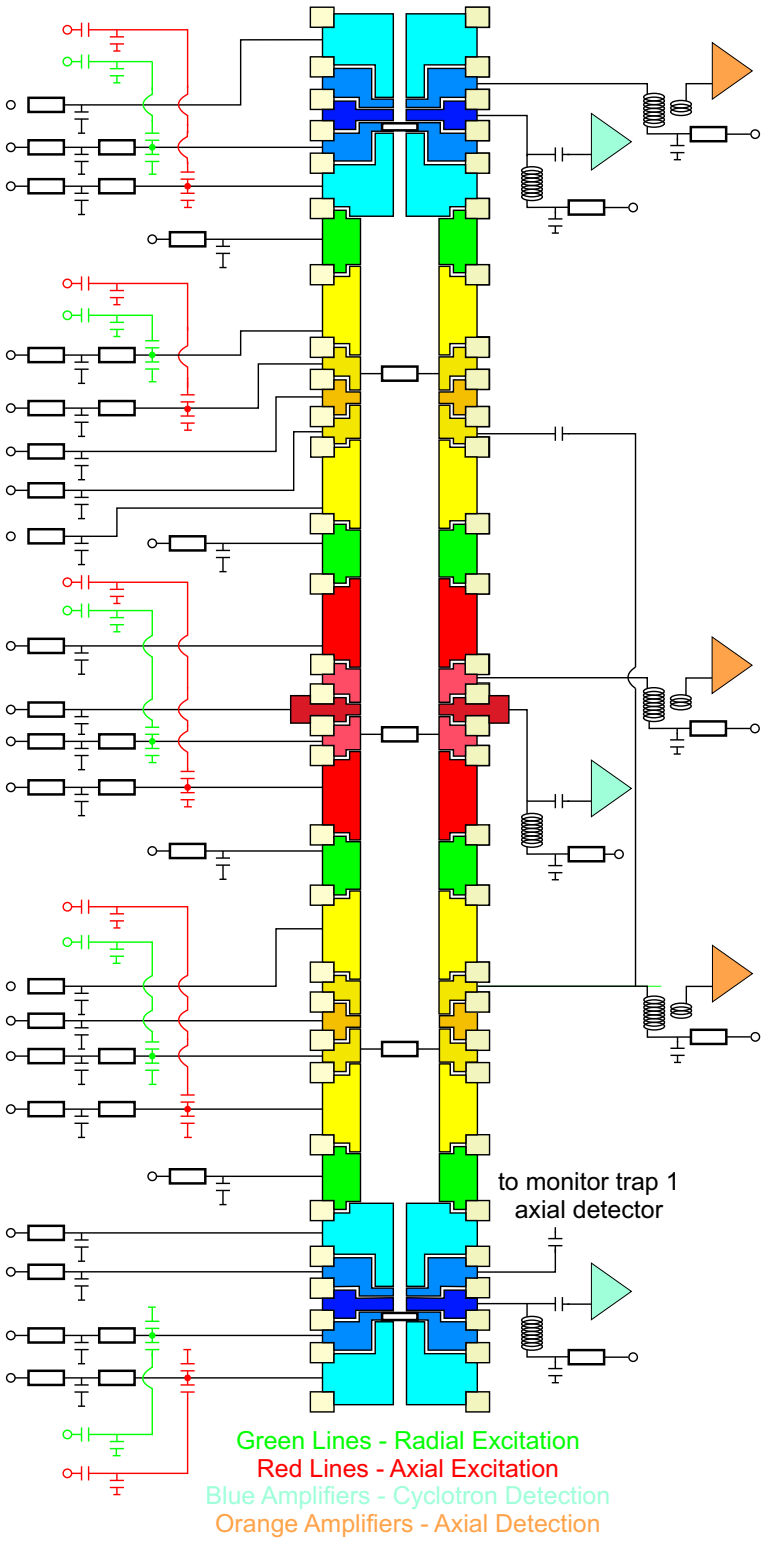

Figure 7.8: Sketch of the detection circuits of the trap-tower. For details see text.

7.5 Monitor traps

Compared to the precision trap the requirements regarding the novel monitor traps are different. Since they are used for a continuous observation of relative changes in the magnetic field the cyclotron frequency has to be detected. No special care was taken regarding the homogeneity of the magnetic field. Both traps are identical five-pole cylindrical Penning traps. The inner radius of the electrodes is only 0.5 mm, which ensures a highly efficient cooling of the particle and large signal at small motional amplitudes. In order to estimate the signal the effective electrode distance D_{eff} was calculated in terms of modified Bessel functions. D_{eff} describes the equivalent signal induced in the electrodes of a cylindrical trap, compared to an infinite capacitor [Stah1998]. For resonant pick up at one half of the splitted ring electrode of the trap D_{eff} is given by

$$D_{eff} = \frac{\Lambda\pi}{4}\left[\sum_{k=1}^{\infty}\frac{\sin\left(\frac{(2k-1)\pi}{2\Lambda}z_0\right)}{I_1\left(\frac{(2k-1)\pi}{\Lambda}r_0\right)}\right]^{-1}, \tag{7.12}$$

where Λ is the total length of the trap and I_1 the modified Bessel function of first kind and first order. For the geometry of the monitor traps $D_{eff} \approx 830\,\mu$m is obtained. Compared to standard orthogonalized, compensated Penning traps [Verd2003], this value is a factor of 10 to 20 smaller. Since the cooling time constant τ scales proportional to D_{eff}^2, and the cyclotron dip line-width $\gamma \propto \tau^{-1}$ [Wine1975], in combination with a high-Q detector this trap enables us to monitor the magnetic field, simultaneously with the actual measurement, but at different locations. Therefor, the very sensitive method of the cyclotron dip detection is used. Application of cyclotron side-band cooling to the monitor ion will lead to mK temperatures of the axial and the magnetron eigenmotion [Brow1986]. As a consequence, effects of the non-harmonic electrostatic potential have no longer to be taken into account.

This new Penning trap project for high-precision mass measurements on highly-charged ions will provide the possibility of fast measurement cycles as well as a continuous B-field observation in order to reach highest precision. The next steps of the project shall briefly be mentioned. The mechanical setup of the trap, its full realization including optimization steps, as well as the cryo-electronics for ion detection are presently under design in the thesis works of Julia Repp and Christian Roux. End of 2009, the superconducting magnet will be delivered. After the commissioning of the full setup extensive correlation studies regarding the predictability of the magnetic field in the precision traps from B-field monitoring will be done.

Chapter 8

Summary and outlook

Within this thesis three projects have been elaborated, dealing with high-precision Penning trap mass spectrometry. The major improvement of TOF-ICR mass spectrometry by the adoption of time-separated oscillatory fields, called Ramsey method, to a Penning trap was used for the first time to perform high-precision mass measurements. The resulting mass values of the radionuclides ^{26}Al and ^{38}Ca contributed to tests of the Standard Model of particle physics. In order to extend the applications of precise values the new Penning trap project PENTATRAP has been initiated and started. High-precision mass spectrometry on highly-charged ions at the level of below 10^{-11} will allow mass values to become sensitive probes for tests of fundamental symmetries.

The basic principle of time-separated oscillatory fields applied for the ion motion excitation in a Penning has already been implemented and succesfully tested at ISOLTRAP in my diploma thesis 2005 [Geor2005]. In detail, the method is meant for an efficient improvement of the time-of-flight ion-cyclotron resonance detection technique. Although the main features of this technique have been studied extensively, any damping effects due to collisions of ions with residual gas atoms have been neglected for reasons of simplification. Furthermore, no on-line mass determination has been performed at that time at ISOLTRAP. After including damping effects in the calculations, the theoretical line shapes of a time-of-flight ion-cyclotron resonance, have been derived in a quantum mechanical framework [Kret2008, Geor2009a]. Extensive off-line studies performed at ISOLTRAP and SHIPTRAP demonstrated the validity of the calculated line shapes for both the conventional one-pulse as well as the Ramsey-type excitation. This was especially important to completely understand the resonance line shape obtained by Ramsey-type excitation. Furthermore, these test were the experimental prove of the first analytically calculated damping effects in a Penning trap by Prof. M. Kretzschmar [Kret2008]. For the first time, a correlation between the strength of the damping and the interconversion of the two radial modes in a Penning trap has been experimentally investigated in detail. Thereby it was found that variations within the typical pressure range of a Penning trap experiment lead to a considerable change of the conversion time. A slightly wrong adjusted conversion time reduces the depth of the time-of-flight resonance, which finally increases the uncertainty of the frequency determination.

As presented, the Ramsey method was applied for the first time in an on-line run for

high-precision mass measurements at ISOLTRAP. The problem of Ramsey-type excitation pattern when isomeric contaminations are present in the precision trap has been investigated and discussed in detail in case of the short-lived radioactive nuclide ^{121}In. The isomeric state has an excitation energy of 313 keV. Although the Ramsey excitation has many advantages as discussed in this work, the method is not applicable in such a situation. While the two ion species could be resolved by using a conventioanal one-pulse excitation with a sufficiently long excitation time, the typical fringe patterns obtained by a Ramsey-type excitation are overlapping. Thus, the resonances cannot be distinguished. As a consequence the Ramsey method can only be applied, in case any ion contamination can be excluded. The on-line mass measurements of ^{26,27}Al and ^{38,39}Ca were performed using both the conventional as well as the Ramsey excitation method allowing for a comparison under on-line conditions. The Ramsey method has already been adopted by other Penning trap experiments [Suho2007, Eron2008b, Scie2009] and is meanwhile routinely used. Furthermore, new applications of this excitation method have been found [Eron2008a, Eron2008b].

The mass values ^{26,27}Al and ^{38}Ca were in agreement with the previous accepted values of the AME 2003. In case of ^{27}Al and ^{38}Ca the consideration of the new ISOLTRAP results changes only slightly the AME values. The new value of ^{26}Al shifted by almost one standard deviation, since not only the ISOLTRAP value was included, but an old input value derived from a reaction measurement was excluded due to inconsistency with the new set of data. The ISOLTRAP value of ^{39}Ca is disagreeing with the former AME value by four standard deviations. The mass region around ^{26,27}Al is covered by a number of very precise experimental data derived from both direct mass measurements as well as Q-value reaction measurements. The different types of measurements were disagreeing to some extend. The mass measurements of ISOLTRAP helped to solve this problem of inconsistent data.

Since tests of the CKM unitarity failed by more than two standard deviations at the beginning of this decade, an extensive experimental research program was triggered. ISOLTRAP was one of the leading Penning trap facility performing high-precision mass measurements on superallowed β-emitters in order to derive the first matrix element V_{ud}, which is the most significant one for tests of the unitarity. In addition to mass measurements of ^{22}Mg [Mukh2004], ^{34}Ar [Herf2002], and ^{74}Rb [Kell2004a], ISOLTRAP contributes now with mass values of ^{26}Al and ^{38}Ca as well. Meanwhile the non-unitarity problem is solved, since the second element of the matrix V_{us}, derived from kaon decay measurements, was assigned to a wrong value. New measurements resulted here in a significant change. Today, the test of the CKM unitarity by the first row of the matrix is the most stringent test of the Standard Model. The newest test of the unitarity yields $|V_{ud}|^2 + |V_{us}|^2 + |V_{ub}|^2 = 0.99995 \pm 0.00061$.

A new Penning trap project aiming for high-precision mass measurements of highly-charged ions in order to test fundamental symmetries and the bound-state quantum electrodynamics in extreme fields has been presented in this thesis. Therefore, the new facility is designed to reach a relative precision of better than 10^{-11}. This will allow for example, to determine the binding energy of the last remaining (1s) electron for the first

by a direct measurement, yielding a precision, which is up to now only achieved by X-ray spectroscopy [Stöh2006]. To be provided with highly-charged ions the experiment will be first connected to the EBIT at the Max-Planck-Institut for Nuclear Physics in Heidelberg and later to the HITRAP facility at GSI [Klug2008]. In order to motivate the new design, Penning trap facilities reaching up to now the highest precision world-wide have been briefly discussed with respect to their measurement techniques. In context of their feasibility to highly-charged ions an overall design and measurement principle has been elaborated.

As a starting point of this long-term project the design of the Penning traps, which are the core of the setup, has been done within this thesis. To this end an electrode configuration of five cylindrical Penning traps is proposed for various applications. Three precision Penning traps in the center of the setup will allow storage, manipulation, and high-precision measurements of at least two single ions simultaneously. Two novel monitor traps are added above and below the three inner traps dedicated for a continuous B-field observation. This will allow for a correction of magnetic field fluctuations. The design studies of the electrodes with respect to the electric field as well as their impact on the homogeneity of the magnetic field have been discussed in detail. An operation scheme for the non-destructive ion detection has been figured out. Furthermore, the possibility of fast measurement cycles, up to now not reached in Penning trap mass spectrometry, has been emphasized. The new facility for mass measurements on highly-charged ions will open the access to new applications of high-precision mass spectrometry.

Appendix A

Atomic-Mass Evaluation

Here, the data which are illustrated in the figures of the atomic-mass evaluation in Chap.6 are listed with their corresponding references.

Table A.1: The uncertainties as well as the deviations from the mean value of the mass excess for different measurements of ^{26}Al are shown.

Reaction	uncertainty / keV	deviation / keV	Reference
^{25}Mg(p,γ)^{26}Al	0.11	-0.046	[Berg1985]
^{25}Mg(p,γ)^{26}Al	0.08	-0.036	[Kiks1991]
^{26}Mg(p,n)^{26}Al	0.22	-1.069	[Bark1984]
^{26}Mg(p,n)^{26}Al	0.05	-0.159	[Bark1992]
^{26}Mg(p,n)^{26}Al	0.12	-0.479	[Brin1994]
^{26}Mg(p,n)^{26}Al	0.17	0.521	
^{26}Mg(^{3}He,t)^{26}Al	0.6	0.026	[Vona1977]
^{26}Mg(^{3}He,t)^{26}Al -^{14}N()^{14}O	0.13	0.126	[Kosl1987]
^{42}Ca(^{3}He,t)^{42}Sc -^{26}Mg()^{26}Al	0.23	0.16	[Kosl1987]
PT ^{26}Al^{m}-^{26}Mg	0.16	0.25	[Eron2006a]
PT ^{26}Al-^{23}Na	0.22	0.02	[Geor2008]

Table A.2: Same as Table A.1 but for ^{27}Al.

Reaction	uncertainty / keV	deviation / keV	Reference
^{23}Na(α,γ)^{27}Al	1.3	1.77	[Maas1978a]
^{27}Al(p,α)^{24}Mg	0.7	0.74	[Rytz1963]
^{27}Al(p,α)^{24}Mg	1.0	-2.56	[Brow1965]
^{27}Al(p,α)^{24}Mg	0.5	0.34	[Stau1967]
^{27}Al(p,α)^{24}Mg	0.21	-0.90	[Maas1978a]
^{24}Mg(α,p)^{27}Al	1.0	-2.06	[Brow1965]
^{26}Mg(p,γ)^{27}Al	0.5	0.34	[Ande1959]
^{26}Mg(p,γ)^{27}Al	0.5	-0.06	[Vand1963]
^{26}Mg(p,γ)^{27}Al	0.5	-0.16	[Maas1978b]
^{27}Al(p,γ)^{28}Si	0.30	0.27	[Maas1978a]
^{27}Al(p,γ)^{28}Si	0.14	-0.06	
PT ^{27}Al-^{23}Na	0.23	-0.225	[Geor2008]

Table A.3: Same as Table A.1 but for ^{38}Ca.

Reaction	uncertainty / keV	deviation / keV	Reference
^{40}Ca(p,t)^{38}Ca	25	10	[Hard1966]
^{40}Ca(p,t)^{38}Ca	11	-21	[Padd1972]
^{40}Ca(p,t)^{38}Ca	5.0	3.3	[Seth1974]
^{36}Ar(13He,n)^{38}Ca	21	52	[Shap1969]
^{24}Mg(^{16}O,2n)^{38}Ca	20	-35	[Zion1972]
PT ^{38}Ca-$H_3{}^{16}$O	0.28	-0.08	[Boll2006]
PT ^{38}Ca^{19}F-^{39}K	0.59	0.35	[Geor2007a, Geor2008]

Table A.4: Same as Table A.1 but for ^{39}Ca.

Reaction	uncertainty / keV	deviation / keV	Reference
^{39}Ca(β^+)^{39}K	25	-13	[Kist1958]
^{40}Ca(^{3}He,α)^{39}Ca	20	-8	[Hind1966]
^{40}Ca(^{3}He,α)^{39}Ca	15	24	[Rapa1971]
^{39}K(p,γ)^{39}Ca	6.0	-4.4	[Kemp1970]
^{39}K(p,γ)^{39}Ca	1.8	8.0	[Rao1978]
^{39}Ca^{19}F-^{39}K	0.60	0	[Geor2008]

Bibliography

[Abel2002] H. Abele, M. Astruc Hoffmann, S. Baeßler, D. Dubbers, F. Glück, U. Müller, V. Nesvizhevsky, J. Reich, O. Zimmer, Phys. Rev. Lett. 88 (2002) 211801.

[Alex2004] T. Alexopoulos for the KTeV Collaboration, Phys. Rev. Lett. 93 (2004) 181802.

[Amsl2008] C. Amsler et al. (Particle Data Group), Phys. Lett. B 667 (2008) 1.

[Ande1959] S.L. Andersen, T. Holtebekk, O. Lonsjo, R. Tangen, Nucl. Phys. 13 (1959) 310.

[Ande1962] P.W. Anderson, Phys. Rev. Lett. 9 (1962) 309.

[Ande1964] P.W. Anderson,Y.B. Kim, Rev. Mod. Phys. 39 (1964) 39.

[Asto1919] F.W. Aston, Phil. Mag. 38 (1919) 707.

[Asto1942] F.W. Aston, *Mass Spectra and Isotopes*, second ed., Edward Arnold, London, 1942.

[Audi2003a] G. Audi, O. Bersillon, J. Blachot, A.H. Wapstra, Nucl. Phys. A 729 (2003) 3.

[Audi2003b] G. Audi, A.H. Wapstra, C. Thibault, Nucl. Phys. A 729 (2003) 337.

[Bamb1977] W. Bambynek, H. Berhrens, M.H. Chen, B. Crasemann, M.L. Fitzpatrick, K.D. Ledingham, H. Genz, M. Mutterer, R.L. Intemann, Rev. Mod. Phys. 49 (1977) 77.

[Bark1984] P.H. Barker, R.E. White, D.M.J. Lovelock, R.M. Smythe, *Proc. 7th Int. Conf. Atomic Masses and Fundamental Constants AMCO-7*, 1984.

[Bark1992] P.H. Barker, S. Brindhaban, *Proc. 9th Int. Conf. Atomic Masses and Fundamental Constants AMCO-9, and 6th Int. Conf. Nuclei far from Stability NUFAST-6*, 1992.

[Beck2001] D. Beck, F. Ames, M. Beck, G. Bollen, B. Delauré, P. Schuurmans, S. Schwarz, P. Schmidt, N. Severijns, O. Forstner, Hyperfine Int. 132 (2001) 469.

[Beie1998] P. Beiersdorfer, K. Widmann, J. Crespo López-Urrutia, Hyperfine Int. 114 (1998) 141.

[Berg1985] F.J. Bergmeister, K. Lieb, K. Pampus, M. Uhrmacher, Z. Phys. A 320 (1985) 693.

[Berg2002] I. Bergström, C. Carlberg, T. Fritioff, G. Douysset, J. Schönfelder, R. Schuch, Nucl. Instr. Meth. A 487 (2002) 618.

[Berg2003] I. Bergström, M. Björkhage, K. Blaum, H. Bluhme, T. Fritioff, Sz. Nagy, R. Schuch, Eur. Phys. J. D 22 (2003) 41.

[Blau2002] K. Blaum, G. Bollen, F. Herfurth, A. Kellerbauer, H.-J. Kluge, M. Kuckein, E. Sauvan, C. Scheidenberger, L. Schweikhard, Eur. Phys. J. A 15 (2002) 245.

[Blau2003a] K. Blaum, D. Beck, G. Bollen, F. Herfurth, A. Kellerbauer, H.-J. Kluge, R.B. Moore, E. Sauvan, C. Scheidenberger, S. Schwarz, L. Schweikhard, Nucl. Instr. Meth. B 204 (2003) 478.

[Blau2003b] K. Blaum, G. Bollen, F. Herfurth, A. Kellerbauer, H.-J. Kluge, M. Kuckein, S. Heinz, P. Schmidt, L. Schweikhard, J. Phys. B: At. Mol. Opt. Phys. 36 (2003) 921.

[Blau2004a] K. Blaum, D. Beck, G. Bollen, P. Delahaye, C. Guénaut, F. Herfurth, A. Kellerbauer, H.-J. Kluge, D. Lunney, S. Schwarz, L. Schweikhard, C.Yazidjian, Europhys. Lett. 67 (2004) 586.

[Blau2004b] K. Blaum, G. Audi, D. Beck, G. Bollen, P. Delahaye, C. Guénaut, F. Herfurth, A. Kellerbauer, H.-J. Kluge, D. Lunney, D. Rodríguez, S. Schwarz, L. Schweikhard, C. Weber, C. Yazidjian, Nucl. Phys. A 746 (2004) 305c.

[Blau2005a] K. Blaum, G. Audi, D. Beck, G. Bollen, P. Delahaye, S. George, C. Guénaut, F. Herfurth, A. Herlert, A. Kellerbauer, H.-J. Kluge, D. Lunney, M. Mukherjee, S. Schwarz, L. Schweikhard, C. Yazidjian, Nucl. Phys. A 752 (2005) 317c.

[Blau2005b] K. Blaum, D. Beck, G. Bollen, P. Delahaye, C. Guénaut, F. Herfurth, A. Kellerbauer, H.-J. Kluge, U. Köster, D. Lunney, S. Schwarz, L. Schweikhard, C. Yazidjian, Hyperfine Int. 162 (2005) 173.

[Blau2005c] K. Blaum, G. Audi, D. Beck, G. Bollen, M. Brodeur, P. Delahaye, **S. George**, C. Guénaut, F. Herfurth, A. Herlert, A. Kellerbauer, H.-J. Kluge, D. Lunney, M. Mukherjee, D. Rodríguez, S. Schwarz, L. Schweikhard, C. Yazidjian, J. Phys. G 31 (2005) S1775.

[Blau2006] K. Blaum, Phys. Rep. 425 (2006) 1.

[Bloc2005] M. Block, D. Ackermann, D. Beck, K. Blaum, M. Breitenfeldt, A. Chauduri, A. Doemer, S. Eliseev, D. Habs, S. Heinz, F. Herfurth, F. Heßberger, S. Hofmann, H. Geissel, H.-J. Kluge, V. Kolhinen, G. Marx, J. Neumayr, M. Mukherjee, M. Petrick,

W. Plass, W. Quint, S. Rahaman, C. Rauth, D. Rodríguez, C. Scheidenberger, L. Schweikhard, M. Suhonen, P. Thirolf, Z. Wang, C. Weber, and the SHIPTRAP Collaboration, Eur. Phys. J. A 25 S01 (2005) 49.

[Boll1989] G. Bollen: *Erste Messungen an instabilen Isotopen mit Hilfe einer Penningfalle* PhD thesis Johannes Gutenberg-Universität Mainz (1989).

[Boll1990] G. Bollen, R.B. Moore, G. Savard, H. Stolzenberg, J. Appl. Phys. 68 (1990) 4355.

[Boll1992a] G. Bollen, H.-J. Kluge, M. König, T. Otto, G. Savard, H. Stolzenberg, R.B. Moore, G. Rouleau, G. Audi, ISOLDE Collaboration, Phys. Rev. C 46 (1992) R2140.

[Boll1992b] G. Bollen, H.-J. Kluge, T. Otto, G. Savard, H. Stolzenberg, Nucl. Instr. Meth. B 70 (1992) 490.

[Boll1996] G. Bollen, S. Becker, H.-J. Kluge, M. König, R.B. Moore, T. Otto, H. Raimbault-Hartmann, G. Savard, L. Schweikhard, H. Stolzenberg, ISOLDE Collaboration, Nucl. Instr. Meth. A 368 (1996) 675.

[Boll2001] G. Bollen, Nucl. Phys. A 693 (2001) 3.

[Boll2004] G. Bollen, Lect. Notes Phys. 651 (2004) 169.

[Boll2006] G. Bollen, D. Davies, M. Facina, J. Huikari, E. Kwan, P.A. Lofy, D.J. Morrissey, A. Prinke, R. Ringle, J. Savory, P. Schury, S. Schwarz, C. Sumithrarachchi, T. Sun, L. Weissman, Phys. Rev. Lett. 96 (2006) 152501.

[Born2005] L. Bornschein, for the KATRIN-Collaboration, Nucl. Phys. A 752 (2005) 14c.

[Bosc2003] F. Bosch, J. Phys. B 36 (2003) 585.

[Bene1979] W. Benenson, E. Kashy, Rev. Mod. Phys. 51 (1979) 527.

[Brad1999] M.P. Bradley, J.V. Porto, S. Rainville, J.K. Thompson, D.E. Pritchard, Phys. Rev. Lett. 83 (1999) 4510.

[Brin1994] S.A. Brindhaban, P.H. Barker, Phys. Rev. C 49 (1994) 2401.

[Brow1965] C.P. Browne, W.E. Dorenbusch, F.H. O'Donnell, Nucl. Phys. 72 (1965) 194.

[Brow1982] L.S. Brown, G. Gabrielse, Phys. Rev. A 25 (1982) 2423.

[Brow1986] L.S. Brown, G. Gabrielse, Rev. Mod. Phys. 58 (1986) 233.

[Caki2005] R.B. Cakirli, D.S. Brenner, R.F. Casten, E.A. Millman, Phys. Rev. Lett. 94 (2005), 092501 and Phys. Rev. Lett. 95 (2005) 119903.

[Char2005] J. Charles, A. Höcker, H. Lacker, S. Laplace, F.R. Le Diberder , J. Malclés, J. Ocariz, M. Pivk, L. Roos, Eur. Phys. C 41 (2005) 1.

[Comi1974] M.B. Comisarow, A.L. Marshall, Chem. Phy. Lett. 25 (1974) 282.

[Comi1996] M.B. Comisarow, A.L. Marshall, J. Mass Spectr. 31 (1996) 581.

[Corn1992] E.A. Cornell, K.R. Boyce, D.L.K. Fygenson, D. Pritchard, Phys. Rev. A 45 (1992) 3049.

[Dehm1990] H. Dehmelt, Rev. Mod. Phys. 62 (1990) 525.

[Dela2006] P. Delahaye, G. Audi, K. Blaum, F. Carrel, S. George, F. Herfurth, A. Herlert, A. Kellerbauer, H.-J. Kluge, D. Lunney, L. Schweikhard, C. Yazidjian, Phys. Rev. C 74 (2006) 034331.

[Delh2006] P. Delheij, L. Blomeley, M. Froese, G. Gwinner, V. Ryjkov, M. Smith, J. Dilling, Hyperfine Int. 173 (2006) 123.

[DiFi1994] F. DiFilippo, V. Natarajan, K.R. Boyce, D.E. Pritchard, Phys. Rev. Lett. 73 (1994) 1481.

[Dill2000] J. Dilling, D. Ackermann, J. Bernard, F.P. Heßberger, S. Hofmann, W. Hornung, H. J. Kluge, E. Lamour, M. Maier, R. Mann, G. Marx, R. B. Moore, G. Münzenberg, W. Quint, D. Rodríguez, M. Schädel, J. Schönfelder, G. Sikler, C. Toader, L. Vermeeren, C. Weber, G. Bollen, O. Engels, D. Habs, P. Thirolf, H. Backe, A. Dretzke, W. Lauth, W. Ludolphs, M. Sewtz, Hyperfine Int. 127 (2000) 491.

[Dill2001] J. Dilling, D. Ackermann, F.P. Heßberger, S. Hofmann, H.-J. Kluge, G. Marx, G. Münzenberg, Z. Patyk, W. Quint, D. Rodríguez, C. Scheidenberger, J. Schönfelder, G. Sikler, A. Sobiczewski, C. Toader, C.Weber, Hyperfine Int. **132** (2001) 495.

[Douy2001] G. Douysset, T. Fritioff, C. Carlberg, Phys. Rev. Lett. 86 (2001) 4259.

[Duck1950] H.E. Duckworth, Rev. Sci. Instr. 21 (1950) 54.

[Dyck1992] R.S. Van Dyck, Jr., D.L. Farnham, P.B. Schwinberg, J. Mod. Opt. 39 (1992) 243.

[Eide2004] S. Eidelman *et al.* (Particle Data Group), Phys. Lett. B 592 (2004) 1.

[Eins1905] A. Einstein, Annal. Phys. 18 (1905) 639.

[Eron2006a] T. Eronen, V. Elomaa, U. Hager, J. Hakala, J.C. Hardy, A. Jokinen, A. Kankainen, I. Moore, H. Penttilä, S. Rahaman, J. Rissanen, A. Saastamoinen, T. Sonoda, J. Äysto, Phys. Rev. Lett. 97 (2006) 232501.

[Eron2006b] T. Eronen, V. Elomaa, U. Hager, J. Hakala, A. Jokinen, A. Kankainen, V.S. Kolhinen, I. Moore, H. Penttilä, S. Rahaman, S. Rinta-Antila, A. Saastamoinen, T. Sonoda, J. Äysto, A. Bey, B. Blank, G. Canchel, C. Dossat,J. Giovinazzo, I. Matea, N. Adimi, Phys. Lett. B 636 (2006) 191.

[Eron2008a] T. Eronen, V. Elomaa, U. Hager, J. Hakala, A. Jokinen, A. Kankainen, S. Rahaman, J. Rissanen, C. Weber, J. Äysto, Nucl. Instr. Meth. B 266 (2008) 4527.

[Eron2008b] T. Eronen, V. Elomaa, U. Hager, J. Hakala, A. Jokinen, A. Kankainen, S. Rahaman, J. Rissanen, C. Weber, J. Äysto, Phys. Rev. Lett. 100 (2008) 132502.

[Fisc1959] E. Fischer, Z. Phys. 156 (1959) 1.

[Froe2006] M. Froese, C. Champagne, J.R. Crespo López-Urrutia, S. Epp, G. Gwinner, A. Lapierre, J. Pfister, G. Sikler, J. Ullrich, J. Dilling, Hyperfine Int. 173 (2006) 85.

[Gabr1984] G. Gabrielse, F.C. Mackinosh, Int. J. Mass. Spectr. 57 (1984) 1.

[Gabr1989] G. Gabrielse, L. Haarsma, S.L. Rolston, Int. J. Mass Spec. 88 (1989) 319.

[Gabr1993] G. Gabrielse, W. Jhe, D. Phillips, W. Quint, L. Haarsma, K. Abdullah, H. Kalinowsky, J. Gröbner, Hyperfine Int. 81 (1993) 5.

[Gabr1999] G. Gabrielse, A. Khabbaz, D.S. Hall, C. Heimann, H. Kalinowsky, W. Jhe, Phys. Rev. Lett. 82 (1999) 3198.

[Gabr2009] G. Gabrielse, Int. J. Mass. Spectr. 279 (2009) 107.

[Geit2009] W. Geithner, T. Neff, G. Audi, K. Blaum, P. Delahaye, H. Feldmeier, S. George, C. Guénaut, F. Herfurth, A. Herlert, S. Kappertz, M. Keim, A. Kellerbauer, H.-J. Kluge, M. Kowalska, P. Lievens, D. Lunney, K. Marinova, R. Neugart, L. Schweikhard, S. Wilbert, C. Yazidjian, Phys. Rev. Lett. 101 (2009) 252502.

[Geor2005] S. George: *Application of the Ramsey method in high-precision Penning trap mass spectrometry*, Diploma thesis, Westfälische Wilhelms-Universität Münster (2005).

[Geor2007a] S. George, S. Baruah, B. Blank, K. Blaum, M. Breitenfeldt, U. Hager, F. Herfurth, A. Herlert, A. Kellerbauer, H.-J. Kluge, M. Kretzschmar, D. Lunney, R. Savreux, S. Schwarz, L. Schweikhard, C. Yazidjian, Phys. Rev. Lett. 98 (2007) 162501.

[Geor2007b] S. George, K. Blaum, F. Herfurth, A. Herlert, M. Kretzschmar, S. Nagy, S. Schwarz, L. Schweikhard, C. Yazidjian, Int. J. Mass. Spectr. 264 (2007) 110.

[Geor2008] S. George, G. Audi, B. Blank, K. Blaum, M. Breitenfeldt, U. Hager, F. Herfurth, A. Herlert, A. Kellerbauer, H.-J. Kluge, M. Kretzschmar, D. Lunney, R. Savreux, S. Schwarz, L. Schweikhard, C. Yazidjian, Europhys. Lett. 50005 (2008) 1.

[Geor2009a] S. George *et al., in preparation*

[Geor2009b] S. George *et al., in preparation*

[Ghos1995] P.K. Ghosh, *Ion Traps*, International Series of Monographs on Physics, vol. 90, Clarendon Press, Oxford, 1995.

[Gore2005] A. Gorelov, D. Melconian, W.P. Alford, D. Ashery, G. Ball, J.A. Behr, P.G. Bricault, J.M. D'Auria, J. Deutsch, J. Dilling, M. Dombsky, P. Dube, J. Fingler, U. Giesen, F. Glück, S. Gu, O. Häusser, K.P. Jackson, B.K. Jennings, M.R. Pearson, T.J. Stocki, T.B. Swanson, M. Trinczek, Phys. Rev. Lett. 94 (2005) 142501.

[Gräf1980] G. Gräff, H. Kalinowsky, J. Traut, Z. Phys. A 297 (1980) 35.

[Guen2005] C. Guénaut, G. Audi, D. Beck, K. Blaum, G. Bollen, P. Delahaye, F. Herfurth, A. Kellerbauer, H.-J. Kluge, D. Lunney, S. Schwarz, L. Schweikhard, C. Yazidjian, Eur. Phys. J. A 25 (s01) (2005) 33.

[Guen2006] C. Guénaut, G. Audi, D. Beck, K. Blaum, G. Bollen, P. Delahaye, F. Herfurth, A. Kellerbauer, H.-J. Kluge, J. Libert, D. Lunney, S. Schwarz, L. Schweikhard, C. Yazidjian, Phys. Rev. C 75 (2007) 044303.

[Hann2008] D. Hanneke, S. Fogwell, G. Gabrielse, Phys. Rev. Lett. 100 (2008) 120801.

[Hard1966] J.C. Hardy, D.J. Skyrme, I.S. Towner, Phys. Lett. 23 (1966) 487.

[Hard1990] J.C. Hardy, I.S. Towner, V.T. Koslowsky, E. Hagberg, H. Schmeing, Nucl. Phys. A 509 (1990) 429.

[Hard2001] J.C. Hardy, I.S. Towner, Hyperfine Int. 132 (2001) 115.

[Hard2005a] J.C. Hardy, I.S. Towner, Phys. Rev. C 71 (2005) 055501.

[Hard2005b] J.C. Hardy, I.S. Towner, Phys. Rev. Lett. 94 (2005) 092502.

[Hard2008] J.C. Hardy, I.S. Towner, arXiv:0812.1202v1 (2008).

[Häns2006] T.W. Hänsch, Rev. Mod. Phys. 78 (2006) 1297.

[Herf2001a] F. Herfurth, J. Dilling, A. Kellerbauer, G. Bollen, S. Henry, H.-J. Kluge, E. Lamour, D. Lunney, R.B. Moore, C. Scheidenberger, S. Schwarz, G. Sikler, J. Szerypo, Nucl. Instr. Meth. A 469 (2001) 254.

[Herf2001b] F. Herfurth, J. Dilling, A. Kellerbauer, G. Audi, D. Beck, G. Bollen, S. Henry, H.-J. Kluge, D. Lunney, R. B. Moore, C. Scheidenberger, S. Schwarz, G. Sikler, J. Szerypo, ISOLDE Collaboration, in: Proc. "Atomic Physics at Accelerators: Mass Spectrometry (APAC 2000)", Cargèse, France, 2000 (eds. D. Lunney, G. Audi, H.-J. Kluge), Hyperfine Int. 132 (2001) 309.

[Herf2002] F. Herfurth, F. Ames, G. Audi, D. Beck, K. Blaum, G. Bollen, O. Engels, A. Kellerbauer, H.-J. Kluge, D. Lunney, R.B. Moore, M. Oinonen, E. Sauvan, C. Scheidenberger, S. Schwarz, G. Sikler, C. Weber, the ISOLDE Collaboration, Eur. Phys. J. A 15 (2002) 17.

[Herf2003] F. Herfurth, F. Ames, G. Audi, D. Beck, K. Blaum, G. Bollen, A. Kellerbauer, H.-J. Kluge, M. Kuckein, D. Lunney, R.B. Moore, M. Oinonen, D. Rodríguez, E. Sauvan, C. Scheidenberger, S. Schwarz, G. Sikler, C. Weber, ISOLDE Collaboration, J. Phys. B 36 (2003) 931.

[Herm1999] N.H. Hermanspahn: *Das magnetische Moment des gebundenen Elektrons in wasserstoffartigem Kohlenstoff (C^{5+})* PhD thesis Johannes Gutenberg-Universität Mainz (1999).

[Hind1966] S. Hinds, R. Middleton, Nucl. Phys. 84 (1966) 651.

[Huss1989] R.J. Hussey, J. Wilson: *Advanced Technical Ceramics Directory and Databook*, Chapman & Hall (1998).

[ISOL1992] ISOLDE Collaboration, G. Bollen, H.-J. Kluge, M. König, T. Otto, G. Savard, H. Stolzenberg, R.B. Moore, G. Rouleau, G. Audi, Phys. Rev. C 46 (1992) R2140.

[Jänn1988] J. Jänecke, P.J. Masson, At. Data Nucl. Data Tab. 39 (1988) 265.

[Jeff1983] J.B. Jeffries, S.E. Barlow, G.H. Dunn, Int. J. Mass Spectr. Ion Process. 54 (1983) 169.

[Jert1993] D. Beck, I. Bergström, G. Bollen, H. Borgenstrand, C. Carlberg, J. Emmes, H.-J. Kluge, G. Rouleau, E. Schark, R. Schuch, S. Schwarz, T. Schwarz, L. Schweikhard, P. Senne, F. Söderberg, Physica Scripta 48 (1993) 399.

[Kaep1998] F. Kaeppeler, F.K. Thielemann, M. Wiescher, Annu. Rev. Nucl. Part. Sci. 48 (1998) 175.

[Kell2001] A. Kellerbauer, T. Kim, R.B. Moore, P. Varfalvy, Nucl. Instr. Meth. A 469 (2001) 276.

[Kell2003] A. Kellerbauer, K. Blaum, G. Bollen, F. Herfurth, H.-J. Kluge, M. Kuckein, E. Sauvan, C. Scheidenberger, L. Schweikhard, Eur. Phys. J. D 22 (2003) 53.

[Kell2004a] A. Kellerbauer, G. Audi, D. Beck, K. Blaum, G. Bollen, B.A. Brown, P. Delahaye, C. Guénaut, F. Herfurth, H.-J. Kluge, D. Lunney, S. Schwarz, L. Schweikhard, C.Yazidjian, Phys. Rev. Lett. 93 (2004) 072502.

[Kell2004b] A. Kellerbauer, G. Audi, D. Beck, K. Blaum, G. Bollen, P. Delahaye, F. Herfurth, H.-J. Kluge, V. Kolhinen, M. Mukherjee, D. Rodríguez, S. Schwarz, Nucl. Phys. A 746 (2004) 635c.

[Kell2007] A. Kellerbauer, G. Audi, D. Beck, K. Blaum, G. Bollen, C. Guénaut, F. Herfurth, H.-J. Kluge, D. Lunney, S. Schwarz, L. Schweikhard, C. Weber, C.Yazidjian, Phys. Rev. C 76 (2007) 024308.

[Kemp1970] K.W. Kemper, C.M. McKenna, J.W. Nelson, Phys. Rev. C 2 (1970) 213.

[Kete2008] J. Ketelaer, J. Krämer, D. Beck, K. Blaum, M. Block, K. Eberhardt, G. Eitel, R. Ferrer, C. Geppert, **S. George**, F. Herfurth, J. Ketter, Sz. Nagy, D. Neidherr, R. Neugart, W. Nörtershäuser, J. Repp, C. Smorra, N. Trautmann, C. Weber, Nucl. Instr. Meth. A 594 (2008) 162.

[Kiks1991] S.W. Kikstra, Z. Guo, C. van der Leun, P.M. Endt, S. Raman, T.A. Walkiewicz, J.W. Starner, E.T. Jurney, I.S. Towner, Nucl. Phys. A 529 (1991) 39.

[Kist1958] O.C. Kistner, B.M. Rustad, Phys. Rev. 112 (1959) 1972.

[Klap2004] H.V. Klapdor-Kleingrothaus, I.V. Krivosheina, A. Dietz, O. Chkvorets, Phys. Lett. B 586 (2004) 198.

[Klug2008] H.-J. Kluge, T. Beier, K. Blaum, L. Dahl, S. Eliseev, F. Herfurth, B. Hofmann, O. Kester, S. Koszudowski, C. Kozhuharov, G. Maero, W. Nörtershäuser, J. Pfister, W. Quint, U. Ratzinger, A. Schempp, R. Schuch, Th. Stöhlker, R.C. Thompson, M. Vogel, G. Vorobjev, D.F.A. Winters, G. Werth, Adv. Quantum Chem. 53 (2008) 83.

[Koba1973] M. Kobayashi, T. Maskawa. Prog. Theor. Phys. 49 (1973) 652.

[Köni1995] M. König, G. Bollen, H.-J. Kluge, T. Otto, J. Szerypo, Int. J. Mass Spec. Ion Process. 142 (1995) 95.

[Köst2003] U. Köster, V.N. Fedoseyev, V.I. Mishin, Spectrochim. Acta B 58 (2003) 1047.

[Kosl1987] V.T. Koslowsky, J.C. Hardy, E. Hagberg, R.E. Azuma, G.C. Ball, E.T.H. Clifford, W.G. Davies, H. Schmeing, U.J. Schrewe, K.S. Sharma, Nucl. Phys. A 472 (1987) 419.

[Kret1991] M. Kretzschmar, Eur. J. Phys. 12 (1991) 240.

[Kret1992] M. Kretzschmar, Physica Scripta 46 (1992) 544.

[Kret2007] M. Kretzschmar, Int. J. Mass. Spectr. 264 (2007) 122.

[Kret2008] M. Kretzschmar, Eur. Phys. J. D 48 3 (2008) 313.

[Kugl2000] E. Kugler, Hyperfine Int. 129 (2000) 23.

[Lind2003] M. Lindroos, The CERN ISOLDE team, the REX-ISOLDE Collaboration, the ISOLDE Collaboration, Nucl. Instr. Meth. B 204 (2003) 730.

[Lunn2003] D. Lunney, J.M. Pearson, C. Thibault, Rev. Mod. Phys. 75 (2003) 1021.

[Maas1978a] J.W. Maas, E. Somorjai, H.D. Graber, C.A. van der Wijngaart, C. van der Leun, P.M. Endt, Nucl. Phys. A 301 (1978) 213.

[Maas1978b] J.W. Maas, A. Holvast, A. Baghus, H. Aarts, P.M. Endt, Nucl. Phys. A 301 (1978) 237.

[Mann1986] R. Mann, Z. Phys. D 3 (1986) 85.

[Mari2008] M. Marie-Jeanne, J. Alonso, K. Blaum, S. Djekic, M. Dworschak, U. Hager, A. Herlert, Sz. Nagy, R. Savreux, L. Schweikhard, S. Stahl, C. Yazidjian, Nucl. Instr. Meth. A 587 (2008) 464.

[Maso1988] E.A. Mason, E.W. McDaniel *Transport Properties of Ions in Gases*, John Wiley and Sons, New York (1988).

[Majo2005] F.G. Major, V.N. Gheorghe, G. Werth, *Charged Particle Traps*, Physics and Techniques of Charged Particle Field Confinement (Springer Series on Atomic, Optical, and Plasma Physics, Vol. 37). Springer, Berlin (2005).

[Moor2002] R.B. Moore, *Buffer Gas Cooling of Ion Beams* (2002), www.physics.mcgill.ca/ moore/Notes/BeamCooling.pdf

[Mukh2004] M. Mukherjee, A. Kellerbauer, D. Beck, K. Blaum, G. Bollen, F. Carrel, P. Delahaye, J. Dilling, S. George, C. Guénaut, F. Herfurth, A. Herlert, H.-J. Kluge, U. Köster, D. Lunney, S. Schwarz, L. Schweikhard, C. Yazidjian, Phys. Rev. Lett. 93 (2004) 150801.

[Mukh2008a] M. Mukherjee, D. Beck, K. Blaum, G. Bollen, J. Dilling, S. George, F. Herfurth, A. Herlert, A. Kellerbauer, H.-J. Kluge, S. Schwarz, L. Schweikhard, C. Yazidjian, Eur. Phys. J. A 35 (2008) 1.

[Mukh2008b] M. Mukherjee, D. Beck, K. Blaum, G. Bollen, P. Delahaye, J. Dilling, S. George, C. Guénaut, F. Herfurth, A. Herlert, A. Kellerbauer, H.-J. Kluge, U. Köster, D. Lunney, S. Schwarz, L. Schweikhard, C. Yazidjian, Eur. Phys. J. A 35 (2008) 31.

[Münz1979] G. Münzenberg, H. Ewald, W. Faust, K. Günter, S. Hofmann, P. Armbruster, Nucl. Instrum. Meth. 161 (1979) 65.

[Nagy2006] Sz. Nagy, T. Fritioff, M. Björkhage, I. Bergström, R. Schuch, Europhys. Lett. 74 (2006) 404-410.

[Navi2008] O. Naviliat-Cuncic, N. Severijns, arXiv:0809.0994v1 (2008).

[Neid2008] D. Neidherr, K. Blaum, M. Block, R. Ferrer, F. Herfurth, J. Ketelaer, Sz. Nagy, C. Weber, Nucl. Instrum. Meth. Phys. Res. B 266 (2008) 4556.

[Neid2009] D. Neidherr, G. Audi, D. Beck, K. Blaum, M. Breitenfeldt, Ch. Böhm, R.B. Cakirli, R.F. Casten, S. George, F. Herfurth, A. Herlert, A. Kellerbauer, M. Kowalsla, D. Lunney, E. Minaya-Ramirez, S. Naimi, E. Noah, L. Penescu, M. Rosenbusch, S. Schwarz, T. Stora, Phys. Rev. Lett. *in print* (2009).

[Neum2006] J. B. Neumayr, L. Beck, D. Habs, S. Heinz, J. Szerypo, P.G. Thirolf, V. Varentsov, F. Voit, D. Ackermann, D. Beck, M. Block, Z. Di, S.A. Eliseev, H. Geissel, F. Herfurth, F.P. Heßberger S. Hofmann, H.-J. Kluge, M. Mukherjee, G. Münzenberg,

M. Petrick, W. Quint, S. Rahaman, C. Rauth, D. Rodríguez, C. Scheidenberger, G. Sikler, Z. Wang, C. Weber, W.R. Plaß, M. Breitenfeldt, A. Chaudhuri, G. Marx, L. Schweikhard, A.F. Dodonov, Y. Novikov, M. Suhonen, Nucl. Instr. Meth. B 244 (2006) 489.

[Nico2005] J.S. Nico, M.S. Dewey, D.M. Giliiam, F.E. Wietfeldt, X. Fei, W.M. Snow, G.L. Greene, J. Pauwels, R. Eykens, A. Lamberty, J. VanGestel, R.D. Scott, Phys. Rev. C 71 (2005) 055502.

[Nier1951] A.O. Nier, T.R. Roberts, Phys. Rev. 81 (1951) 507.

[Padd1972] R.A. Paddock, Phys. Rev. C 5 (1972) 485.

[Paul1953] W. Paul, H. Steinwedel, Z. Naturf. 8a (1953) 448.

[Paul1955] W. Paul, M. Raether, Z. Phys. 140 (1955) 262.

[Paul1958] W. Paul, H.P. Reinhard, U.v. Zahn, Z. Phys. 152 (1958) 143.

[Paul1990] W. Paul, Rev. Mod. Phys. 62 (1990) 531.

[Penn1936] F.M. Penning, Physica 3 (1936) 563.

[Pier1949] J.R. Pierce, in: *Theory and Design of Electron Beams*, D. van Nostrand Co., New York 1949, Chap 3.

[Poca2004] D. Pocanič, E. Frlež, W. Bertl, Ch. Brönnimann, M. Bychkov, J.F. Crawford, M. Daum, N.V. Khomutov, A.S. Korenchenko, S.M. Korenchenko, T. Kozlowski, N.P. Kravchuk, N.A. Kuchinsky, W. Li, R.C. Minehart, D. Mzhavia, B.G. Ritchie, S. Ritt, A.M. Rozhdestvensky, V.V. Sidorkin, L.C. Smith, I. Supek, Z. Tsamalaidze, B.A. VanDevender, Y. Wang, H.-P. Wirtz, K.O.H. Ziock, Phys. Rev. Lett. 93 (2004) 181803.

[Port2001] J.V. Porto, Phys. Rev. A 64 (2001) 023403.

[Qui1998] T.J. Quinn, I.M. Mills, in: The International System of Units (SI), The SI Brochure, 7th Edition, Bureau International des Poids et Mesures, Sèvres, France, 1998, p. 152.

[Raha2008] S. Rahaman, V.-V. Elomaa, T. Eronen, J. Hakala, A. Jokinen, J. Julin, A. Kankainen, A. Saastamoinen, J. Suhonen, C. Weber, J. Äystö, Phys. Lett. B 662 (2008) 111.

[Raim1997] H. Raimbault-Hartmann, D. Beck, G. Bollen, M. König, H.-J. Kluge, E. Schark, J. Stein, S. Schwarz, J. Szerypo, Nucl. Instr. Meth. B 126 (1997) 378.

[Rain2003] S. Rainville *A Two-Ion Balance for High Precision Mass Spectrometry* PhD thesis at the Masschusetts Institue of Technology (2003).

[Rain2004] S. Rainville, J.K. Thompson, D.E. Pritchard, Science 303 (2004) 334.

[Rams1990] N.F. Ramsey, Rev. Mod. Phys. 62 (1990) 541.

[Rao1978] G.R. Rao, G. Azuelos, J.C. Kim, J.P. Martin, P. Taras, Phys. Rev. C 8 (1978) 1085.

[Rapa1971] J. Rapaport, W.E. Dorenbusch, T.A. Belote, Nucl. Phys. A 177 (1971) 307.

[Ravn1992] H.L. Ravn, Nucl. Instrum. Meth. B 70 (1992) 107.

[Reds2007] M. Redshaw, E. Wingfield, J. McDaniel, E.G. Myers, Phys. Rev. Lett. 98 (2007) 053003.

[Reds2008] M. Redshaw, J. McDaniel, E.G. Myers, Phys. Rev. Lett. 100 (2008) 093002.

[Reds2009] M. Redshaw, B.J. Mount, E.G. Myers, Phys. Rev. A 79 (2008) 012507.

[Rodr2003] D. Rodríguez, *An RFQ buncher for accumulation and cooling of heavy radionuclides at SHIPTRAP and high precision mass measurements on unstable Kr isotopes at ISOLTRAP*, Ph.D. Thesis, University of Valencia, Spain (2003).

[Rodr2004] D. Rodríguez, V.S. Kolhinen, G. Audi, J. Äystö, D. Beck, K. Blaum, G. Bollen, F. Herfurth, A. Jokinen, A. Kellerbauer, H.-J. Kluge, M. Oinonen, H. Schatz, E. Sauvan, S. Schwarz, Phys. Rev. Lett. 93 (2004) 161104.

[Rolf1988] C.E. Rolfs, W.S. Rodney, *Cauldrons in the Cosmos - Nuclear Astrophysics*, University of Chicago Press, Chicago and London, 1988.

[Roos2004] J. Van Roosbroeck, C. Guénaut, G. Audi, D. Beck, K. Blaum, G. Bollen, J. Cederkall, P. Delahaye, H. De Witte, D. Fedorov, V.N. Fedoseyev, S. Franchoo, H. Fynbo, M. Gorska, F. Herfurth, K. Heyde, M. Huyse, A. Kellerbauer, H.-J. Kluge, U. Köster, K. Kruglov, D. Lunney, A. De Maesschalck, V.I. Mishin, W.F. Müller, S. Nagy, S. Schwarz, L. Schweikhard, N.A. Smirnova, K. Van de Vel, P. Van Duppen, A. Van Dyck, W.B. Walters, L. Weissmann, C. Yazidjian, Phys. Rev. Lett. 92 (2004) 112501.

[Ryjk2008] V.L. Ryjkov, M. Brodeur, T. Brunner, M. Smith, R. Ringle, A. Lapierre, F. Ames, P. Bricault, M. Dombsky, P. Delheij, D. Lunney, M. R. Pearson, J. Dilling, Phys. Rev. Lett. 101 (2008) 012501.

[Rytz1963] A. Rytz, H.H. Staub, H. Winkler, F. Zamboni, Nucl. Phys. 43 (1993) 229.

[Sava1991] G. Savard, St. Becker, G. Bollen, H.-J. Kluge, R.B. Moore, Th. Otto, L. Schweikhard, H. Stolzenberg, U. Wiess, Phys. Lett. A 158 (1991) 247.

[Sava2004] G. Savard, J.A. Clark, F. Buchinger, J.E. Crawford, S. Gulick, J.C. Hardy, A.A. Hecht, V.E. Jakob, J.K.P. Lee, A.F. Levand, B.F. Lundgren, N.D. Scielzo, K.S. Sharma, I. Tanihata, I.S. Towner, W. Trimble, J.C. Wang, Y. Wang, Z. Zhou, Phys. Rev. C. 70 (2004) 042501(R).

[Sava2005] G. Savard, F. Buchinger, J.A. Clark, J.E. Crawford, S. Gulick, J.C. Hardy, A.A. Hecht, J.K.P. Lee, A.F. Levand, N.D. Scielzo, H. Sharma, K.S. Sharma, I. Tanihata, A.C.C. Villari, Y. Wang, Phys. Rev. Lett. 95 (2005) 102501.

[Scha1998] H. Schatz, A. Aprahamian, J. Görres, M. Wiescher, T. Rauscher, J.F. Rembges, F.-K. Thielemann, B. Pfeiffer, P. Möller, K.-L. Kratz, H. Herndl, B.A. Brown, H. Rebel, Phys. Rep. 294 (1998) 167.

[Schn1994] D. Schneider, D.A. Church, G. Weinberg, J. Steiger, B. Beck, J. McDonald, E. Magee, E. Knapp, Rev. Sci. Instrum. 65 (1994) 3472.

[Schw1993] S. Schwarz: *Aufbau und Test einer Laserdesorptionsquelle für das CERN-Massenexperiment*, Master's thesis, Johannes Gutenberg-Universität Mainz (1993).

[Schw2001] S. Schwarz, F. Ames, G. Audi, D. Beck, G. Bollen, C. De Coster, J. Dilling, O. Engels, R. Fossion, J.-E. Garcia Ramos, S. Henry, F. Herfurth, K. Heyde, A. Kellerbauer, H.-J. Kluge, A. Kohl, E. Lamour, D. Lunney, I. Martel, R.B. Moore, M. Oinonen, H. Raimbault-Hartmann, C. Scheidenberger, G. Sikler, J. Szerypo, C.Weber, ISOLDE Collaboration, Nucl. Phys. A 693 (2001) 533.

[Scie2009] N.D. Scielzo, S. Caldwell, G. Savard, J.A. Clark, C.M. Deibel, J. Fallis, S. Gulick, D. Lascar, A.F. Levand, G. Li, J. Mintz, E.B. Norman, K.S. Sharma, M. Sternberg, T. Sun, J. Van Schelt, arXiv:0902.2376v1 (2009).

[Seve2008] N. Severijns, M. Tandecki, T. Phalet, I.S. Towner, arXiv:0807.2202v1 (2008).

[Seth1974] K.K. Seth, A. Saha, W. Benenson, W.A. Lanford, H. Nann, B.H. Wildenthal, Phys. Rev. Lett. 33 (1974) 233.

[Shap1969] M.H. Shapiro, C. Moss, W.M. Denny, Nucl. Phys. A 128 (1969) 73.

[Sher2003] A. Sher, R. Appel, G.S. Atoyan, B. Bassalleck, D.R. Bergman, N. Cheung, S. Dhawan, H. Do, J. Egger, S. Eilerts, H. Fischer, W. Herold, V.V. Issakov, H. Kaspar, D.E. Kraus, D.M. Lazarus, P. Lichard, J. Lowe, J. Lozano, H. Ma, W. Majid, S. Pislak, A.A. Poblaguev, P. Rehak, A. Sher, J.A. Thompson, P. Truöl, M.E. Zeller, Phys. Rev. Lett. 91 (2003) 261802.

[Shi2005] W. Shi, M. Redshaw, E.G. Myers, Phys. Rev. A 72 (2005) 022510.

[Sikl2003] G. Sikler, *Massenspektrometrie kurzlebiger Sr- und Sn- Isotope und Aufbau der SHIPTRAP-Penningfallen*, Ph.D. Thesis, University of Heidelberg, Germany (2003).

[Smit2008] M. Smith, M. Brodeur, T. Brunner, S. Ettenauer, A. Lapierre, R. Ringle, V.L. Ryjkov, F. Ames, P. Bricault, G.W.F. Drake, P. Delheij, D. Lunney, J. Dilling, Phys. Rev. Lett. 101 (2008) 202501.

[Stah1998] S. Stahl: *Aufbau eines Experiments zu Bestimmung elektronischer g-Faktoren einzelner wasserstoffähnlicher Ionen*, PhD thesis, Johannes Gutenberg-Universität Mainz (1998).

[Stau1967] H.H. Staub, *Proc. Intern. Conf. Atomic Masses, 3rd*, Univ. Manitoba Press, 1967.

[Stöh2006] T. Stöhlker, H.F. Beyer, A. Gumberidze, A. Kumar, D. Liesen, R. Reuschl, U. Spillmann, M. Trassinelli, Hyperfine Int. 172 (2006) 135.

[Suho2007] M. Suhonen, I. Bergström, T. Fritioff, Sz. Nagy, A. Solders, R. Schuch, J. Inst. (2007) P06003.

[Tach1988] T. Tachibana, M. Uno, M. Yamada, S. Yamada, At. Data Nucl. Data Tab. 39 (1988) 251.

[Thom1897] J.J. Thomson, Phil. Mag. 3 (1897) 293.

[Thom1899] J.J. Thomson, Phil. Mag. 5 (1899) 547.

[Thom2003] J.K. Thompson *Two-Ion Control and Polarization Forces for Precise Mass Comparisons* PhD thesis, at the Masschusetts Institute of Technology (2003).

[Town1995] I.S. Towner, J.C. Hardy, in *Symmetries and Fundamental Interactions in Nuclei*, eds. W.C. Haxton and E.M. Henley, (World-Scientific, Singapore, 1995) pp. 183-249.

[Town1999] I.S. Towner, J.C. Hardy, in *Proceedings of the V International WEIN Symposium: Physics Beyond the Standard Model*, Santa Fe, NM 1998, eds. P. Herzeg, C.M. Hoffman and H.V. Klapdor-Kleingrothaus, (World-Scientific, Singapore, 1999) pp. 338-359.

[Town2002] I.S. Towner, J.C. Hardy, Phys. Rev. C 66 (2002) 035501.

[Town2008] I.S. Towner, J.C. Hardy, Phys. Rev. C 77 (2008) 025501.

[Vand1963] C. van der Leun, P.M. Endt, Physica 29 (1963) 990.

[VanD1989] R.S. Van Dyck Jr., F.L. Moore, D.L. Farnham, P.B. Schwinberg, Phys. Rev. A 40 (1989) 6308.

[VanD1999] R.S. Van Dyck, D.L. Farnham, S.L. Zafonte, P.B. Schwinberg, Rev. Sci. Instrum. 70 (1999) 1665.

[VanD1992] R.S. Van Dyck Jr., D.L. Farnham, P.B. Schwinberg, J. Mod. Opt. 39 (1992) 243.

[VanD2004] R.S. Van Dyck Jr., S.L. Zafonte, S. Van Liew, D.B. Pinegar, P.B. Schwinberg, Phys. Rev. Lett. 92 (2004) 220802.

[Verd2001] J.L. Verdú: *One experiment for the high precision measurement of the g_j-factor of the electron bound in hydrogenlike ions*, Master's thesis, Johannes Gutenberg-Universität Mainz (2001).

[Verd2003] J.L. Verdú: *Ultrapräzise Messung des elektronischen g-Faktors in wasserstoffähnlichem Sauerstoff*, PhD thesis, Johannes Gutenberg-Universität Mainz (2003).

[Vona1977] H. Vonach, P. Glassel, P. Maier-Komor, H. Rosler, H.J. Scheerer, H. Paul, D. Semrad, Nucl. Phys. A 278 (1977) 189.

[Wall1997] G. Wallerstein, I. Iben, P. Parker, A.M. Boesgaard, G.M. Hale, A.E. Champagne, C.A. Barnes, F. Käppeler, V.V. Smith, R.D. Hoffmann, F.X. Timmes, C. Sneden, R.N. Boyd, B.S. Meyer, D.L. Lambert, Rev. Mod. Phys. 69 (1997) 995.

[Waps2003] A.H. Wapstra, G. Audi, C. Thibault, Nucl. Phys. A 729 (2003) 129.

[Wine1975] D.J. Wineland, H.G. Dehmelt, J. Appl. Phys. 46 (1975) 919.

[Webe2005] C. Weber, G. Audi, D. Beck, K. Blaum, G. Bollen, F. Herfurth, A. Kellerbauer, H.-J. Kluge, D. Lunney, S. Schwarz, Phys. Lett. A 347 (2005) 81.

[Webe2008] C. Weber, V.-V. Elomaa, R. Ferrer, C. Fröhlich, D. Ackermann, J. Äystö, G. Audi, L. Batist, K. Blaum, M. Block, A. Chaudhuri, M. Dworschak, S. Eliseev, T. Eronen, U. Hager, J. Hakala, F. Herfurth, F.P. Heßberger, S. Hofmann, A. Jokinen, A. Kankainen, H.-J. Kluge, K. Langanke, A. Martín, G. Martínez-Pinedo, M. Mazzocco, I.D. Moore, J.B. Neumayr, Yu.N. Novikov, H. Penttilä, W.R. Plaß, A.V. Popov, S. Rahaman, T. Rauscher, C. Rauth, J. Rissanen, D. Rodríguez, A. Saastamoinen, C. Scheidenberger, L. Schweikhard, D.M. Seliverstov, T. Sonoda, F.-K. Thielemann, P.G. Thirolf, G.K. Vorobjev, Phys. Rev. C 78 (2008) 054310.

[West1984] B.J. West, K. Lindenberg, Phys. Rev. 102A (1984) 189.

[Yazi2006] C. Yazidjian, K. Blaum, R. Ferrer, F. Herfurth, A. Herlert, L. Schweikhard, Hyperfine Int. 173 (2006) 181

[Yazi2007] C. Yazidjian, G. Audi, D. Beck, K. Blaum, S. George, C. Guénaut, F. Herfurth, A. Herlert, A. Kellerbauer, H.-J. Kluge, D. Lunney, L. Schweikhard, Phys. Rev. C 76 (2007) 024308.

[Zion1972] J. Zioni, A.A. Jaffe, E. Friedman, N. Haik, R. Schectman, D. Nir, Nucl. Phys. A 181 (1972) 465.

List of publications (February 2009)

1. The mass of ^{22}Mg
   M. Mukherjee, A. Kellerbauer, D. Beck, K. Blaum, G. Bollen, F. Carrel, P. Delahaye, J. Dilling, S. George, C. Guénaut, F. Herfurth, A. Herlert, H.-J. Kluge, U. Köster, D. Lunney, S. Schwartz, L. Schweikhard, C. Yazidjian
   Phys. Rev. Lett. 93 (2004) 150801.

2. Mass spectrometry of atomic ions produced by in-trap decay of short-lived nuclides
   A. Herlert, D. Beck, K. Blaum, F. Carrel, P. Delahaye, S. George, C. Guénaut, F. Herfurth, A. Kellerbauer, H.-J. Kluge, D. Lunney, M. Mukherjee, L. Schweikhard, C. Yazidjian
   New J. Phys. 7, 44 (2005) 1-11.

3. ISOLTRAP mass measurements of exotic nuclides at $\delta m/m = 10^{-8}$
   K. Blaum, G. Audi, D. Beck, G. Bollen, P. Delahaye, S. George, C. Guénaut, F. Herfurth, A. Herlert, A. Kellerbauer, H.-J. Kluge, D. Lunney, M. Mukherjee, S. Schwarz, L. Schweikhard, C. Yazidjian
   Nucl. Phys. A 752 (2005) 317c-320c.

4. ISOLTRAP pins down masses of exotic nuclides
   K. Blaum, G. Audi, D. Beck, G. Bollen, M. Brodeur, P. Delahaye, S. George, C. Guénaut, F. Herfurth, A. Herlert, A. Kellerbauer, H.-J. Kluge, D. Lunney, M. Mukherjee, D. Rodríguez, S. Schwarz, L. Schweikhard, C. Yazidjian
   J. Phys. G 31 (2005) S1775-S1778.

5. Recent high-precision mass measurements with the Penning trap spectrometer ISOLTRAP
   F. Herfurth, G. Audi, D. Beck, K. Blaum, G. Bollen, P. Delahaye, S. George, C. Guénaut, A. Herlert, A. Kellerbauer, H.-J. Kluge, D. Lunney, M. Mukherjee, S. Rahaman, S. Schwarz, L. Schweikhard, C. Weber, C. Yazidjian
   Eur. J. Phys. A 25, s01 (2005) 17-21.

6. ISOLTRAP Mass Measurements for Weak-Interaction Studies
   A. Kellerbauer, G. Audi, D. Beck, K. Blaum, G. Bollen, P. Delahaye, S. George, C. Guénaut, F. Herfurth, A. Herlert, H.-J. Kluge, D. Lunney, M. Mukherjee, D. Rodríguez, S. Schwarz, L. Schweikhard, C. Weber, C. Yazidjian
   FINUSTAR Conference, Kos, Griechenland 2005
   AIP Conference Proceedings 831 (2006) 49-54.

7. High-accuracy mass measurements on neutron deficient neon isotopes
   A. Herlert, S. Baruah, K. Blaum, P. Delahaye, S. George, C. Guénaut, F. Herfurth, H.-J. Kluge, D. Lunney, S. Schwarz, L. Schweikhard, C. Weber, C. Yazidjian
   FINUSTAR Conference, Kos, Griechenland 2005
   AIP Conference Procedings, 831 (2006) 152-156.

8. High-precision mass measurements for reliable nuclear astrophysical calculations
   A. Herlert, S. Baruah, K. Blaum, P. Delahaye, S. George, C. Guénaut, F. Herfurth, H.-J. Kluge, D. Lunney, S. Schwarz, L. Schweikhard, C. Weber, C. Yazidjian
   International Symposium on Nuclear Astrophysics-Nuclei in the Cosmos-IX, CERN, Genf, Schweiz 2006
   Proceedings of Science (NIC-IX) 051 (2006)

9. High-accuracy mass measurements for a test of the Standard Model
   A. Herlert, G. Audi, D. Beck, K. Blaum, G. Bollen, P. Delahaye, S. George, C. Guénaut, F. Herfurth, A. Kellerbauer, H.-J. Kluge, D. Lunney, M. Mukherjee, D. Rodríguez, S. Schwarz, L. Schweikhard, C. Weber, C. Yazidjian
   in "Proceedings of the EPS-13 Conference 'Beyond Einstein' - Physics for the 21st Century" (Bern, Switzerland, July 11-15, 2005)
   ESA SP-637 (2006)
   ISBN 92-9291-201-X, ISSN 1609-042X (CD-ROM)

10. Towards high-accuracy mass spectrometry of highly charged short-lived ions at ISOLTRAP
    A. Herlert, S. Baruah, K. Blaum, P. Delahaye, M. Dworschak, S. George, C. Guénaut, U. Hager, F. Herfurth, A. Kellerbauer, M. Marie-Jeanne, S. Schwarz, L. Schweikhard, C. Yazidjian
    Int. J. Mass Spectrom. 251 (2006) 131-137.

11. High-accuracy mass measurements of neutron-rich Kr isotopes
    P. Delahaye, G. Audi, K. Blaum, F. Carrel, S. George, F. Herfurth, A. Herlert, A. Kellerbauer, H.-J. Kluge, D. Lunney, L. Schweikhard, C. Yazidjian
    Phys. Rev. C 74 (2006) 034331.

12. Spin-related aspects of mass determination of radionuclides
    A. Herlert, S. Baruah, K. Blaum, P. Delahaye, M. Dworschak, S. George, C. Guénaut, U. Hager, F. Herfurth, A. Kellerbauer, H.-J. Kluge, D. Lunney, S. Schwarz, L. Schweikhard, C. Weber, C. Yazidjian
    Czech. J. Phys. 56 (2006) F277.

13. Penning trap mass spectrometry for nuclear structure studies
    K. Blaum, D. Beck, M. Breitenfeldt, S. George, F. Herfurth, A. Herlert, A. Kellerbauer, H.-J. Kluge, D. Lunney, R. Savreux, S. Schwarz, L. Schweikhard, C. Yazidjian
    Hyperfine Interact. 171 (2006) 83-91.

14. Ramsey Method of Separated Oscillatory Fields for High-Precision Penning Trap Mass Spectrometry
    S. George, S. Baruah, B. Blank, K. Blaum, M. Breitenfeldt, U. Hager, F. Herfurth, A. Herlert, A. Kellerbauer, H.-J. Kluge, M. Kretzschmar, D. Lunney, R. Savreux, S. Schwarz, L. Schweikhard, C. Yazidjian
    Phys. Rev. Lett. 98 (2007) 162501.

15. The Ramsey method in high-precision mass spectrometry with Penning traps: Experimental results
S. George, K. Blaum, F. Herfurth, A. Herlert, M. Kretzschmar, S. Nagy, S. Schwarz, L. Schweikhard, C. Yazidjian
Int. J. Mass Spectrom. 264 (2007) 110-121.

16. Evidence for a breakdown of the isobaric multiplet mass equation: A study of the A=35, T=3/2 isospin quartet
C. Yazidjian, G. Audi, D. Beck, K. Blaum, S. George, C. Guénaut, F. Herfurth, A. Herlert, A. Kellerbauer, H.-J. Kluge, D. Lunney, L. Schweikhard
Phys. Rev. C 76 (2007) 024308.

17. Die Ramsey-Methode in der Präzisions-Massenspektrometrie
S. George, K. Blaum, M. Kretzschmar, L. Schweikhard
Physik in unserer Zeit 38 (2007) 163-164.

18. Restoration of the N=82 Shell Gap from Direct Mass Measurements of ^{132,134}Sn
M. Dworschak, G. Audi, K. Blaum, P. Delahaye, S. George, U. Hager, F. Herfurth, A. Herlert, A. Kellerbauer, H.-J. Kluge, D. Lunney, L. Schweikhard, C. Yazidjian
Phys. Rev. Lett. 100 (2008) 072501.

19. ISOLTRAP: An on-line Penning trap for mass spectrometry on short-lived nuclides
M. Mukherjee, D. Beck, K. Blaum, G. Bollen, J. Dilling, S. George, F. Herfurth, A. Herlert, A. Kellerbauer, H.-J. Kluge, S. Schwarz, L. Schweikhard, C. Yazidjian
Eur. Phys. J. A 35 (2008) 1-29.

20. Mass measurements and evaluation around A=22
M. Mukherjee, D. Beck, K. Blaum, G. Bollen, P. Delahaye, J. Dilling, S. George, C. Guénaut, F. Herfurth, A. Herlert, A. Kellerbauer, H.-J. Kluge, U. Köster, D. Lunney, S. Schwarz, L. Schweikhard, C. Yazidjian
Eur. Phys. J. A 35 (2008) 31-37.

21. Time-separated oscillatory fields for high-precision mass measure-ments on short-lived Al and Ca nuclides
S. George, G. Audi, B. Blank, K. Blaum, M. Breitenfeldt, U. Hager, F. Herfurth, A. Herlert, A. Kellerbauer, H.-J. Kluge, M. Kretzschmar, D. Lunney, R. Savreux, S. Schwarz, L. Schweikhard, C. Yazidjian
Europhys. Lett. 82 (2008) 50005.

22. TRIGA-SPEC: A setup for mass spectrometry and laser spectroscopy at the research reactor TRIGA Mainz
J. Ketelaer, J. Krämer, D. Beck, K. Blaum, M. Block, K. Eberhardt, G. Eitel, R. Ferrer, C. Geppert, S. George, F. Herfurth, J.Ketter, Sz. Nagy, D. Neidherr, R. Neugart, W. Nörtershäuser, J. Repp, C. Smorra, N. Trautmann, C. Weber
Nucl. Instr. Meth. A 495 (2008) 162-177.

23. Mass measurements beyond the major r-process waiting point ^{80}Zn
S. Baruah, G. Audi, K. Blaum, M. Dworschak, S. George, C. Guénaut, U. Hager, F. Herfurth, A. Herlert, A. Kellerbauer, H.-J. Kluge, D. Lunney, H. Schatz, L. Schweikhard, C. Yazidjian
Phys. Rev. Lett. 101 (2008) 262501.

24. Masses and charge radii of 17-22Ne and the two-proton halo candidate ^{17}Ne
W. Geithner, T. Neff, G. Audi, K. Blaum, P. Delahaye, S. George, C. Guénaut, F. Herfurth, A. Herlert, S. Kappertz, M. Keim, A. Kellerbauer, H.-J. Kluge, M. Kowalska, P. Lievens, D. Lunney, K. Marinova, R. Neugart, L. Schweikhard ,S. Wilbert, C. Yazidjian
Phys. Rev. Lett. 101 (2008) 262502.

25. Electric and magnetic field optimization procedure for Penning trap mass spectrometers
D. Beck, K. Blaum, G. Bollen, S. George, C. Guénaut, F. Herfurth, A. Herlert, D. Lunney, L. Schweikhard, C. Yazidjian
Nucl. Instr. and Meth. A 598 (2009) 635-641.

26. Recent developments in ion detection techniques for penning trap mass spectrometry at TRIGA-TRAP
J. Ketelaer, K. Blaum, M. Block, K. Eberhardt, M. Eibach, R. Ferrer, S. George, F. Herfurth, J. Ketter, Sz. Nagy, J. Repp, L. Schweikhard, C. Smorra, S. Sturm, S. Ulmer
Eur. Phys. J. A (2009) *DOI: 10.1140/epja/i2008-10711-6.*

27. Discovery of ^{229}Rn and the structure of the heaviest Rn and Ra isotopes from Penning trap mass measurements
D. Neidherr, G. Audi, D. Beck, K. Blaum, Ch. Böhm, M. Breitenfeldt, R.B. Cakirli, R.F. Casten, S. George, F. Herfurth, A. Herlert, A. Kellerbauer, M. Kowalska, D. Lunney, E. Minaya-Ramirez, S. Naimi, E. Noah, L. Penescu, M. Rosenbusch, S. Schwarz, L. Schweikhard, T. Stora
Phys. Rev. Lett., *in print* (2009).

28. Position-sensitive ion detection in precision Penning trap mass spectrometry
G. Eitel, K. Blaum, M. Block, A. Czasch, M. Dworschak, S. George, O. Jagutzki, J. Ketelaer, J. Ketter, S. Nagy, D. Rodríguez, C. Smorra
Nucl. Inst. Meth. Phys. Res. A, submitted (2009).

29. Preparing a journey to the east of ^{208}PB with ISOLTRAP. Isobaric purification at A=209 and new masses for $^{211-213}$Fr and ^{211}Ra.
M. Kowalska, S. Naimi, J. Agramunt, A. Algora, G. Audi, D. Beck, B. Blank, K. Blaum, Ch. Böhm, M. Breitenfeldt, E. Estevez, L.M. Fraile, S. George, F. Herfurth, A. Herlert, A. Kellerbauer, D. Lunney, E. Minaya-Ramirez, D. Neidherr, B. Olaizola, K. Riisager, M. Rosenbusch, B. Rubio, S. Schwarz, L. Schweikhard, U. Warring.
Eur. Phys. J. A, submitted (2009).